Copy 248
RM L57B04

RESEARCH MEMORANDUM

EXPERIMENTAL STATIC AERODYNAMIC FORCES AND MOMENTS AT HIGH SUBSONIC SPEEDS ON A MISSILE MODEL DURING SIMULATED LAUNCHING FROM UNSWEPT-, SWEPTBACK-, AND MODIFIED-DELTA-WING—FUSELAGE COMBINATIONS AT ZERO SIDESLIP

By William J. Alford, Jr., and Thomas J. King, Jr.

Langley Aeronautical Laboratory
Langley Field, Va.

NATIONAL ADVISORY COMMITTEE
FOR AERONAUTICS

WASHINGTON

March 19, 1957

NATIONAL ADVISORY COMMITTEE FOR AERONAUTICS

RESEARCH MEMORANDUM

EXPERIMENTAL STATIC AERODYNAMIC FORCES AND MOMENTS AT HIGH SUBSONIC SPEEDS ON A MISSILE MODEL DURING SIMULATED LAUNCHING FROM UNSWEPT-, SWEPTBACK-, AND MODIFIED-DELTA-WING—FUSELAGE COMBINATIONS AT ZERO SIDESLIP

By William J. Alford, Jr., and Thomas J. King, Jr.

SUMMARY

An investigation was made at high subsonic speeds in the Langley high-speed 7- by 10-foot tunnel to determine the static aerodynamic forces and moments on a missile model during simulated launching from the midsemispan locations of unswept- and sweptback-wing—fuselage combinations and from the midsemispan and one-quarter semispan locations of a modified-delta-wing—fuselage combination (including tests with the wing removed). The results indicated that variation in the missile longitudinal location produced significant effects upon the missile aerodynamic characteristics for each of the airplane wing plan forms investigated, as evidenced by large gradients in the various forces and moments. Increasing the angle of attack caused increases in the absolute magnitudes of the missile forces and moments relative to those of the isolated missile. Increasing the Mach number had little effect on the variations with angle of attack of the missile force and moment characteristics except that nonlinearities were incurred at smaller angles of attack for the higher Mach numbers. The flow disturbance effects, due to airplane finite wing thickness, on the missile characteristics increased with increasing Mach number. The primary effects of variations in airplane wing plan form were most noticeable in the missile yawing-moment characteristics in that the sweptback- and modified-delta-wing combinations produced considerably larger deviations with variations in chordwise distance than did the unswept-wing—fuselage combination. The effect of moving the missile from the midsemispan to the one-quarter semispan location was to cause an increase in the severity of the chordwise gradients of the pitching moments and normal forces and to cause a decrease in the severity in the chordwise gradients of the yawing moments and side forces. The wing plus wing-fuselage interference effects were found to be the prime factors in producing the large force and moment variations when compared with the isolated missile.

INTRODUCTION

The National Advisory Committee for Aeronautics is conducting investigations to determine the nature and origin of the mutual interference experienced by various combinations of wing-fuselage models and externally carried missiles. Previous investigations (refs. 1 to 9) have shown the existence of these large and generally objectionable interference effects, and references 1 to 4 have shown that they are primarily due, at low speeds, to the nonuniform flow field generated by the airplane.

The manner in which first-order estimations of the static forces and moments existing on the missile model can be accomplished, with consideration for the airplane nonuniform flow fields, have been demonstrated in references 1 and 2. The ability of potential theory to predict the flow characteristics beneath swept and unswept wings has been reported in reference 3. Additional and more extensive low-speed flow-field characteristics near swept- and unswept-wing—fuselage combinations, at zero sideslip, have been reported in reference 4. The low-speed aerodynamic forces and moments existing on a missile model similar to the one of the present investigation during simulated launching, from several spanwise and vertical locations of a 45° sweptback-wing—fuselage combination have been presented in references 5 and 7. Similar low-speed information has been obtained on a canard missile model and has been reported in reference 6. The static forces and moments existing on the canard missile at high subsonic speeds during simulated launching from the sweptback-wing—fuselage combination of this investigation have been presented in reference 8. The high-subsonic-speed force and moment characteristics of the missile model and sweptback-wing—fuselage combination of the present investigation have previously been reported in reference 9, where the effects of chordwise position, the effects of the pylon, the effects of skewing the missile relative to the wing-fuselage combination and the effects of sideslipping the missile with the wing-fuselage combination were investigated. The present investigation extends the results of reference 9 to include the effects of wing plan form for the condition of zero sideslip.

The purposes of the present paper are to present the results of an experimental investigation made at high subsonic speeds to determine the static aerodynamic forces and moments on a missile model during simulated launching from the midsemispan locations of unswept- and sweptback-wing—fuselage combinations and from the midsemispan and one-quarter semispan locations of a modified-delta-wing—fuselage combination (including tests with the wing removed), and to present a qualitative analysis of the missile force and moment characteristics as affected by chordwise position, spanwise position, and airplane wing plan form.

The data for the missile model in the presence of the sweptback-wing—fuselage combination have been reported previously in reference 9 and are repeated in the present paper for comparative purposes.

SYMBOLS

The directions of positive angles, forces, and moments for the body-axes system employed are presented in figure 1.

C_N	missile normal-force coefficient, $\frac{\text{Normal force}}{qS_m}$
C_m	missile pitching-moment coefficient, $\frac{\text{Pitching moment}}{qS_m\bar{c}_m}$
C_Y	missile side-force coefficient, $\frac{\text{Side force}}{qS_m}$
C_n	missile yawing-moment coefficient, $\frac{\text{Yawing moment}}{qS_m b_m}$
C_l	missile rolling-moment coefficient, $\frac{\text{Rolling moment}}{qS_m b_m}$
$C_{L,A}$	airplane wing-fuselage lift coefficient, $\frac{\text{Lift}}{qS_A}$
q	free-stream dynamic pressure, lb/sq ft
V	free-stream velocity, ft/sec
S_m	exposed missile wing area of two panels, 0.0167 sq ft
S_A	included wing area, 2.16, 2.20, and 2.25 sq ft for unswept, modified-delta, and sweptback wings, respectively
b_m	span of missile wings, 0.256 ft
b	span of airplane wing, ft
c	local wing chord of airplane model, ft

$\bar{c}_m$ mean aerodynamic chord of exposed missile wing, 0.114 ft

$\bar{c}_A$ mean aerodynamic chord of airplane wing, 0.90, 1.02, and 0.82 ft for unswept, modified-delta, and sweptback wings, respectively

c_p chord of pylon, in.

d_{max} maximum diameter of missile fuselage, 0.058 ft

x chordwise distance from leading edge of local wing chord to missile center of gravity (positive rearward), ft

y spanwise distance from fuselage center line to missile center line (positive to right), ft

z vertical distance from wing-chord plane to missile center line (positive up), ft

l_s unsupported length of missile sting, ft

β missile skew angle relative to fuselage center line, deg

α missile angle of attack relative to free-stream direction, deg

α_A airplane angle of attack relative to free-stream direction, deg

M Mach number

MODELS AND APPARATUS

The three airplane wing-fuselage models used as the test vehicles are shown in figure 2 and include unswept, sweptback, and modified-delta plan forms. The unswept wing had 6.3° sweepback of the quarter-chord line, an aspect ratio of 3.0, a taper ratio of 0.5, and NACA 65A004 airfoil sections parallel to the free-stream direction. The sweptback wing had a quarter-chord sweepback of 45°, an aspect ratio of 4.0, a taper ratio of 0.3, and NACA 65A006 airfoil sections parallel to the free-stream direction. The modified-delta wing had a quarter-chord sweepback of 36.9°, an aspect ratio of 3.0, a taper ratio of 0.14, and NACA 65A006 airfoil sections parallel to the free-stream direction. The fuselage (with ordinates given in table I) consisted of an ogival nose section,

a cylindrical center section, and a truncated tail cone. The missile model used in this investigation employed an inline cruciform arrangement of its wing and tail, a fuselage that consisted of an ogival nose, and a cylindrical aftersection and is shown in figures 3 and 4 as a part of a typical test setup. Details of the missile model are shown in figure 5. The pylons used in this investigation had an elliptic nose section, a flat center section, and a straight tapered trailing edge. The ordinates of the pylons are given in table II. The vertical lengths of the pylons used with the various airplane-missile combinations were determined from the missile vertical locations (assumed from missile-ground clearance considerations) with allowances for a no-load gap between the pylon and the missile fuselage and also between the missile wing tip and the lower surface of the airplane wing. This gap, capable of accommodating the maximum deflection to be encountered in the vertical plane due to missile-sting flexibility, was $0.12d_{max}$ of the missile fuselage and was constant for all airplane wing plan forms and spanwise locations investigated. A list of the pylon vertical lengths and missile vertical locations in percent of the mean aerodynamic chords of the various airplane wing plan forms is presented in the following table:

Airplane wing-fuselage combination	Spanwise location, $y/\frac{b}{2}$	Pylon vertical length from maximum-thickness location of airplane wing lower surface, percent mean aerodynamic chord	Missile vertical location from airplane wing-chord plane, percent mean aerodynamic chord
Unswept	-0.50	6.9	12.8
Sweptback	-.50	7.5	14.7
Modified delta	-.50	6.2	11.8
Modified delta	-.25	6.0	13.3

The leading edge of the pylon was located 12 percent of the local wing chord behind the leading edge of the local wing chord for all wing plan forms and spanwise locations.

The missile was internally instrumented with a five-component strain-gage balance and was supported from the rear by a sting that could be translated in the longitudinal and lateral planes (figs. 3 and 4). The missile support sting also incorporated a skew-angle pivot support (fig. 3).

TESTS

The tests were made in the Langley high-speed 7- by 10-foot tunnel at Mach numbers of 0.60, 0.80, 0.90, and 0.94 with the corresponding Reynolds number varying from 3.3×10^6 to 3.8×10^6 per foot of a typical dimension. The variation of average Reynolds number with test Mach number is presented in figure 6. The angle-of-attack range generally extended at $M = 0.60$ from -2° to 18°, although at the higher Mach numbers the angle range was restricted by the load limit of the strain-gage balance and therefore varied with the loadings measured for each location of the missile. The tests were made at zero sideslip with the missile model located under the left wing of the airplane wing-fuselage-pylon combinations.

CORRECTIONS AND ACCURACY

Blocking corrections applied to Mach number and dynamic pressure were determined by the method of reference 10. Jet-boundary corrections applied to the angle of attack were calculated by the method of reference 11.

Corrections have been applied to the missile angle of attack to account for the deflection of both the main sting used to support the airplane-missile combinations (fig. 4) and the missile support sting and balance combination (fig. 3). The variation of the corrected airplane model angle of attack due to the main sting under load and due to jet-boundary considerations is presented in figure 7 and the variations in missile angle of attack due to the deflection of the missile sting and balance combination are presented in figure 8. A list is presented in table III of the missile sting lengths for the various missile longitudinal locations associated with the three airplane wing-fuselage combinations. In order to keep the unsupported missile sting lengths to a minimum, the missile sting was clamped to the pylon for positions where the missile model was ahead of the pylon leading edge. The maximum angle of incidence existing between the missile model and the airplane model due to the deflection of the missile sting and balance combination was of the order of 1.9° for the various models and positions investigated. The magnitude of the angle of incidence may be determined for any missile attitude and location investigated from the data presented in figure 8 and table III along with the force and moment data of the missile model. No corrections have been applied to the missile lateral angle, or the vertical and lateral locations because of the deflections of the missile sting and balance. A calibration of these deflections has been made and the results are presented in figure 8.

A study of the strain-gage-balance calibrations and general repeatability of the test data indicated that the accuracy levels of the various force and moment coefficients are approximately as follows:

C_N	±0.05
C_m	±0.05
C_Y	±0.05
C_n	±0.05
C_l	±0.01

RESULTS AND DISCUSSION

Presentation of Results

When the force and moment characteristics of the missile model are analyzed, it should be kept in mind that the missile was located beneath the left wing of the wing-fuselage-pylon combinations and that the positive directions of angles, forces, and moments are as shown in figure 1.

The experimental results of this investigation are presented as listed in the following table:

Airplane wing-fuselage combination	$y/\frac{b}{2}$	Prime variable	Figure
Isolated missile	----------	α	9
Unswept	-0.50	α	10
Sweptback	-0.50	α	11
Modified delta	-0.50	α	12
Modified delta	-0.25	α	13
Fuselage alone	-0.50*	α	14
Fuselage alone	-0.25*	α	15
Unswept	-0.50	x/c	16
Sweptback	-0.50	x/c	17
Modified delta	-0.50	x/c	18
Effects of wing plan form	-0.50	x/c	19
Effect of spanwise position	-0.50 and -0.25	x/c	20
Comparison of fuselage and airplane wing-fuselage effects	-0.50 and -0.25	x/c	21 and 22
Lift characteristics of airplane wing-fuselage combinations	----------	α	23

*Indicates lateral distances based on modified-delta-wing plan form.

Although breakdown tests of the isolated missile were not obtained in the present investigation, this information has been presented in reference 12.

Isolated Missile Characteristics

The results of tare tests made in the clear tunnel (airplane wing-fuselage-pylon combinations removed) to evaluate the interference effects of the lateral sting support (fig. 3) upon the isolated missile aerodynamic characteristics indicated that these interferences were negligible even for the most rearward location of the missile investigated (corresponding to $x/c = 0.50$ of the sweptback-wing—fuselage combination).

A support used to restrain the skew-angle pivot incorporated in the missile sting (fig. 1) is seen from figure 9 to have little effect on the missile normal force and pitching moments except at the higher Mach numbers where some nonlinearity is incurred in the slopes of the pitching-moment curves through zero angle of attack. The effects of the support on the remaining force and moment components were negligible.

Effect of Varying Chordwise Position

In general, variation of missile chordwise position relative to the airplane wing produced pronounced effects upon the missile aerodynamic characteristics, these effects being evidenced by large gradients in the missile forces and moments. (See figs. 16 to 22.)

These large gradients are induced on the missile because of the non-uniform flow field generated primarily by the wings of the airplane wing-fuselage-pylon combinations. The variations of the missile forces and moments with longitudinal position can be explained qualitatively by a consideration of the airplane wing-fuselage flow fields similar to those reported in references 1 to 4. For instance, when the missile center of gravity is located rearward of the leading edge of the local wing chord (figs. 16, 17, and 18) at positive angles of attack, the missile wings are operating in regions of downflow. The missile tail, however, is in a region of slightly higher total angularity (that is, less downflow). The net result is a decreased normal force and a nose-down pitching moment relative to the isolated missile characteristics (fig. 9). As the missile is moved forward, its wings move into regions of upflow (ahead of the leading edge of the local wing chord) and its tail moves into regions of increased downflow (immediately rearward of the leading edge of the local wing chord (refs. 3 and 4)); this condition results in an increased normal force and a nose-up pitching moment. Movement of the missile farther forward causes the wings to operate in regions of decreasing disturbances and the tail to operate in the regions of

upflow; thus, the normal force approaches its free-stream level and the pitching moment decreases its nose-up tendency. With sufficient increases in chordwise distance, the effects of the wing-fuselage flow fields diminish and the missile forces and moments tend to their free-stream levels.

A similar analysis can be effected for the missile lateral forces and moments. References 3 and 4 indicate that large local sidewash or sideslip angularities are generated beneath the wings of the wing-fuselage combinations, even at an angle of sideslip of 0°. The maximum values of these local sideslip angles occur near the leading edge of the local wing chord and are in an outboard direction (toward the wing tip) for positive angles of attack; thus, negative side forces are induced (forces directed toward left wing tip). The missile yawing moments in the presence of the sweptback- and modified-delta-wing airplanes are at first (for the more rearward center-of-gravity locations) nose outboard when the missile wings are in the higher angular regions and then nose inboard when the missile tail enters the maximum sidewash region. (See figs. 17 and 18.) The missile yawing moments are positive over the complete chordwise range when in the presence of the unswept-wing airplane, the largest variations occurring for positions immediately ahead of the leading edge of the local wing chord (fig. 16).

Effects of Angle of Attack and Mach Number

In general, the effects of increasing the angle of attack were to cause substantial changes in the missile forces and moments (figs. 10 to 18) relative to the isolated missile (fig. 9). These changes can be explained (from refs. 1 to 4) by the increases in airplane wing-fuselage circulation strength which result in increases in downwash and sidewash angularity fields in conjunction with a nonuniform but somewhat diminished dynamic pressure field. Reducing the angle of attack to zero did not, however, eliminate the flow-field disturbances since the effects of wing thickness, sweep, and taper still generate sizable flow distortions (ref. 3).

Increasing the Mach number (figs. 10 to 22) had, in general, little effect on the variations of the missile aerodynamic characteristics with angle of attack or chordwise position, except that nonlinearities were incurred at smaller angles of attack for the higher Mach numbers. The flow-disturbance effects due to finite wing thickness (for a given airplane wing plan form) increased with increasing Mach number as evidenced by the displacement of the missile moment curves at an angle of attack of 0°. This result is in accord with theoretical predictions of the effects of Mach number on the flow-field characteristics at zero lift presented in reference 3. The theoretical results of reference 3 for zero lift might be interpreted as saying that, for a given vertical

distance below a wing, the effect of increasing the Mach number (for subcritical speeds) on the flow-field characteristics, and hence on the missile forces and moments, is analogous to the conditions where the Mach number was held constant and the wing above the missile was appropriately thickened and swept back.

Effect of Airplane Wing Geometric Characteristics

Inasmuch as a systematic investigation of the effects of the wing geometric characteristics on the missile aerodynamic characteristics is impracticable because of the large number of variables involved, three plan forms having approximately the same wing areas were selected as being representative of configurations likely to be of present or future interest. These consisted of unswept-, sweptback-, and modified-delta-wing—fuselage combinations.

Examination of figure 19 indicates that the missile normal and side forces, for an angle of attack of 0°, are not affected to any appreciable extent by the variation in the geometric characteristics of the wing. The missile pitching moments have, in general, a similar variation with chordwise distance for the various plan forms. The most noticeable effect of wing plan form is evident in the missile yawing moments; at an angle of attack of 0°, the unswept wing has only a small effect and the sweptback and modified-delta wings induced considerable effect because of their local sweep and taper characteristics (ref. 3). It should be noted that the thickness distributions and sweep and taper characteristics of the wings primarily determine the chordwise variation of the missile pitching and yawing moments (parts (a) and (c) of fig. 19), whereas the lift characteristics of the wings appear to magnify or diminish these variations (parts (b) and (d) of fig. 19). This is also the case for the normal and side forces. The missile rolling-moment characteristics are affected in a more random fashion, possibly because of the localized influence of the pylon as has been reported in reference 9.

Effect of Missile Spanwise Location

A comparison of the missile aerodynamic forces and moments at the midsemispan location of the modified-delta-wing—fuselage combination with those existing at the one-quarter semispan location of the same configuration is presented in figure 20. Examination of the normal-force and pitching-moment data indicates that an inboard movement of the missile causes, in general, larger deviations from the isolated missile characteristics and more severe chordwise gradients. For an angle of attack of 0° (parts (a) and (c) of fig. 20) these deviations are presumed to be due to the increase in maximum thickness and chord length of the wing; this increase distributes the disturbed flow over a longer

length of the missile. As the angle of attack is increased, the deviations from the isolated missile characteristics and chordwise gradients in the normal force and pitching moments become even more severe for the inboard location than for the outboard location, because of the increased downwash angles which occur as the plane of symmetry is approached.

At an angle of attack of 0° the effect of an inboard movement in spanwise location of the missile is to cause a reduction in the severity of the chordwise gradients and in the magnitudes of the missile side forces and yawing moments. As the angle of attack is increased, the missile side force and yawing moments also increase. It should be noted, however, that they are considerably lower than for the midsemispan location. This can be explained from simple vortex considerations which show that the lift-induced sidewash angles approach zero as the plane of symmetry is approached. The variation of spanwise position produced no important effects on the missile rolling-moment characteristics.

Comparison of Wing-Fuselage and Fuselage Effects on the Missile Forces and Moments

Comparisons of the missile forces and moments in the presence of the modified-delta-wing—fuselage with the missile forces and moments in the presence of the fuselage alone for the midsemispan and one-quarter semispan locations are presented in figures 21 and 22, respectively.

Examination of the comparison presented in figure 21 for the midsemispan location indicates that, when the wing is removed, the missile forces and moments differ little from the isolated missile levels. The only noticeable effect due to the fuselage occurs in the missile lateral characteristics in that some small deviations are evident, presumably because of the fuselage thickness, inasmuch as they increase with Mach number but not with angle of attack. Examination of the missile forces and moments for the more inboard lateral location ($y/\frac{b}{2} = -0.25$, fig. 22) indicates that the fuselage contributes slightly more effect on the missile than for the midsemispan location, these effects changing slightly with angle of attack. For both spanwise locations it is evident that the wing plus wing-fuselage interference effects are the primary causes for the missile deviations relative to the isolated missile characteristics. This result is in accord with the flow-field characteristics reported in reference 4.

It should be noted that the effects of removing the wing of the airplane wing-fuselage combination would be similar for the other plan forms investigated.

CONCLUSIONS

The results of an experimental investigation made at high subsonic speed to determine the static aerodynamic forces on a missile model during simulated launching from the midsemispan locations of unswept-, sweptback-, and modified-delta-wing—fuselage combinations and from the one-quarter semispan location of the modified-delta-wing—fuselage combination indicate the following conclusions:

1. Variation in missile longitudinal location produced significant effects upon the missile aerodynamic characteristics for each of the plan forms investigated, these effects being evidenced by large gradients in the various forces and moments.

2. Increasing the angle of attack caused substantial changes in the absolute magnitudes of the missile forces and moments relative to those of the isolated missile. Increasing the Mach number had little effect on the variations with angle of attack of the missile force and moment characteristics, except that nonlinearities were incurred at smaller angles of attack for the higher Mach numbers. The flow disturbance effects, due to finite wing thickness, on the missile characteristics increased with increasing Mach number.

3. The primary effects of variations in wing geometric characteristics were most noticeable in the missile yawing-moment characteristics in that the sweptback and modified-delta-wing combinations produced considerably larger deviations with variation in chordwise location than did the unswept-wing—fuselage combination.

4. The effect of moving the missile from the midsemispan location to the one-quarter semispan location was to cause an increase in the severity of the chordwise gradients of the pitching moments and normal forces and to cause a decrease in the severity in the chordwise gradients of the yawing moments and side forces.

5. A comparison of the missile aerodynamic characteristics in the presence of the wing-fuselage combination and in the presence of the fuselage alone indicated that the wing plus wing-fuselage interference

are the prime factors in producing the large force and moment variations when compared with the missile in the free stream.

Langley Aeronautical Laboratory,
National Advisory Committee for Aeronautics,
Langley Field, Va., January 15, 1957.

REFERENCES

1. Alford, William J., Jr., Silvers, H. Norman, and King, Thomas J., Jr.: Preliminary Low-Speed Wind-Tunnel Investigation of Some Aspects of the Aerodynamic Problems Associated With Missiles Carried Externally in Positions Near Airplane Wings. NACA RM L54J20, 1954.

2. Alford, William J., Jr.: Effects of Wing-Fuselage Flow Fields on Missile Loads at Subsonic Speeds. NACA RM L55E10a, 1955.

3. Alford, William J., Jr.: Theoretical and Experimental Investigation of the Subsonic-Flow Fields Beneath Swept and Unswept Wings With Tables of Vortex-Induced Velocities. NACA TN 3738, 1956.

4. Alford, William J., Jr., and King, Thomas J., Jr.: Experimental Investigation of Flow Fields at Zero Sideslip Near Swept- and Unswept-Wing—Fuselage Combinations at Low Speed. NACA RM L56J19, 1957.

5. Alford, William J., Jr., Silvers, H. Norman, and King, Thomas J., Jr.: Experimental Aerodynamic Forces and Moments at Low Speed of a Missile Model During Simulated Launching From the Midsemispan Location of a 45° Sweptback Wing-Fuselage Combination. NACA RM L54K11a, 1955.

6. Alford, William J., Jr.: Experimental Static Aerodynamic Forces and Moments at Low Speed on a Canard Missile During Simulated Launching From the Midsemispan and Wing-Tip Locations of a 45° Sweptback Wing-Fuselage Combination. NACA RM L55A12, 1955.

7. Alford, William J., Jr., Silvers, H. Norman, and King, Thomas J., Jr.: Experimental Static Aerodynamic Forces and Moments at Low Speed on a Missile Model During Simulated Launching From the 25-Percent-Semispan and Wing-Tip Locations of a 45° Sweptback Wing-Fuselage Combination. NACA RM L55D20, 1955.

8. Alford, William J., Jr., and King, Thomas J., Jr.: Experimental Static Aerodynamic Forces and Moments at High Subsonic Speeds on a Canard Missile During Simulated Launching From the Midsemispan Location of a 45° Sweptback Wing-Fuselage-Pylon Combination at Zero Sideslip. NACA RM L56J15a, 1957.

9. Alford, William J., Jr., and King, Thomas J., Jr.: Experimental Static Aerodynamic Forces and Moments at High Subsonic Speeds on a Missile Model During Simulated Launching From the Midsemispan Location of a 45° Sweptback Wing-Fuselage-Pylon Combination. NACA RM L56J05, 1957.

[redacted]

10. Herriot, John G.: Blockage Corrections for Three-Dimensional-Flow Closed-Throat Wind Tunnels, With Consideration of the Effect of Compressibility. NACA Rep. 995, 1950. (Supersedes NACA RM A7B28.)

11. Gillis, Clarence L., Polhamus, Edward C., and Gray, Joseph L., Jr.: Charts for Determining Jet-Boundary Corrections for Complete Models in 7- by 10-Foot Closed Rectangular Wind Tunnels. NACA WR L-123, 1945. (Formerly NACA ARR L5G31.)

12. Johnson, M. C., and Copley, R. J.: Presentation of Normal Force, Pitching Moment, and Rolling Moment Data from Wind-Tunnel Tests of the 13.3-Percent-Scale Model of the Sparrow 14-B at Mach Numbers of 0.5, 0.7, and 0.8. Rep. No. SM-14334 (Contract Noa(s)51-859), Douglas Aircraft Co., Inc., Dec. 30, 1952.

TABLE I

FUSELAGE ORDINATES

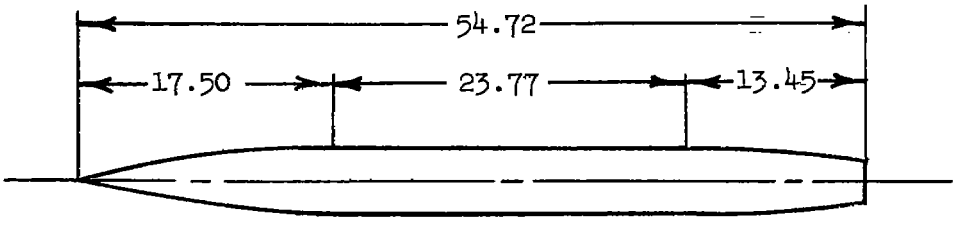

Ordinates

Station, in.	Radius, in.
0	0
2.00	.53
4.00	1.00
6.00	1.44
8.00	1.80
10.00	2.07
12.00	2.30
14.00	2.42
16.00	2.47
17.50	2.50
41.27	2.50
43.27	2.42
45.27	2.35
47.27	2.25
48.30	2.14
54.72	1.65

[redacted]

TABLE II

PYLON ORDINATES

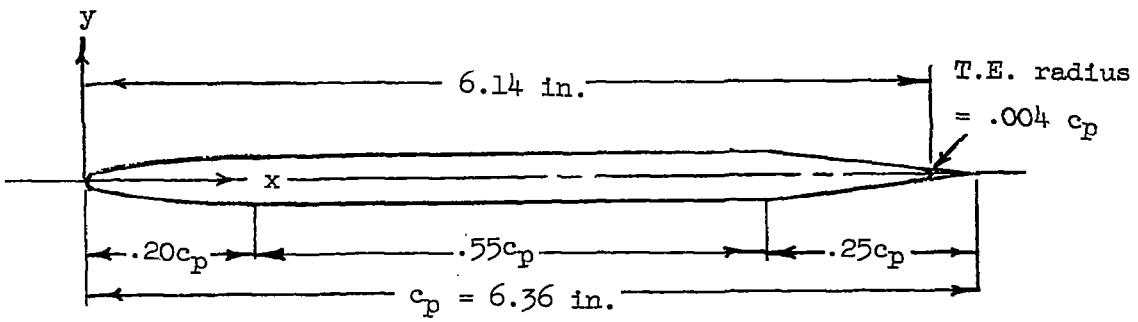

Ordinates

x, percent chord	±y, percent chord
0	0
2.5	.46
5.0	2.00
15.0	2.90
20.0	3.00
75.0	3.00
Straight taper	
100.0	0

TABLE III

MISSILE STING LENGTHS

Unswept $\left(y/\frac{b}{2} = -0.50\right)$

Missile center-of-gravity location, x/c	$l_s/\bar{c}_A$
0.29	1.44
.13	1.59
-.10	1.81
*-.25	.99
*-.44	1.17
*-.58	1.30
*-.74	1.45
*-1.11	1.81

Sweptback $\left(y/\frac{b}{2} = -0.50\right)$

Missile center-of-gravity location, x/c	$l_s/\bar{c}_A$
0.50	1.24
.29	1.44
.13	1.58
-.10	1.79
*-.25	1.01
*-.44	1.08
*-.58	1.31
*-.74	1.35
*-1.11	1.69

Modified delta $\left(y/\frac{b}{2} = -0.50\right)$

Missile center-of-gravity location, x/c	$l_s/\bar{c}_A$
0.48	1.01
.27	1.19
.10	1.32
-.10	1.49
-.25	1.62
*-.44	1.01
*-.58	1.13
*-.74	1.26
*-1.11	1.58

Modified delta $\left(y/\frac{b}{2} = -0.25\right)$

Missile center-of-gravity location, x/c	$l_s/\bar{c}_A$
0.25	1.35
.13	1.57
*-.11	.80
*-.25	.95
*-.46	1.20
*-.58	1.34
*-.71	1.48

*Denotes locations where missile sting was supported from pylon.

[redacted]

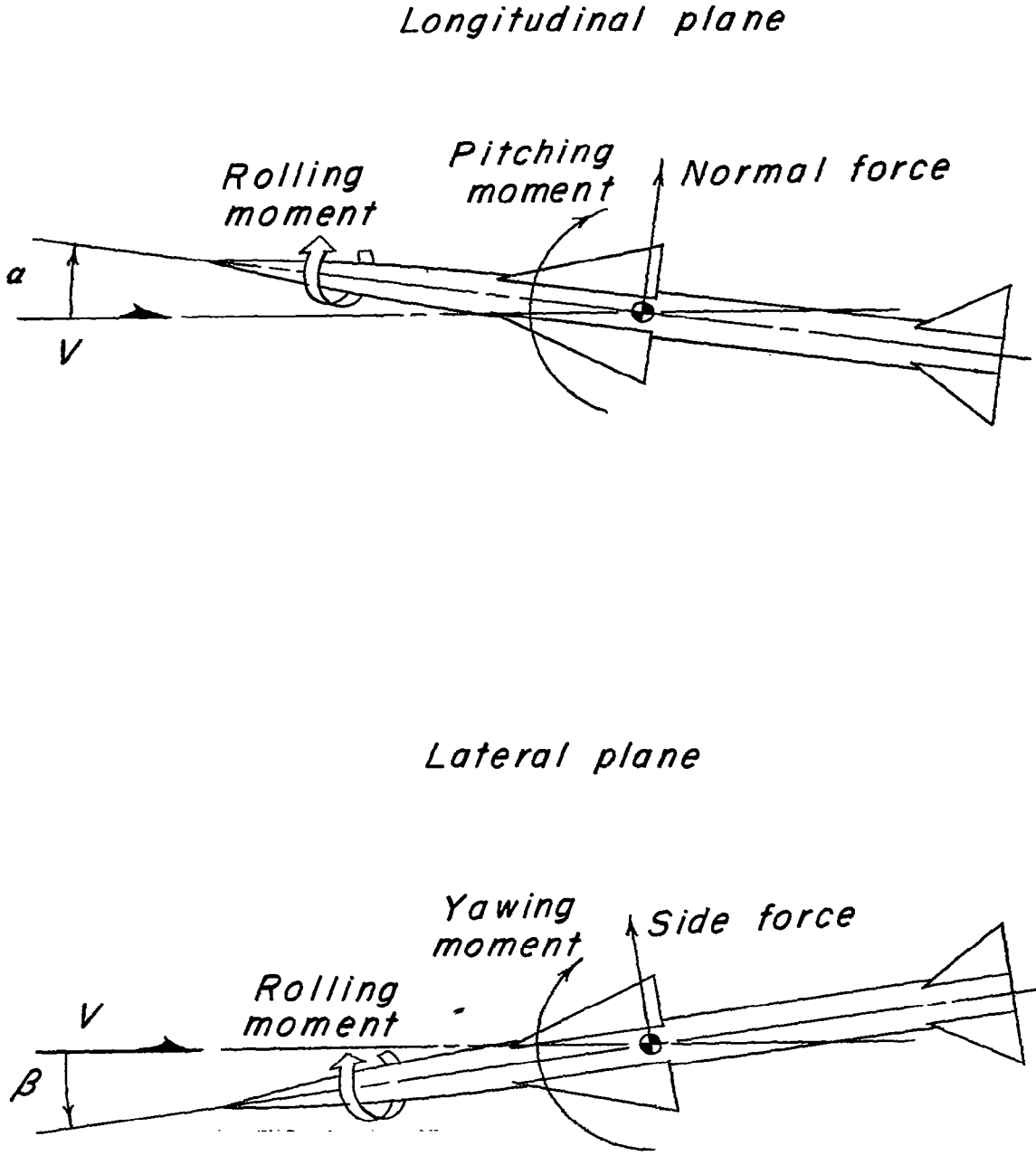

Figure 1.- Positive directions of forces, angles, and moments as measured on the missile.

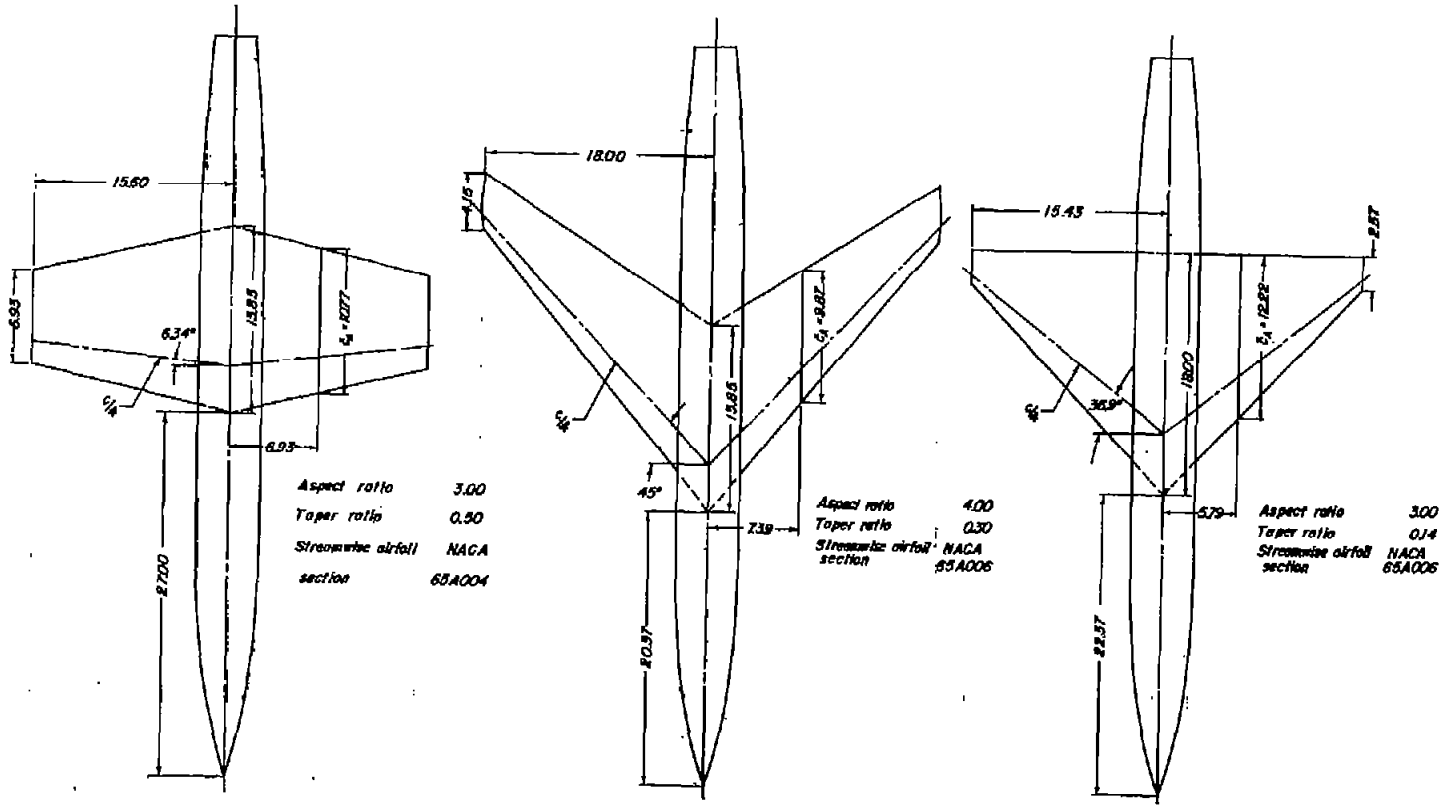

Figure 2.- Geometric characteristics of the wing-fuselage combinations on which the missile model was installed.

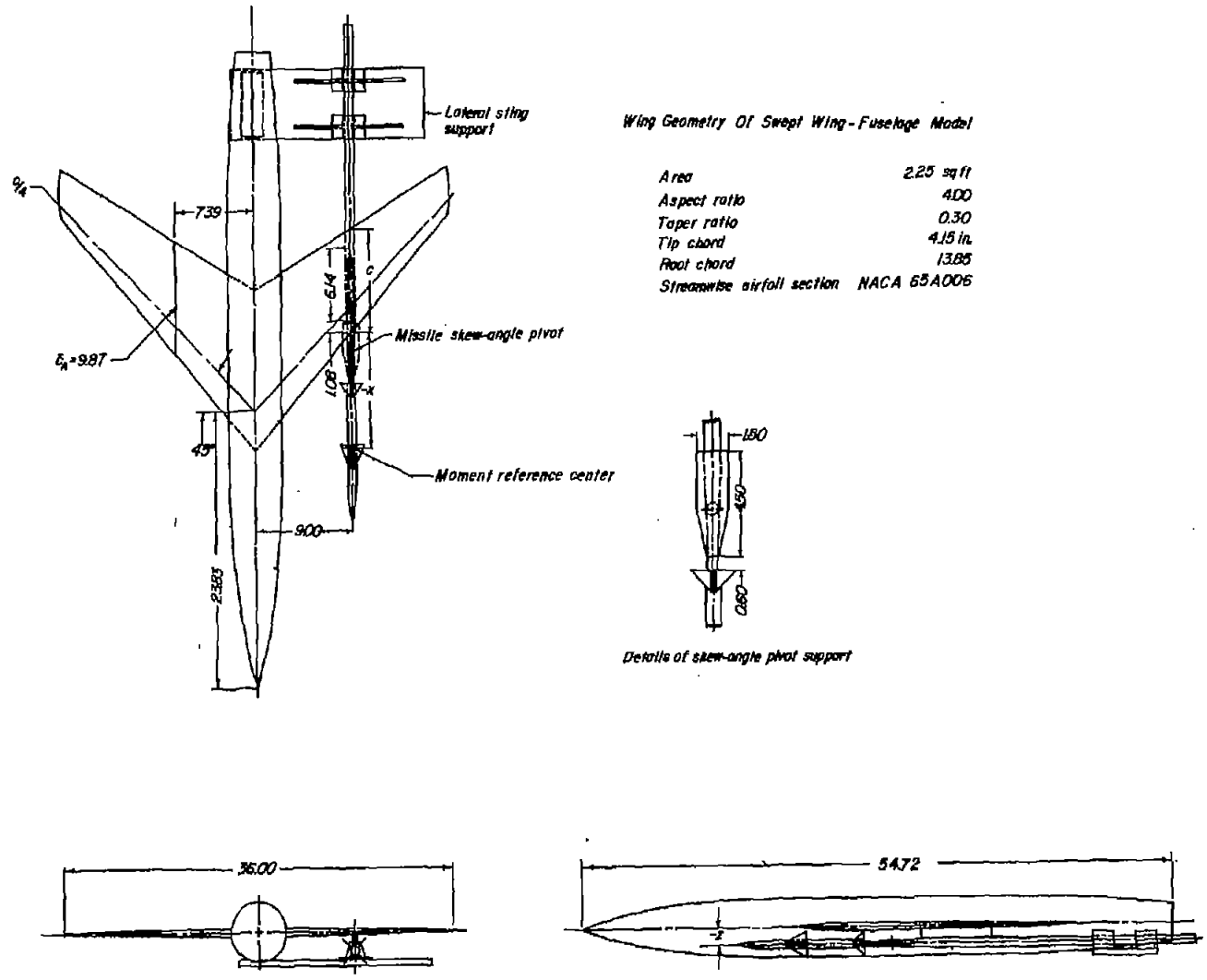

Figure 3.- Three-view drawing of wing-fuselage with missile model installed. All dimensions are in inches except where noted.

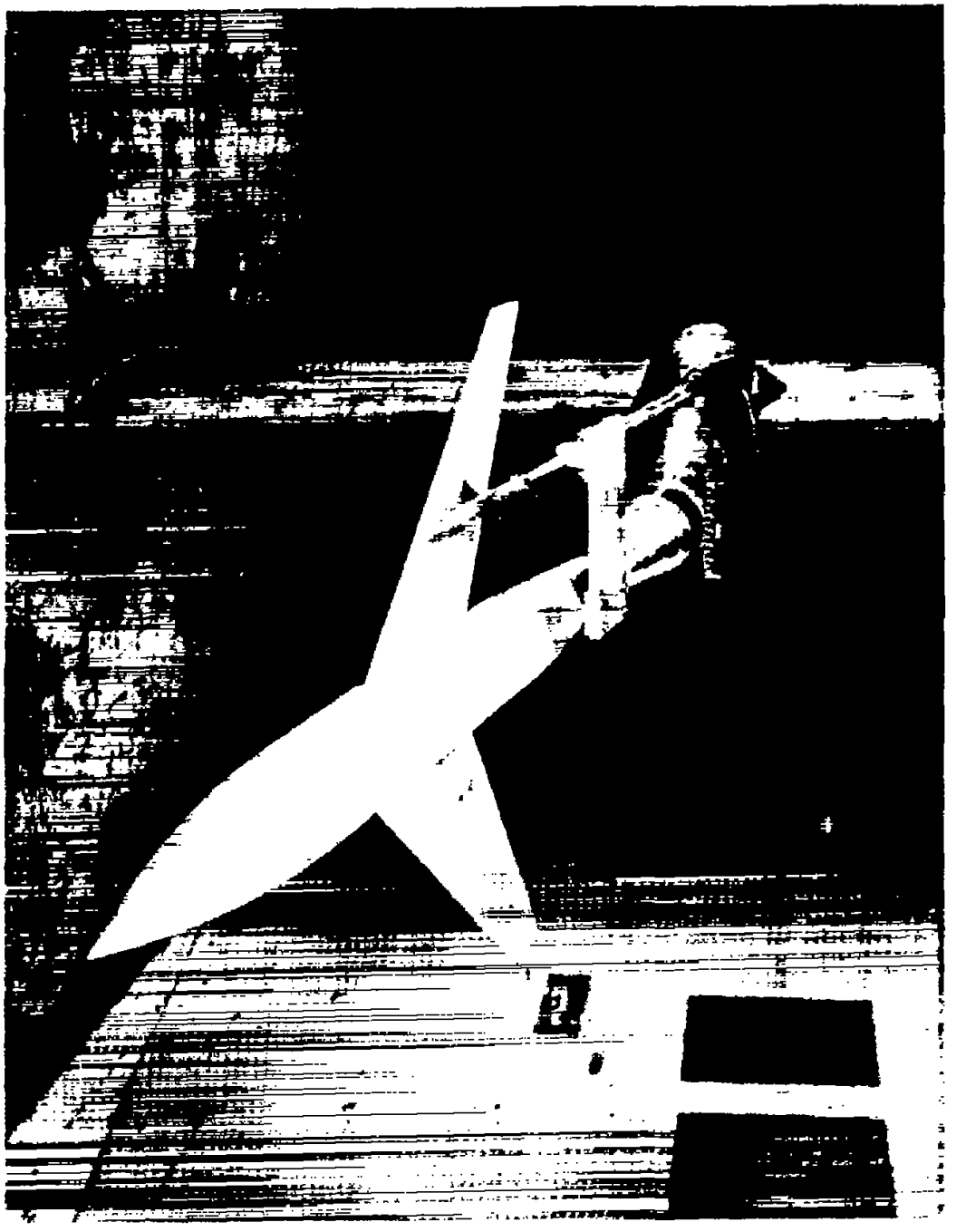

L-90313

Figure 4.- Photograph (inverted for orientation) of typical test setup.

Nose ordinates, inches	
x_m	r
0	0
.500	.082
1.000	.153
1.500	.214
2.000	.264
2.500	.302
3.000	.331
3.500	.348
4.050	.355

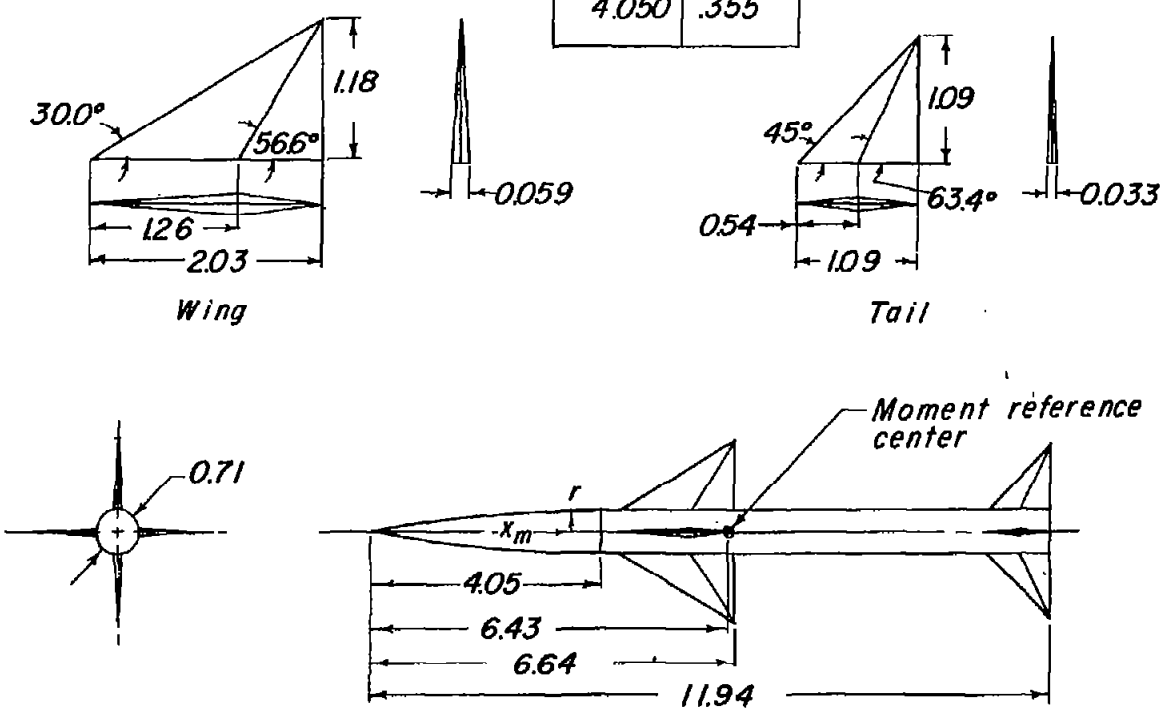

Figure 5.- Drawing of the missile model. All linear dimensions are in inches.

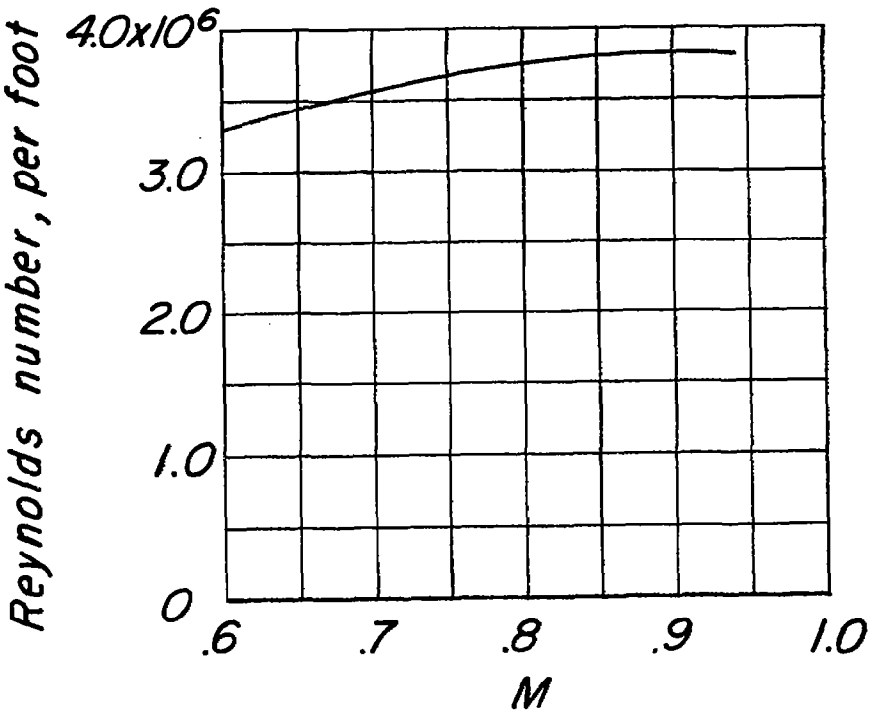

Figure 6.- Variation of average Reynolds number with test Mach number.

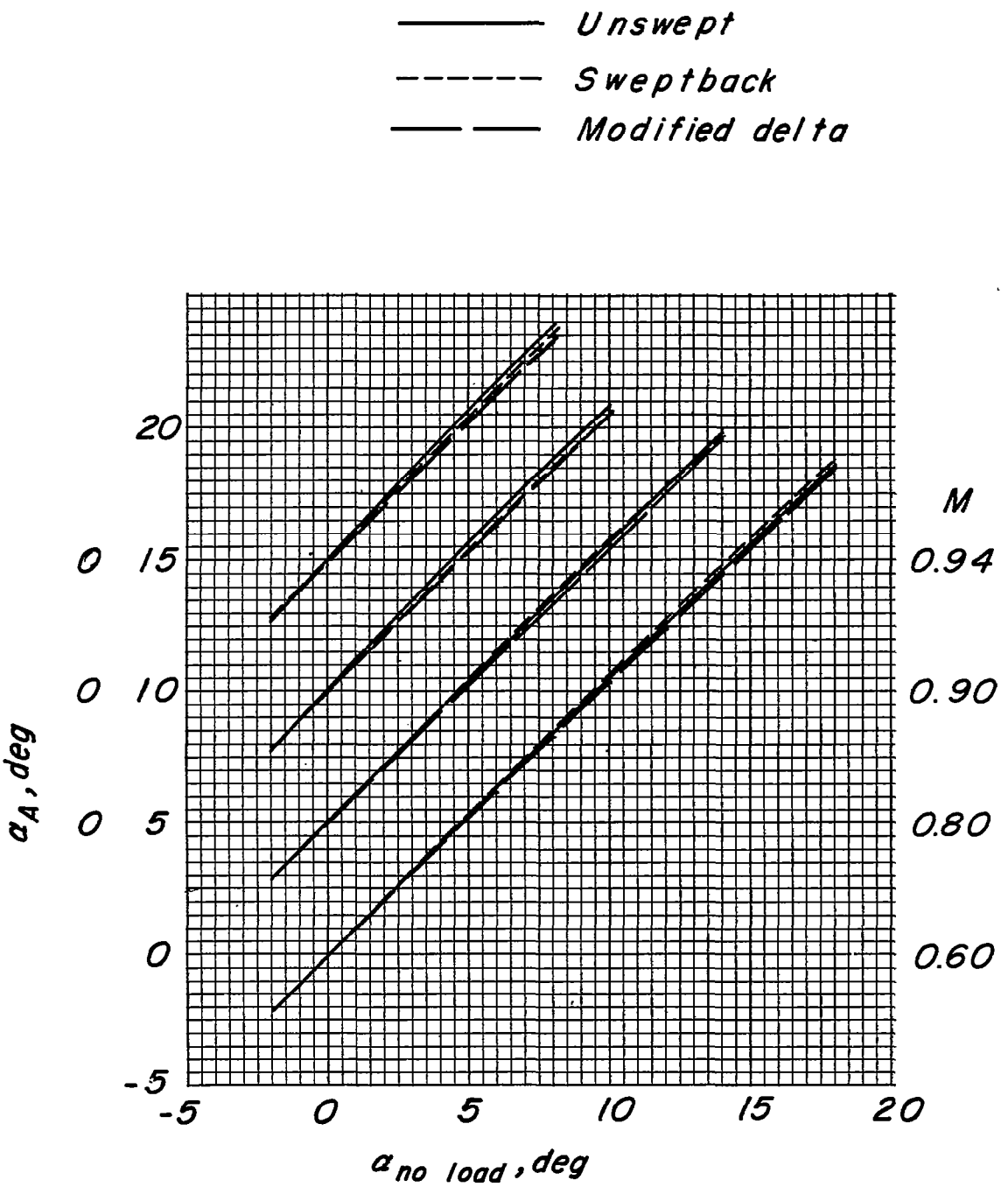

Figure 7.- Variation of corrected angle of attack with reference angle of attack for the wing-fuselage combinations.

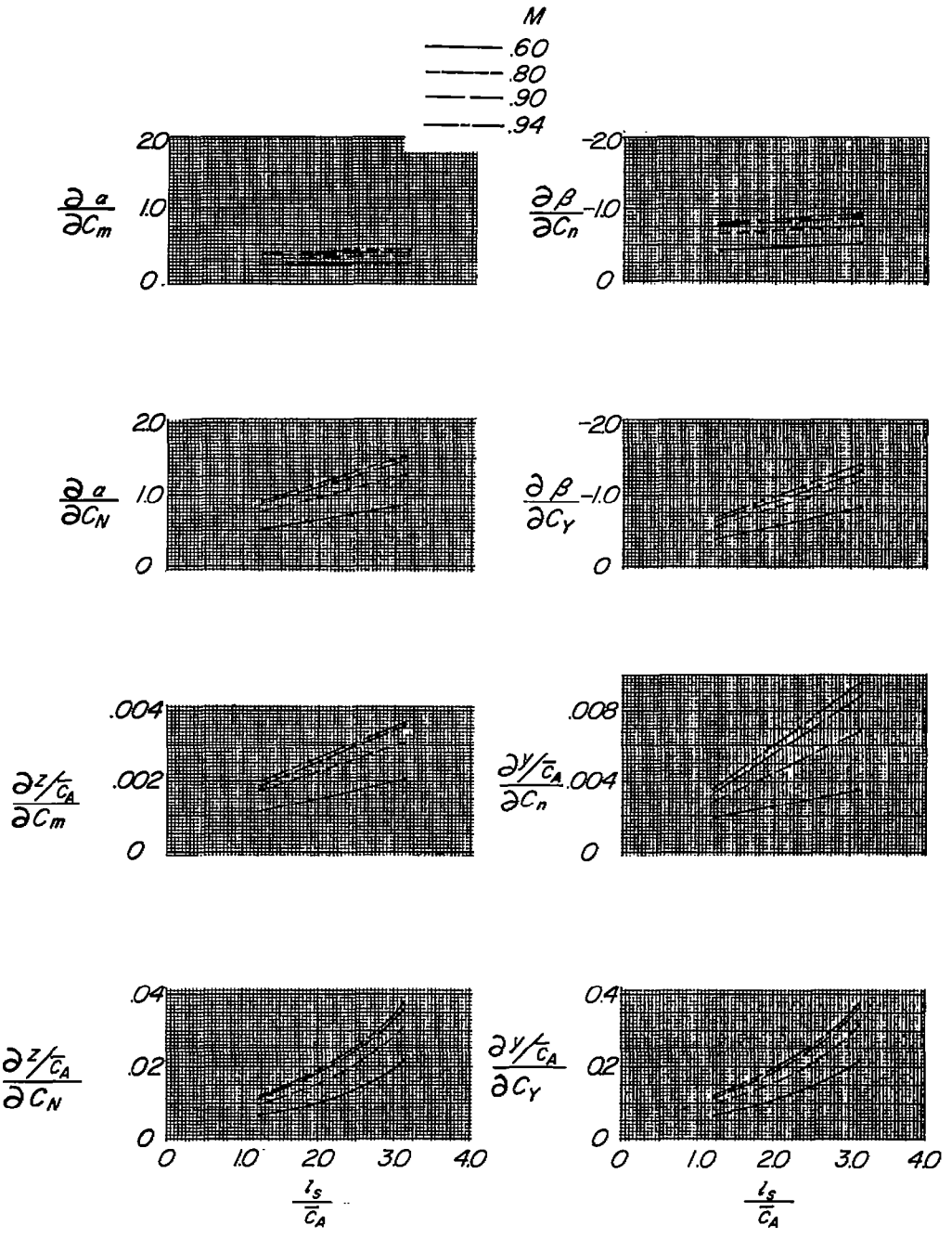

Figure 8.- Deflection characteristics of the sting-balance combination, (angular deflections in degrees) based on mean aerodynamic chord of the swept wing.

[redacted]

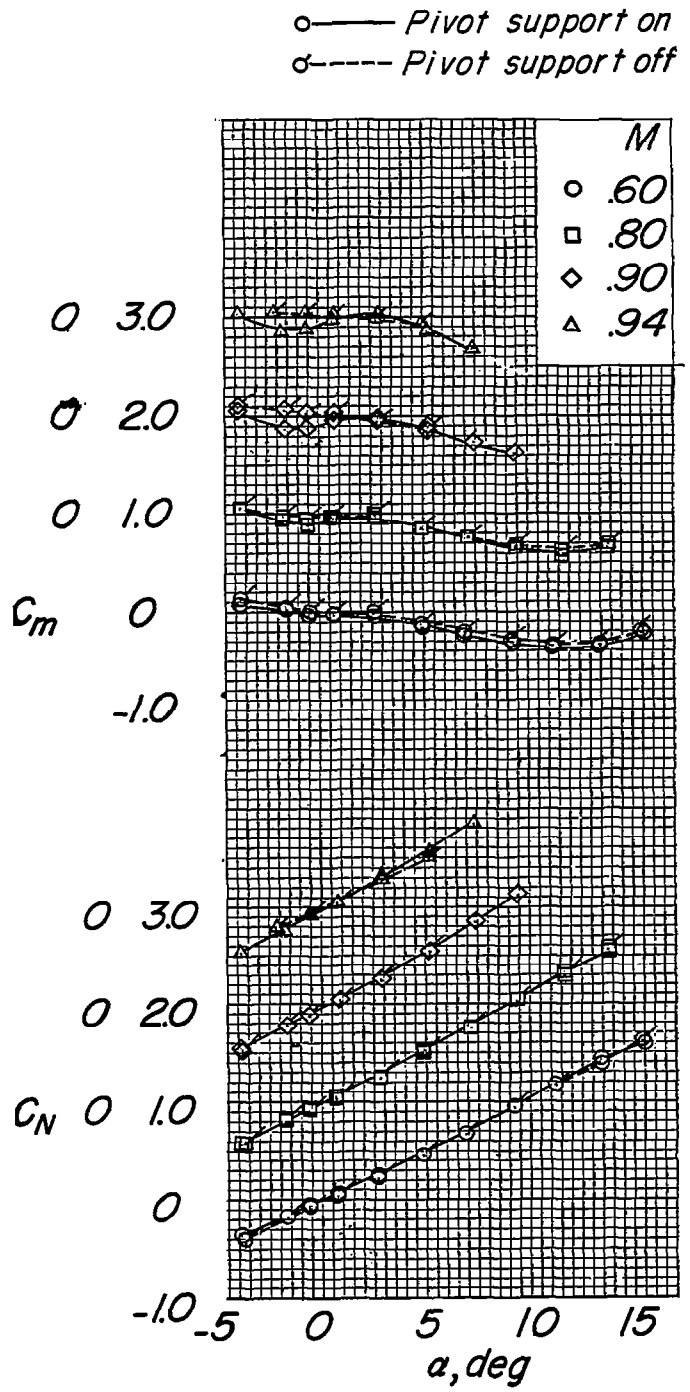

Figure 9.- Aerodynamic forces and moments of the isolated missile.

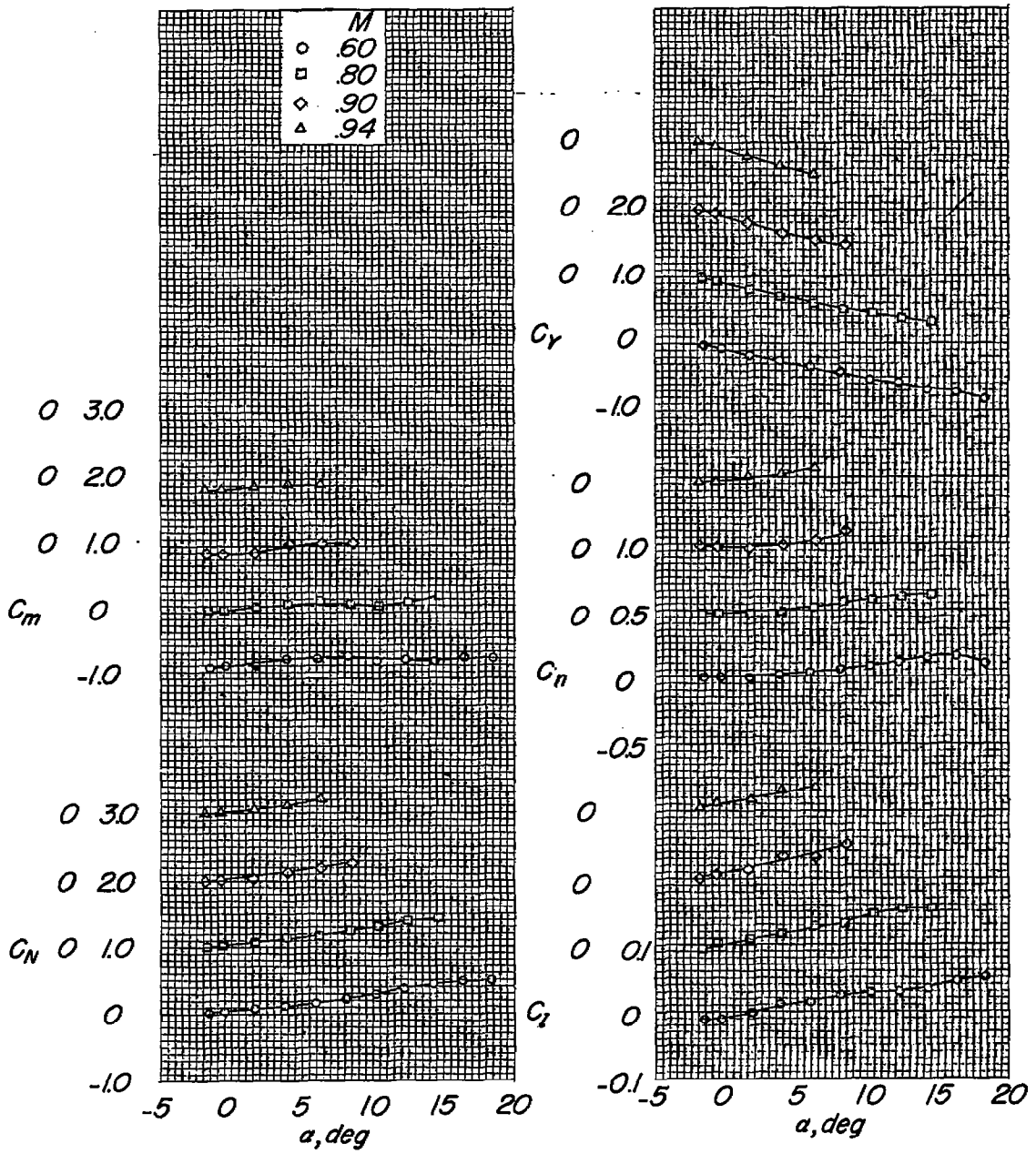

(a) x/c = 0.29.

Figure 10.- Missile aerodynamic forces and moments in the presence of the unswept-wing—fuselage—pylon combination at various Mach numbers. $z/\bar{c}_A$ = -0.13; $y/\frac{b}{2}$ = -0.50.

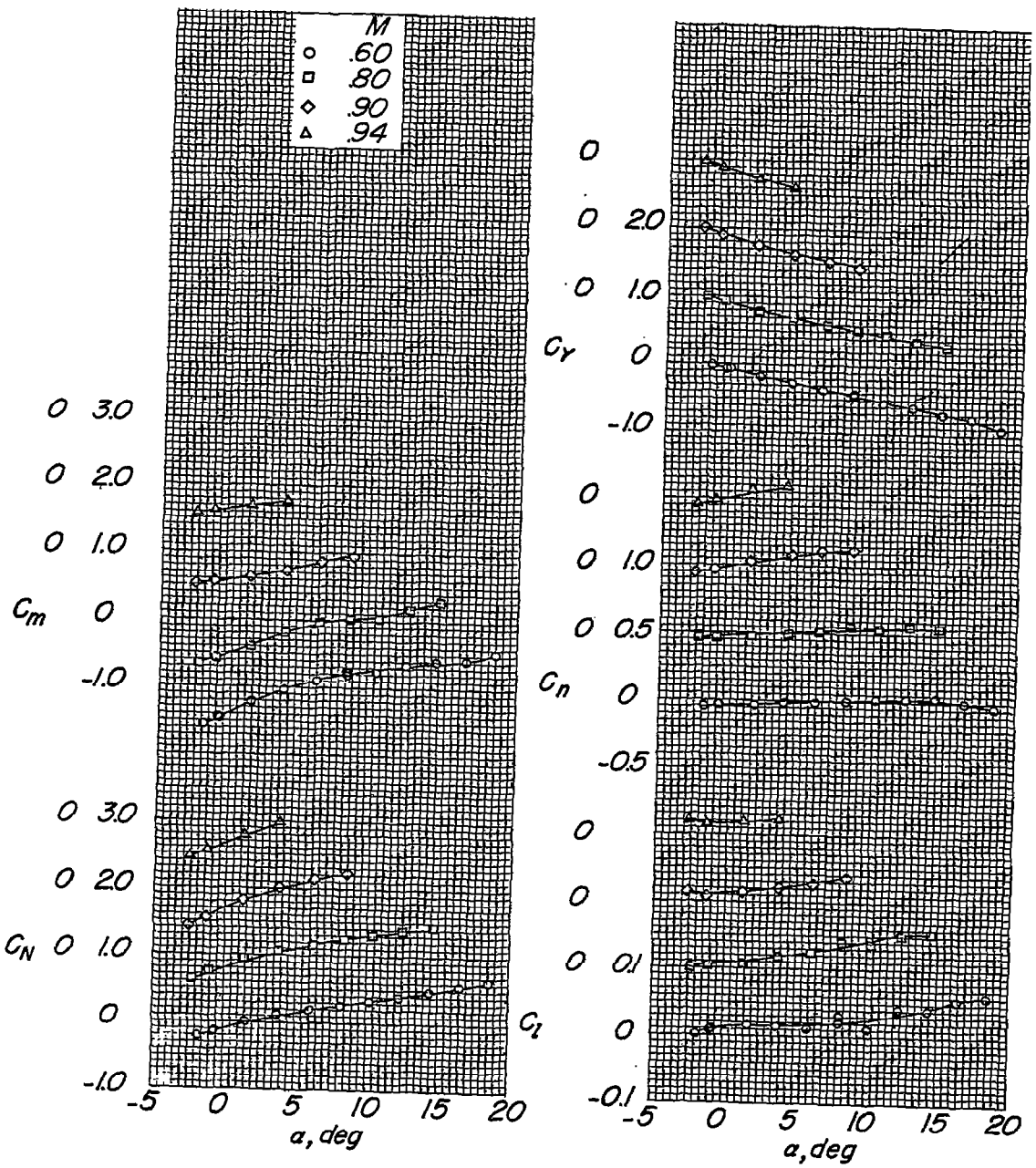

(b) x/c = 0.13.

Figure 10.- Continued.

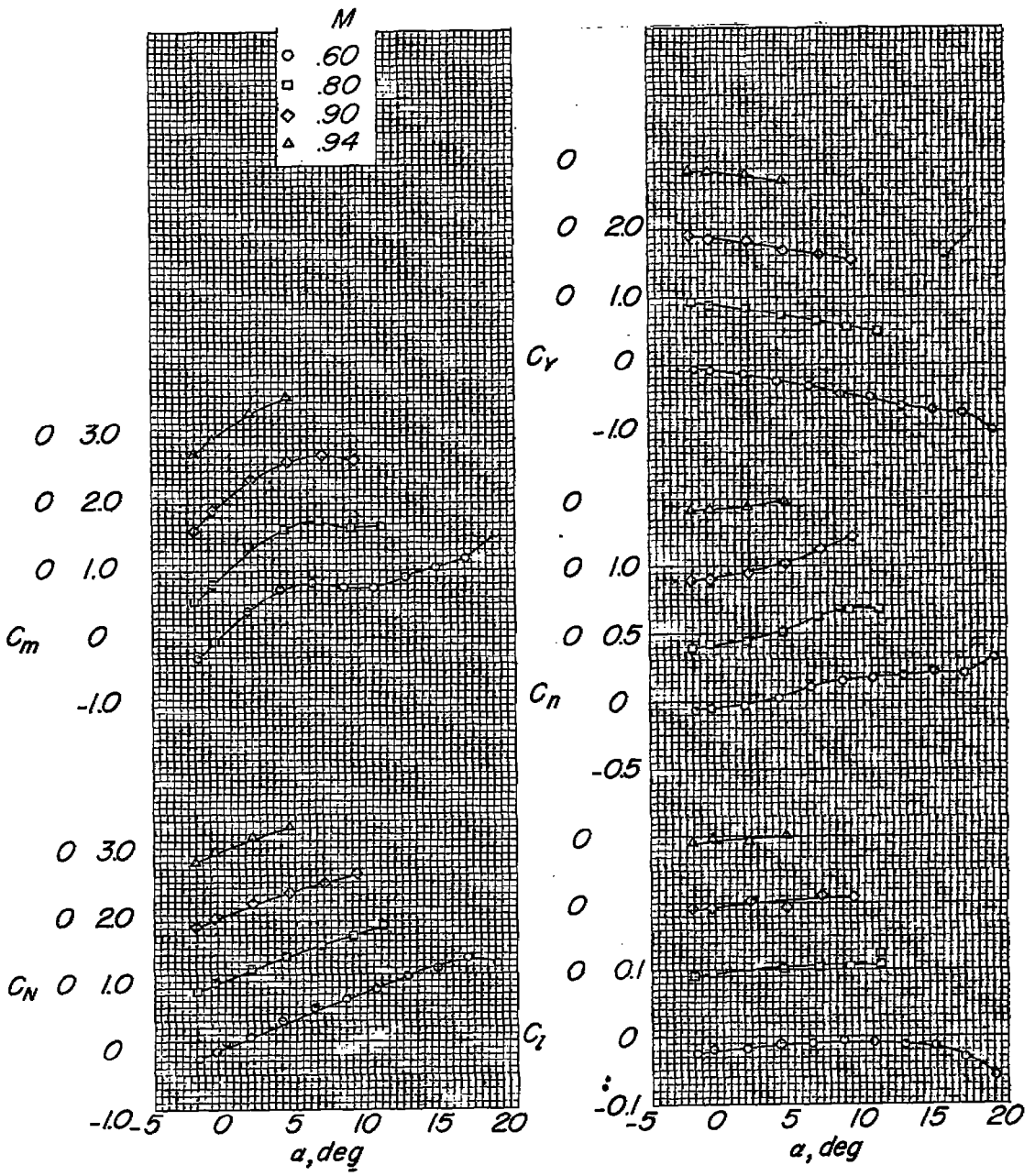

(c) x/c = -0.10.

Figure 10.- Continued.

[redacted]

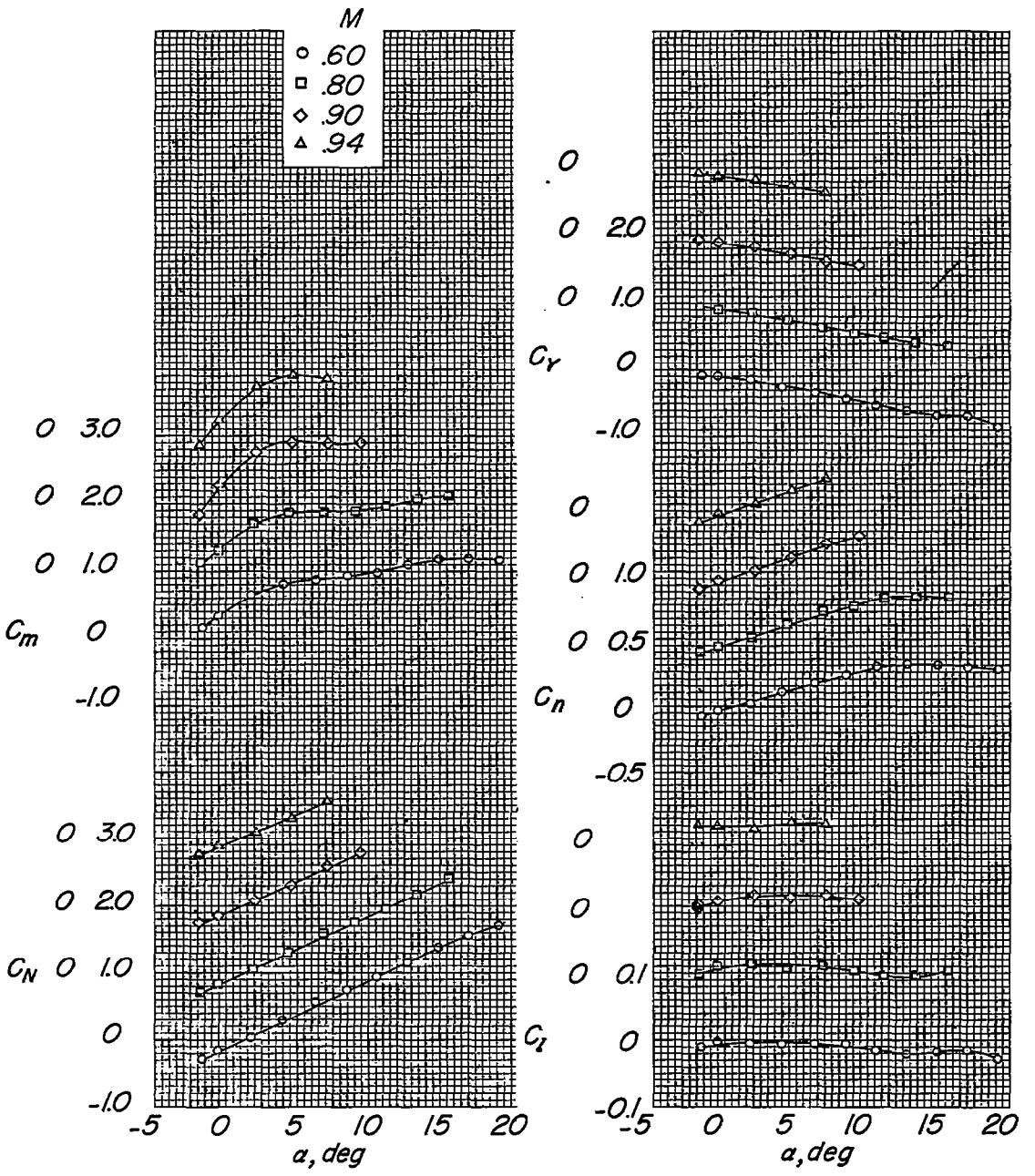

(d) x/c = -0.25.

Figure 10.- Continued.

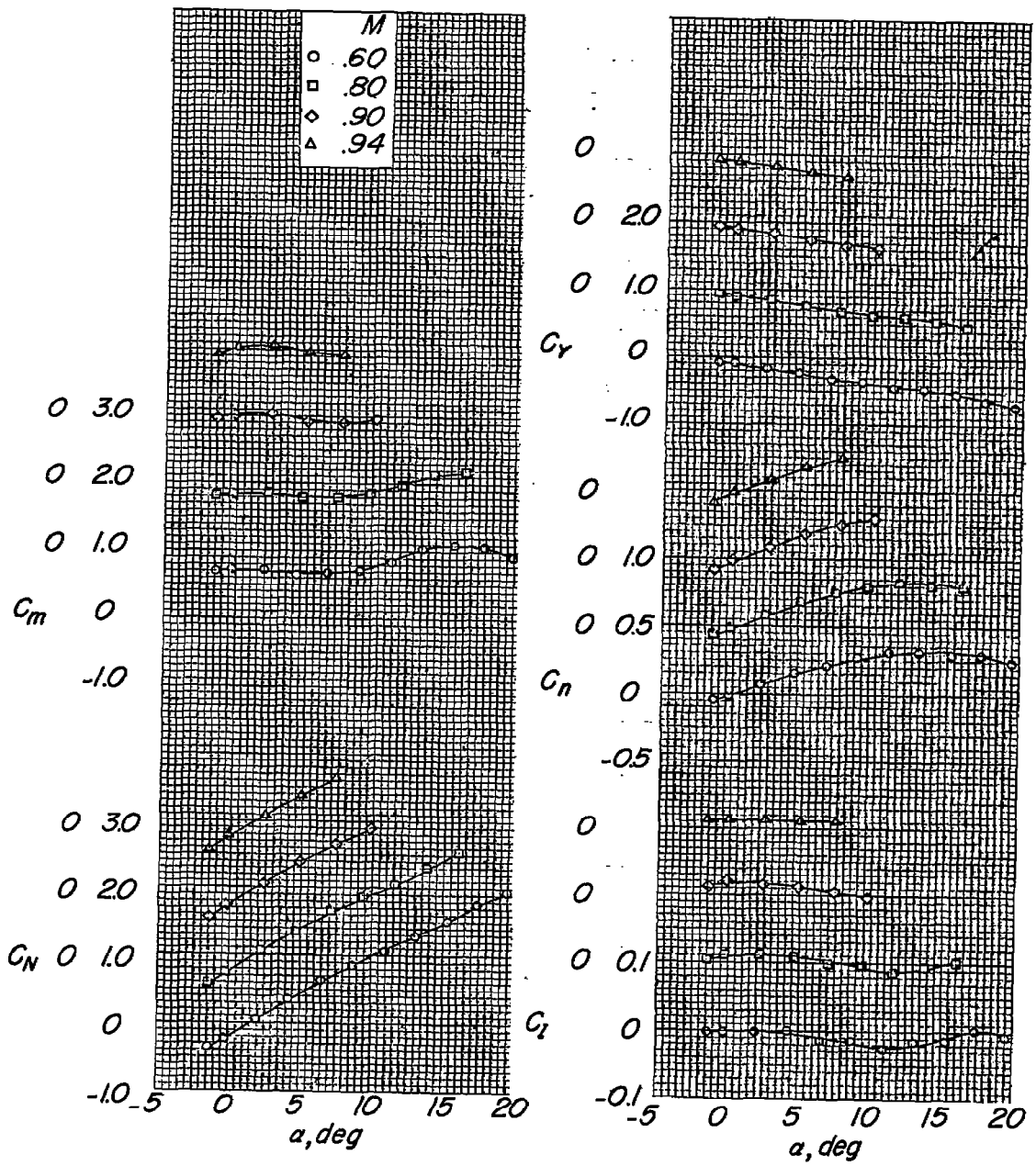

(e) x/c = -0.44.

Figure 10.- Continued.

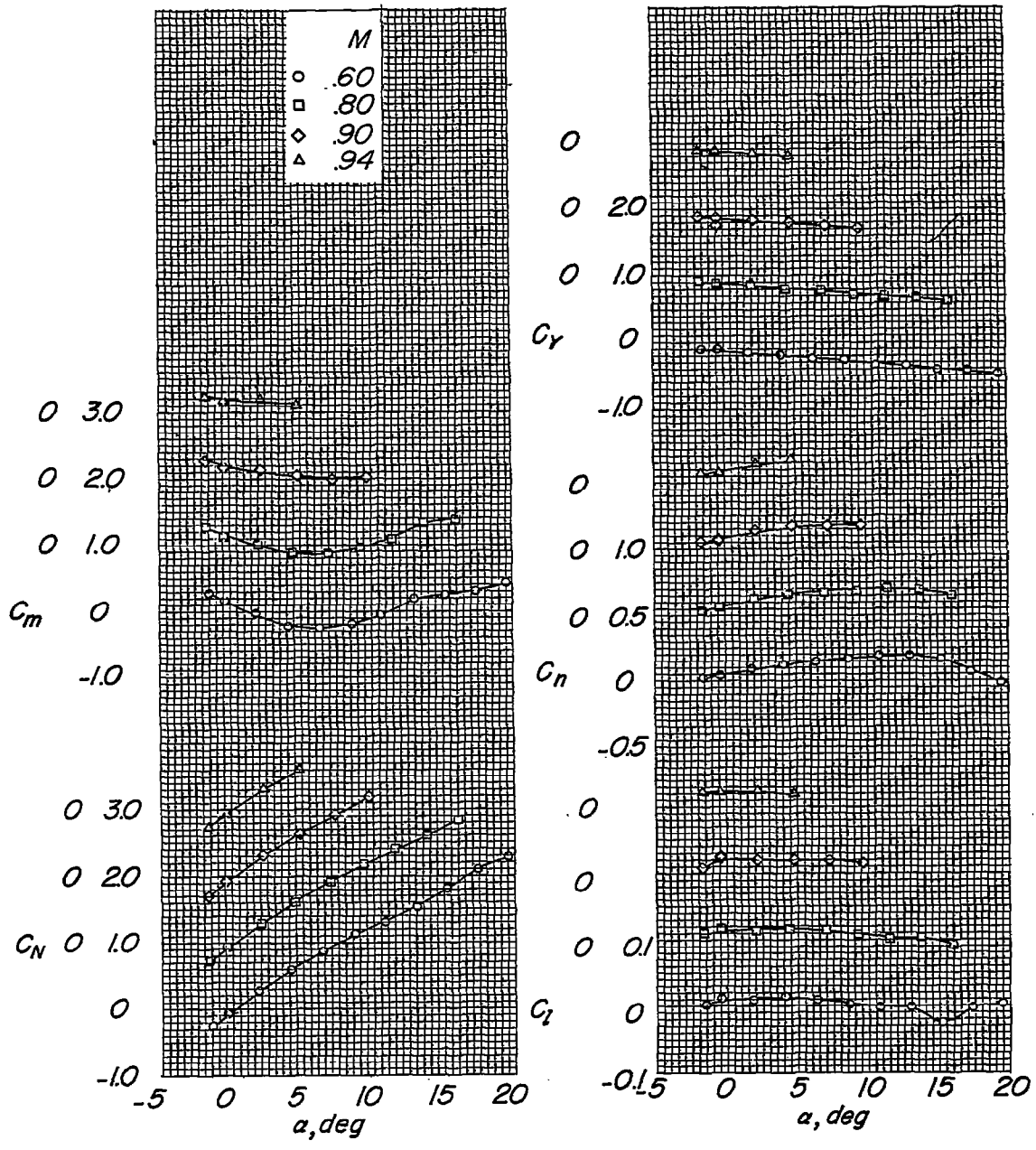

(f) x/c = -0.58.

Figure 10.- Continued.

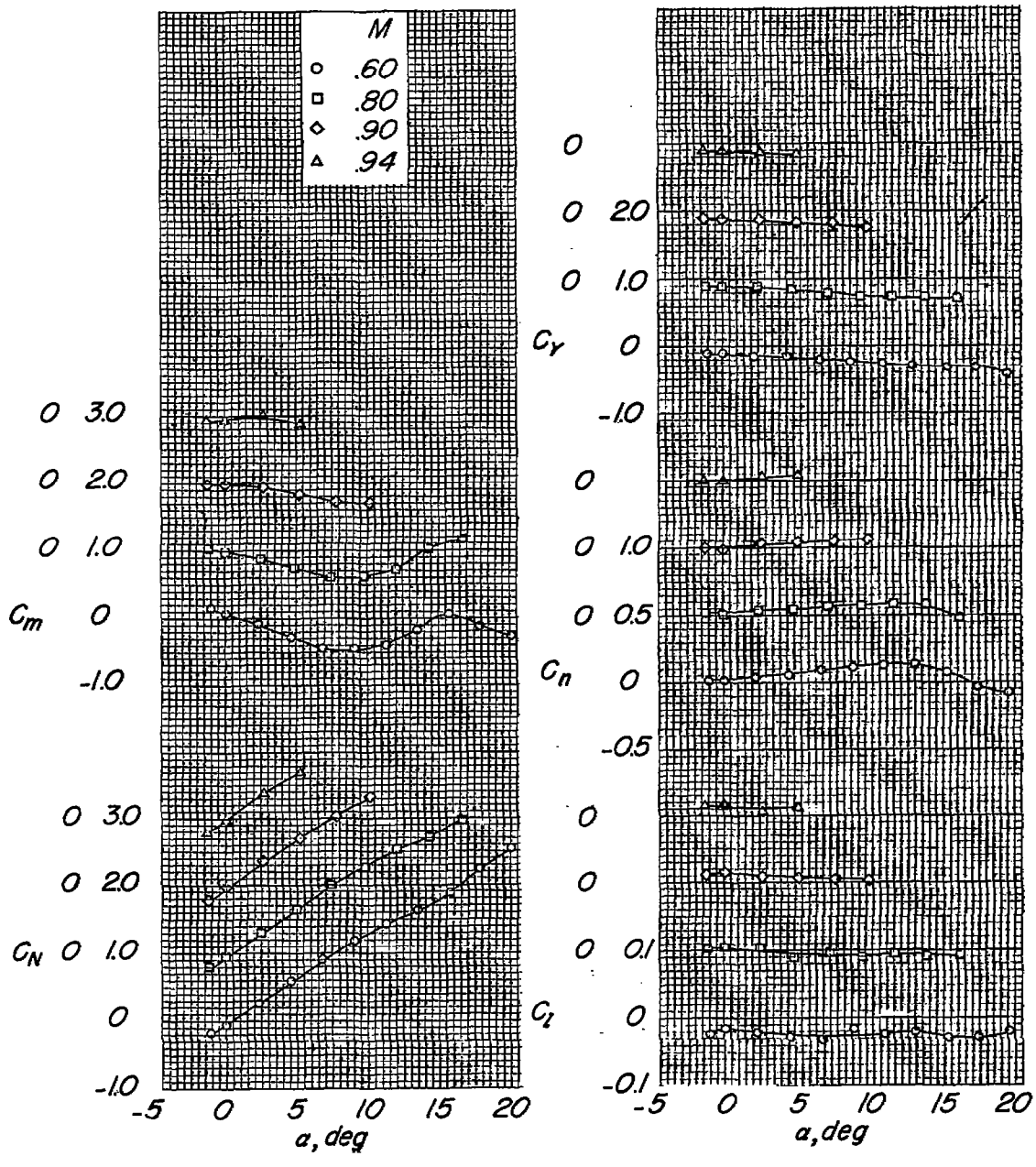

(g) x/c = -0.74.

Figure 10.- Continued.

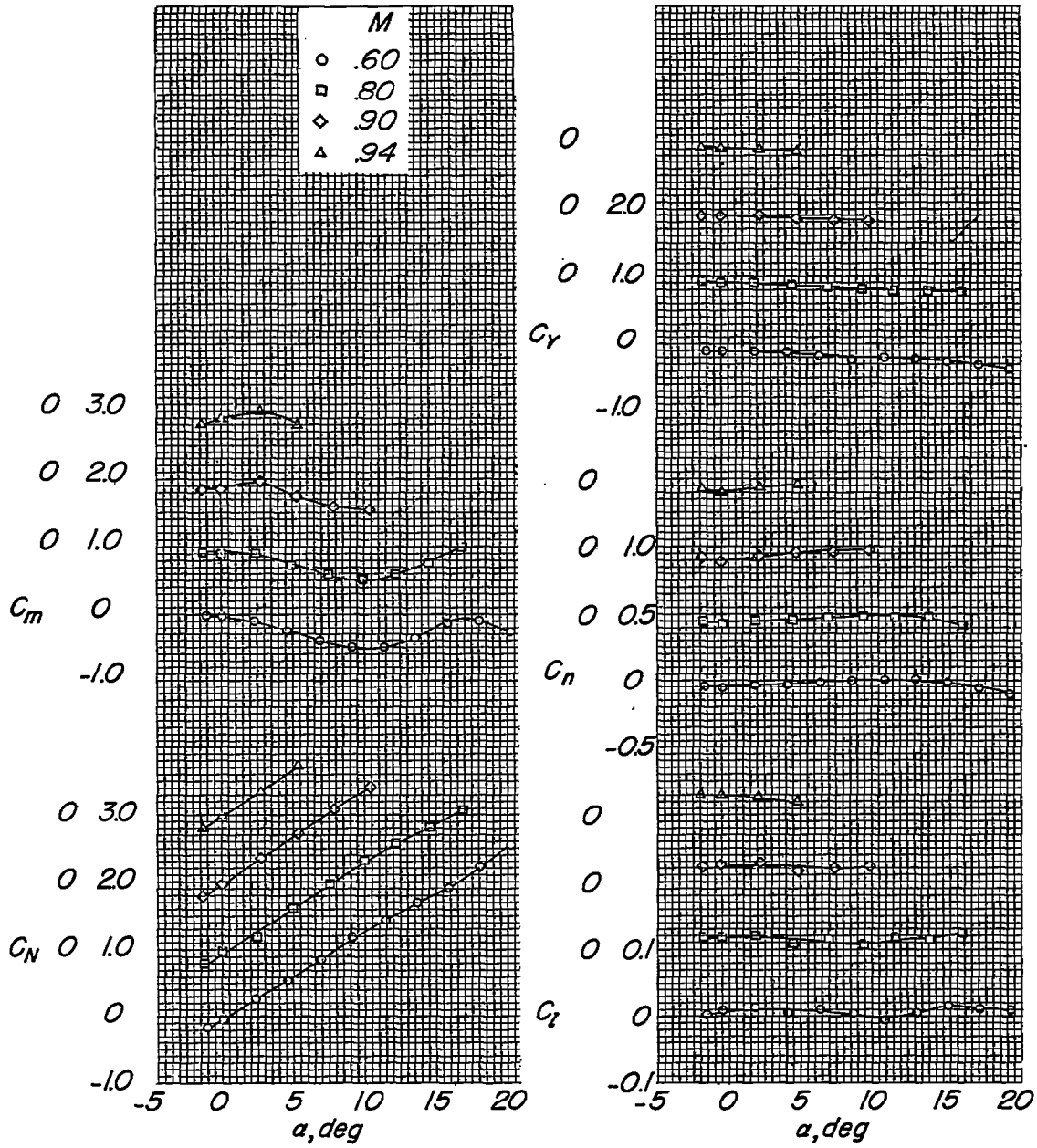

(h) x/c = -1.11.

Figure 10.- Concluded.

[redacted]

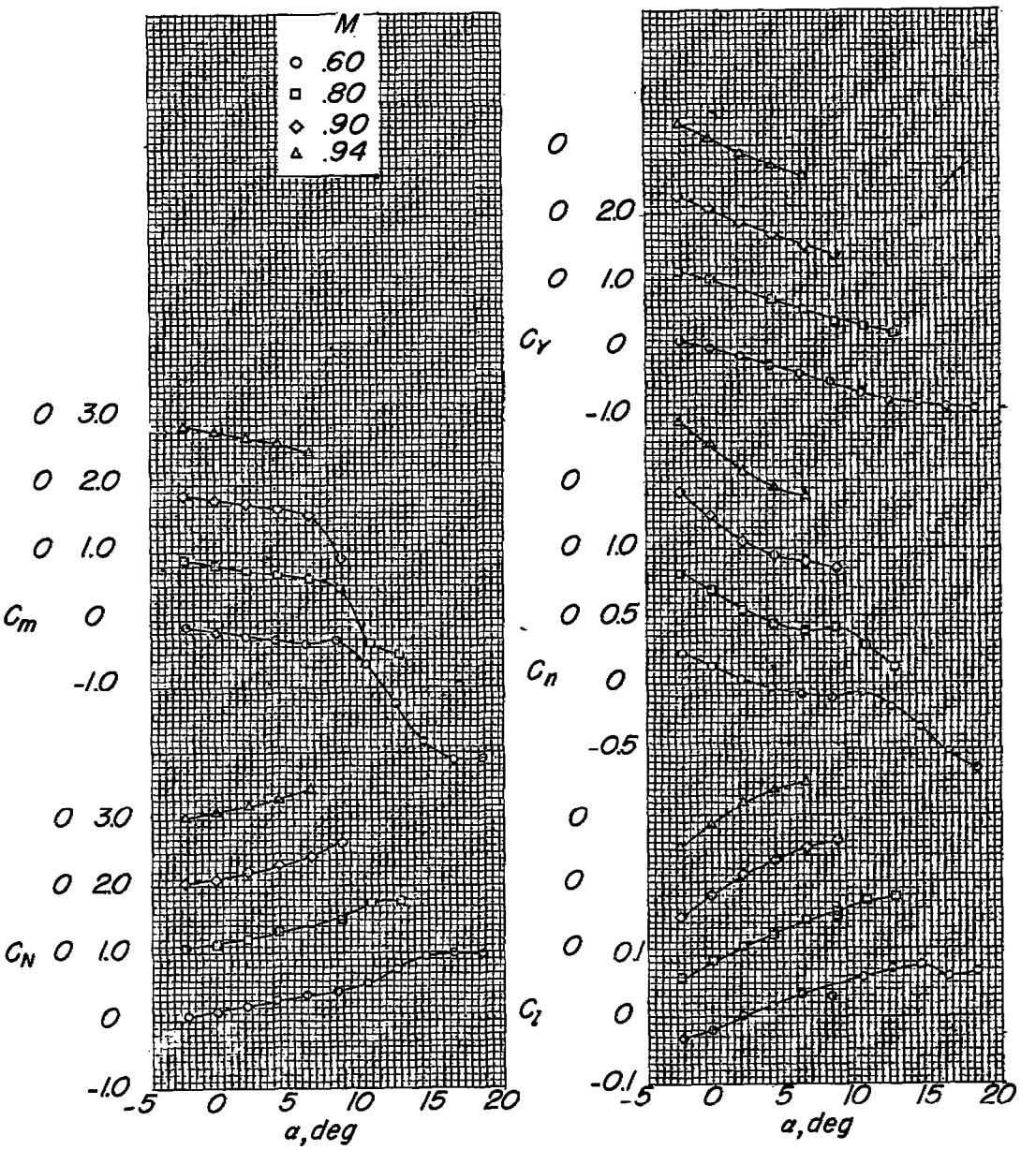

(a) x/c = 0.50.

Figure 11.- Missile aerodynamic forces and moments in the presence of the swept-wing—fuselage—pylon combination for various Mach numbers and chordwise locations. $z/\bar{c}_A = -0.15$; $y/\frac{b}{2} = -0.50$.

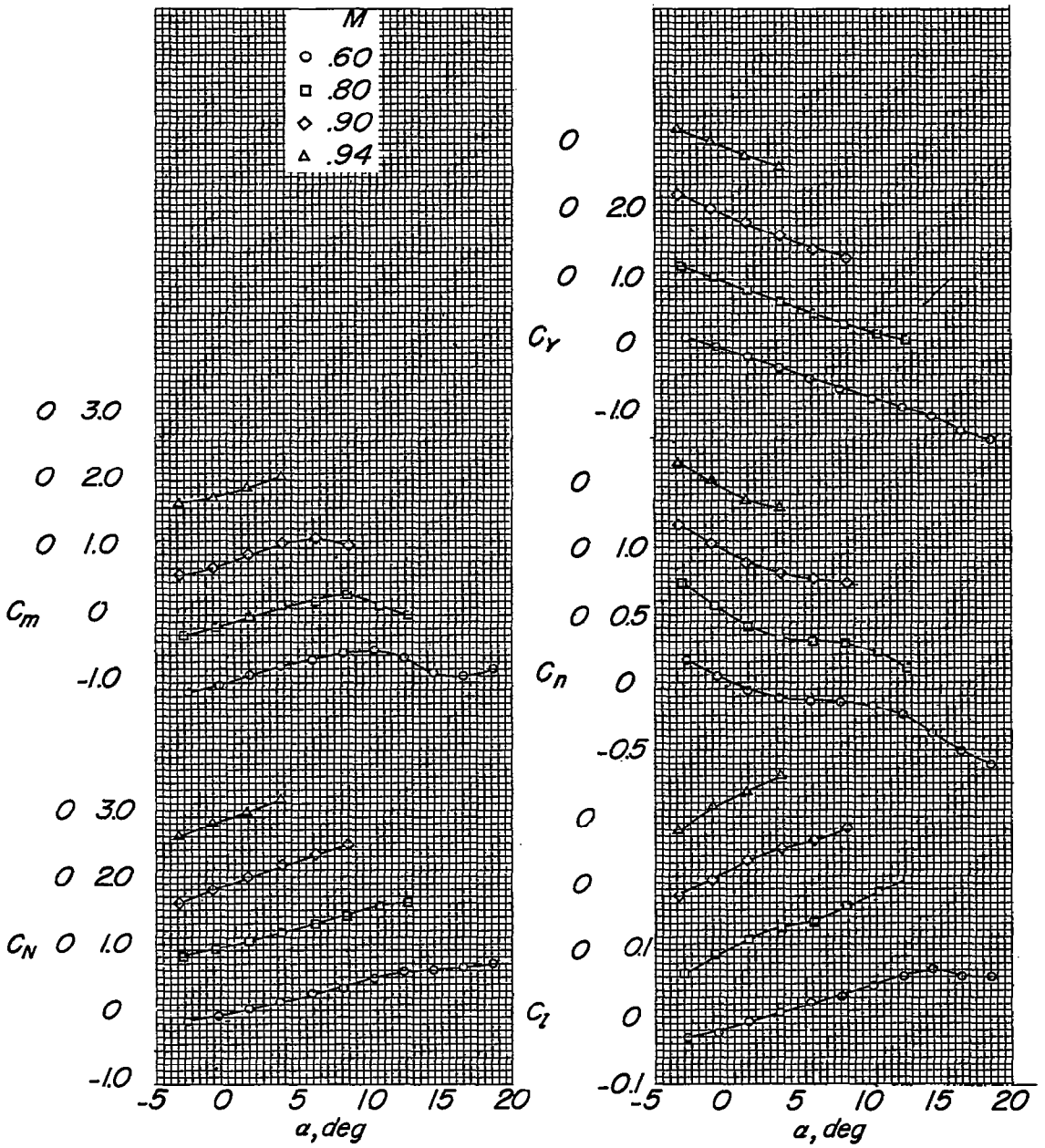

(b) x/c = 0.29.

Figure 11.- Continued.

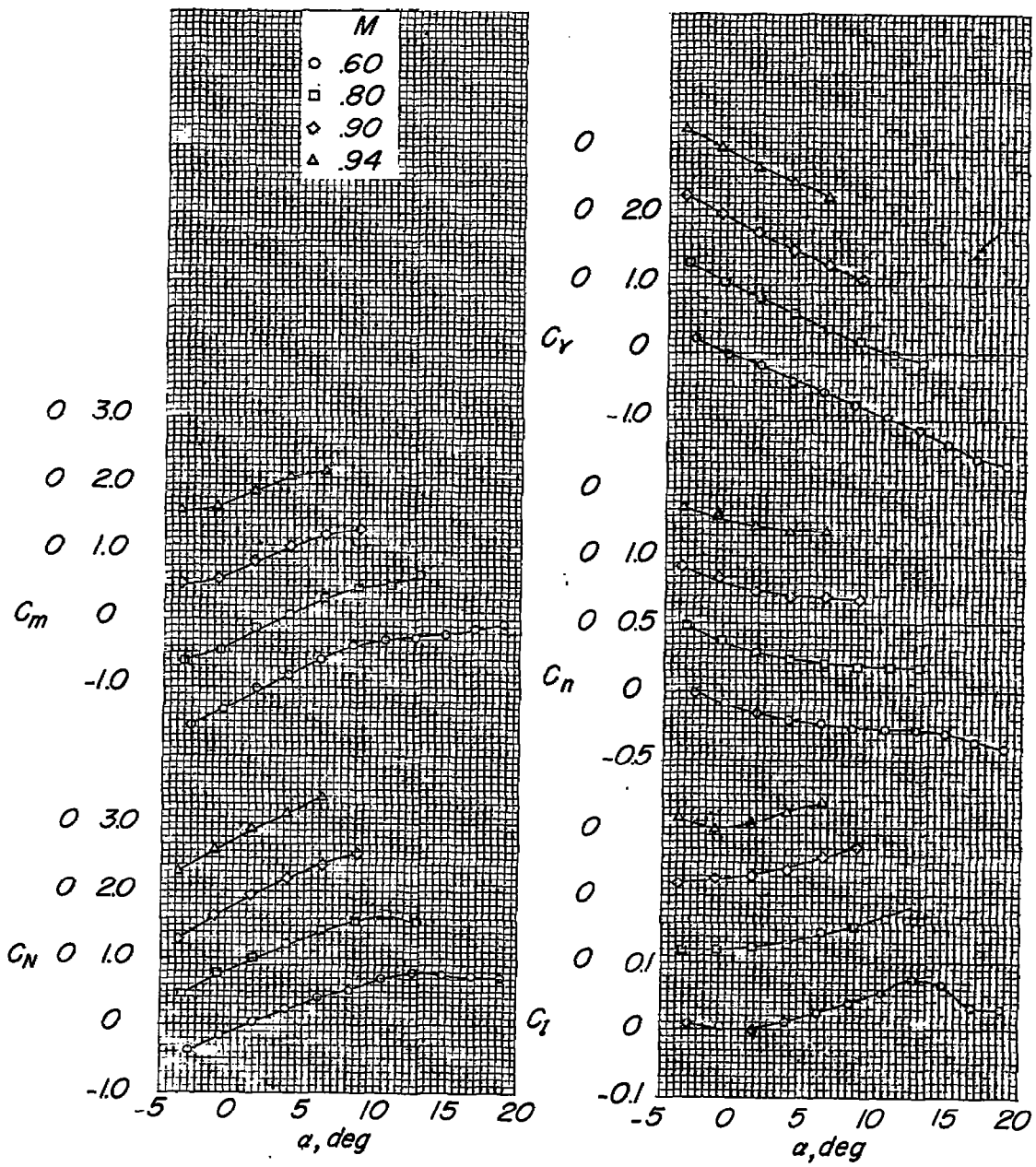

(c) x/c = 0.13.

Figure 11.- Continued.

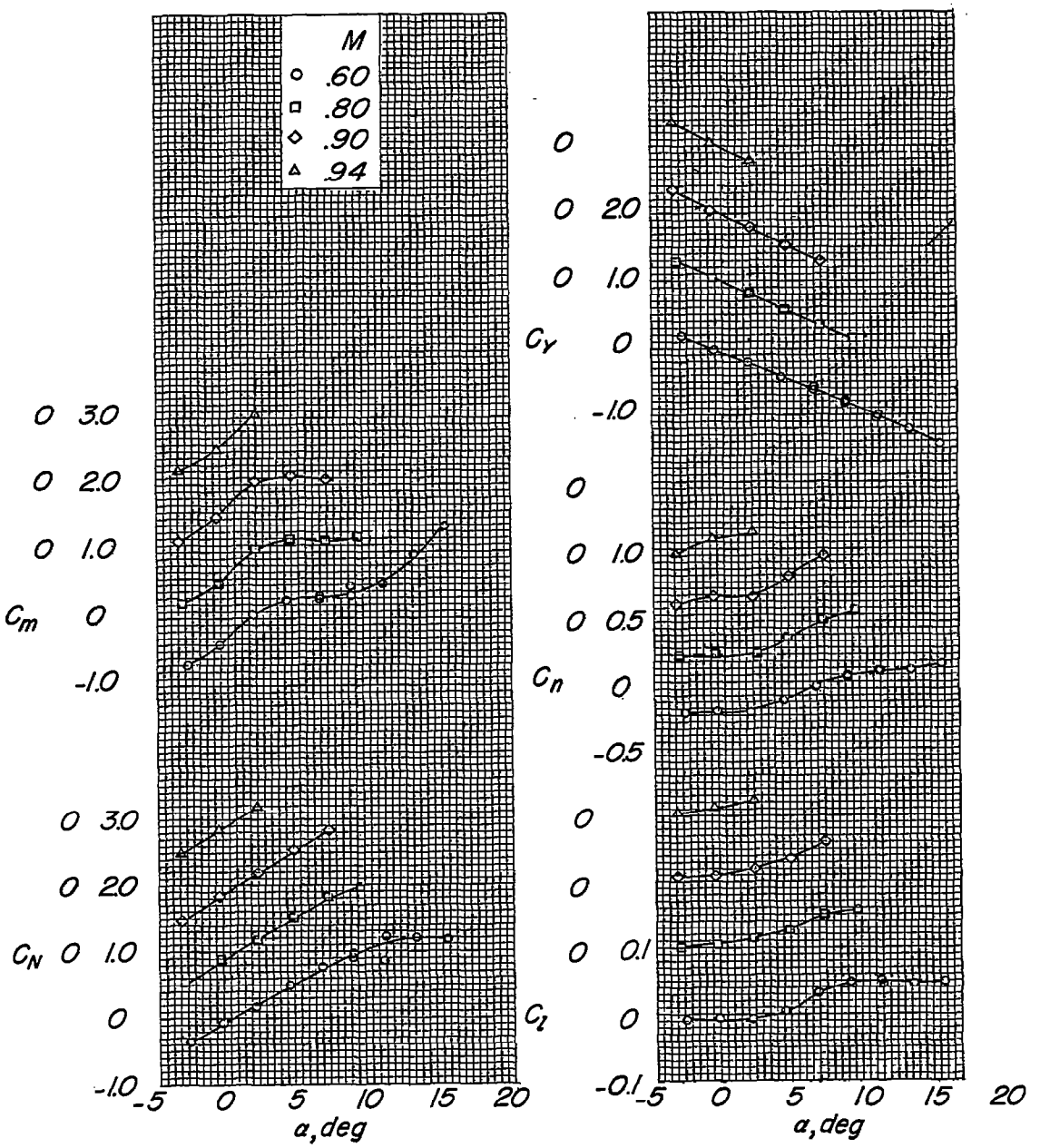

(d) x/c = -0.10.

Figure 11.- Continued.

[redacted]

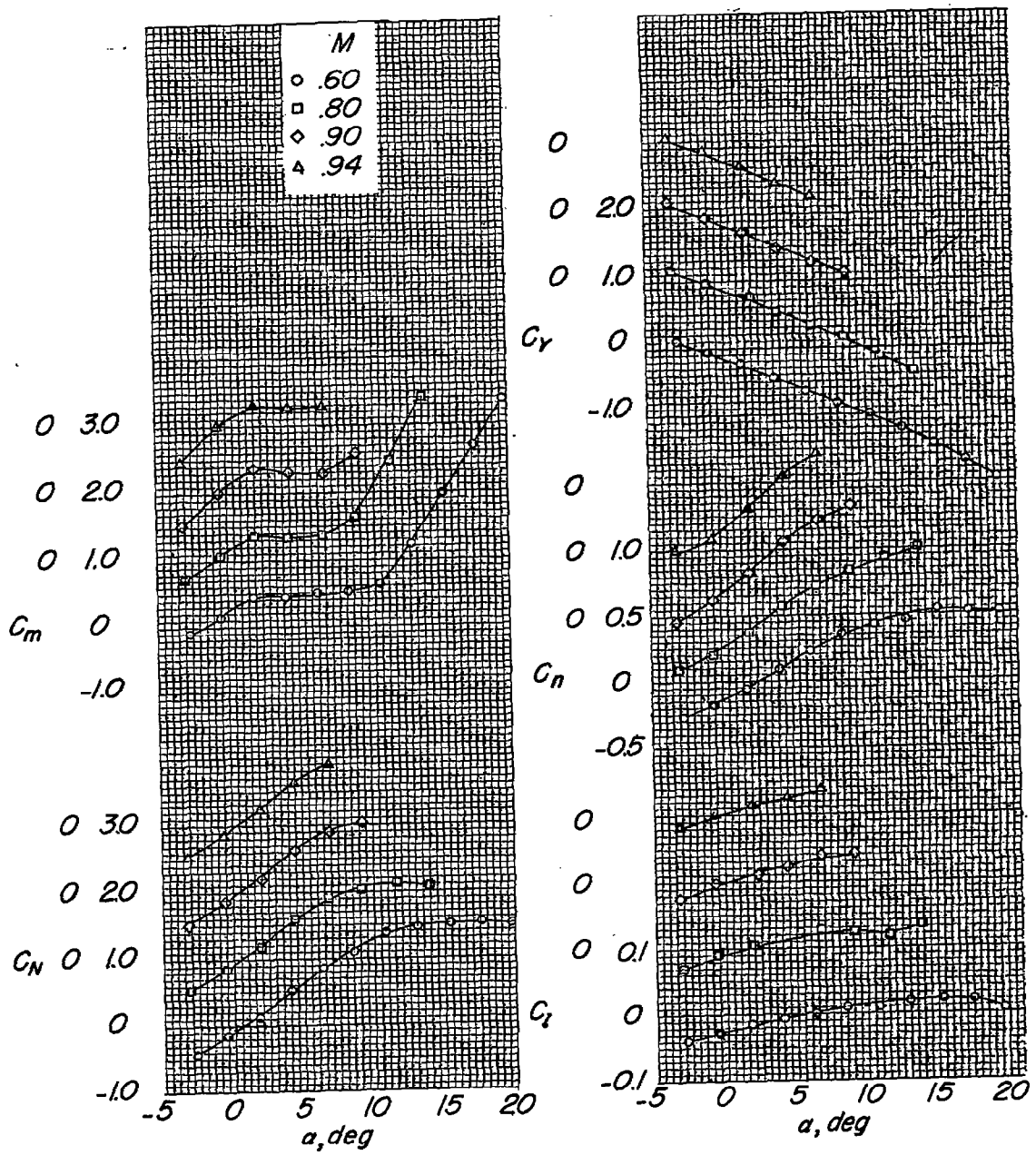

(e) x/c = -0.25.

Figure 11.- Continued.

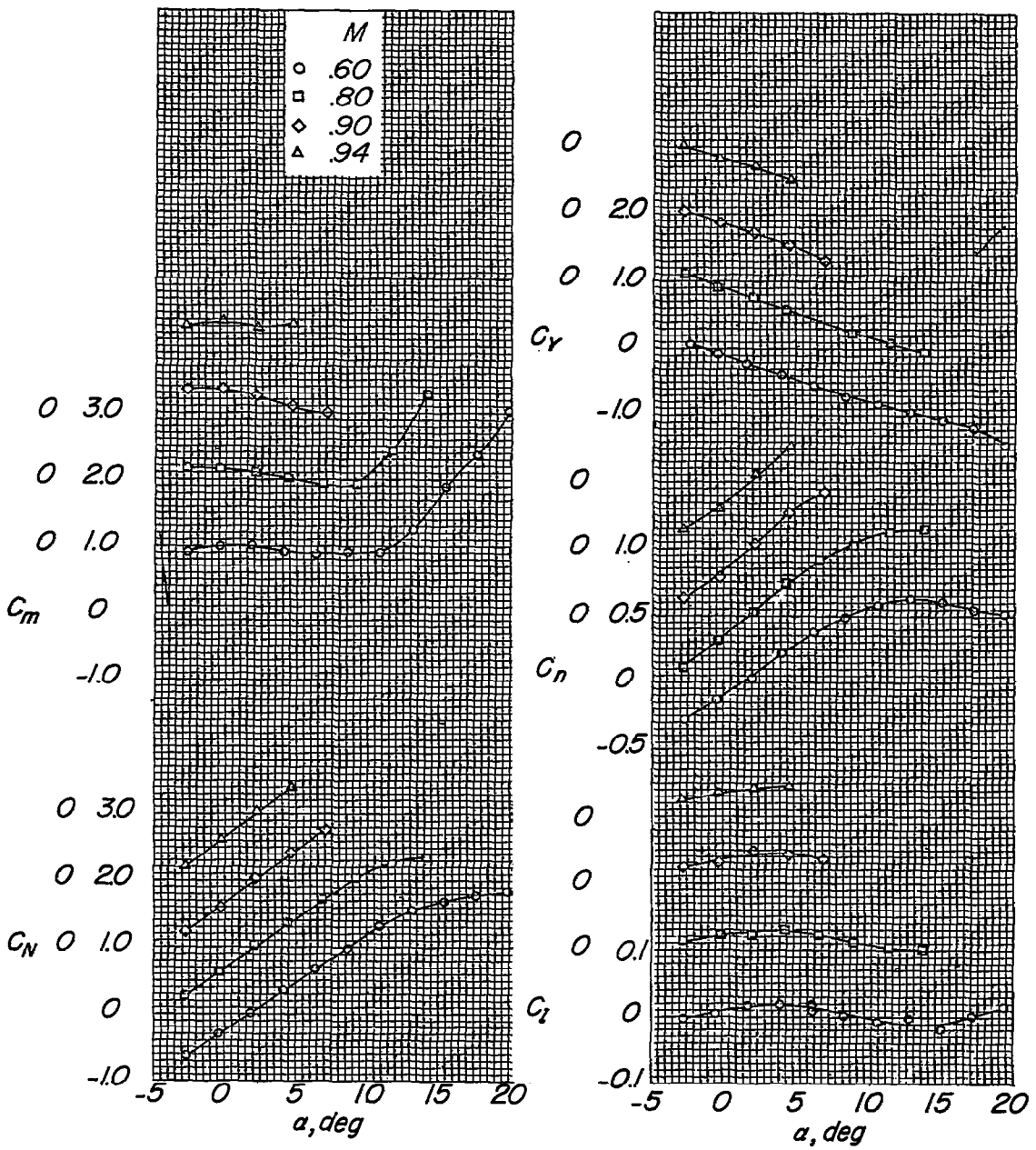

(f) x/c = -0.44.

Figure 11.- Continued.

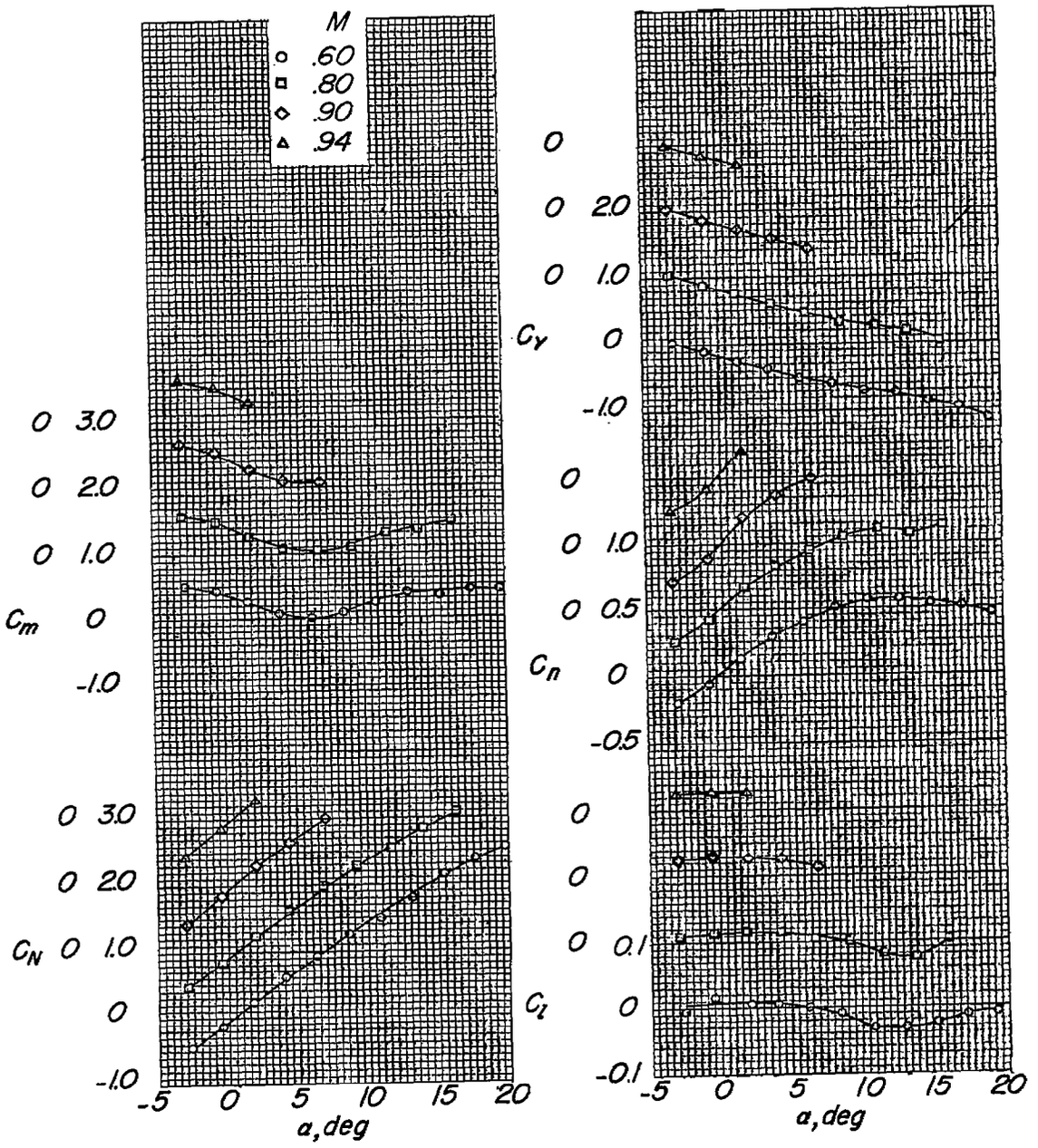

(g) x/c = -0.58.

Figure 11.- Continued.

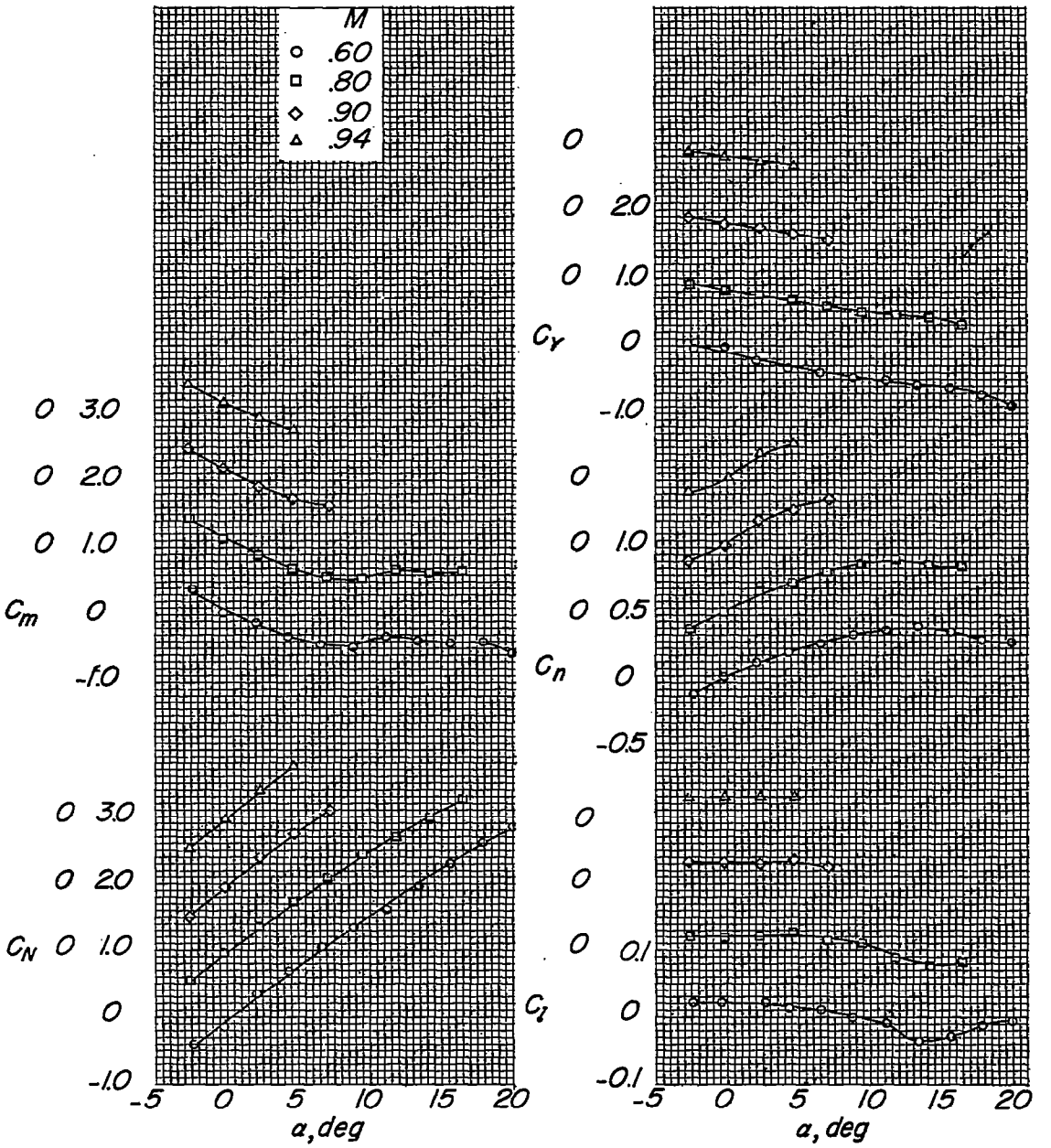

(h) x/c = -0.74.

Figure 11.- Continued.

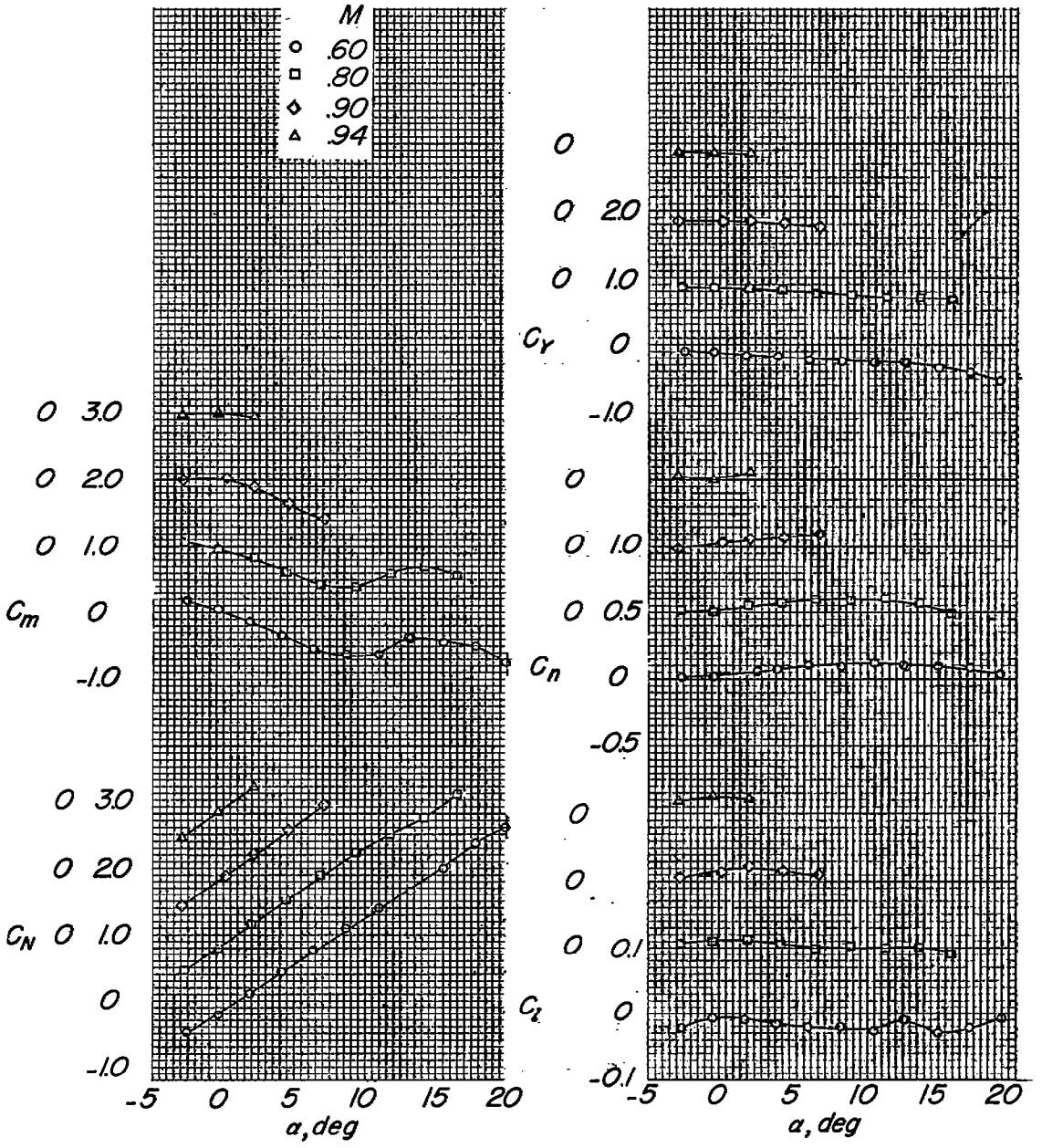

(i) x/c = -1.11.

Figure 11.- Concluded.

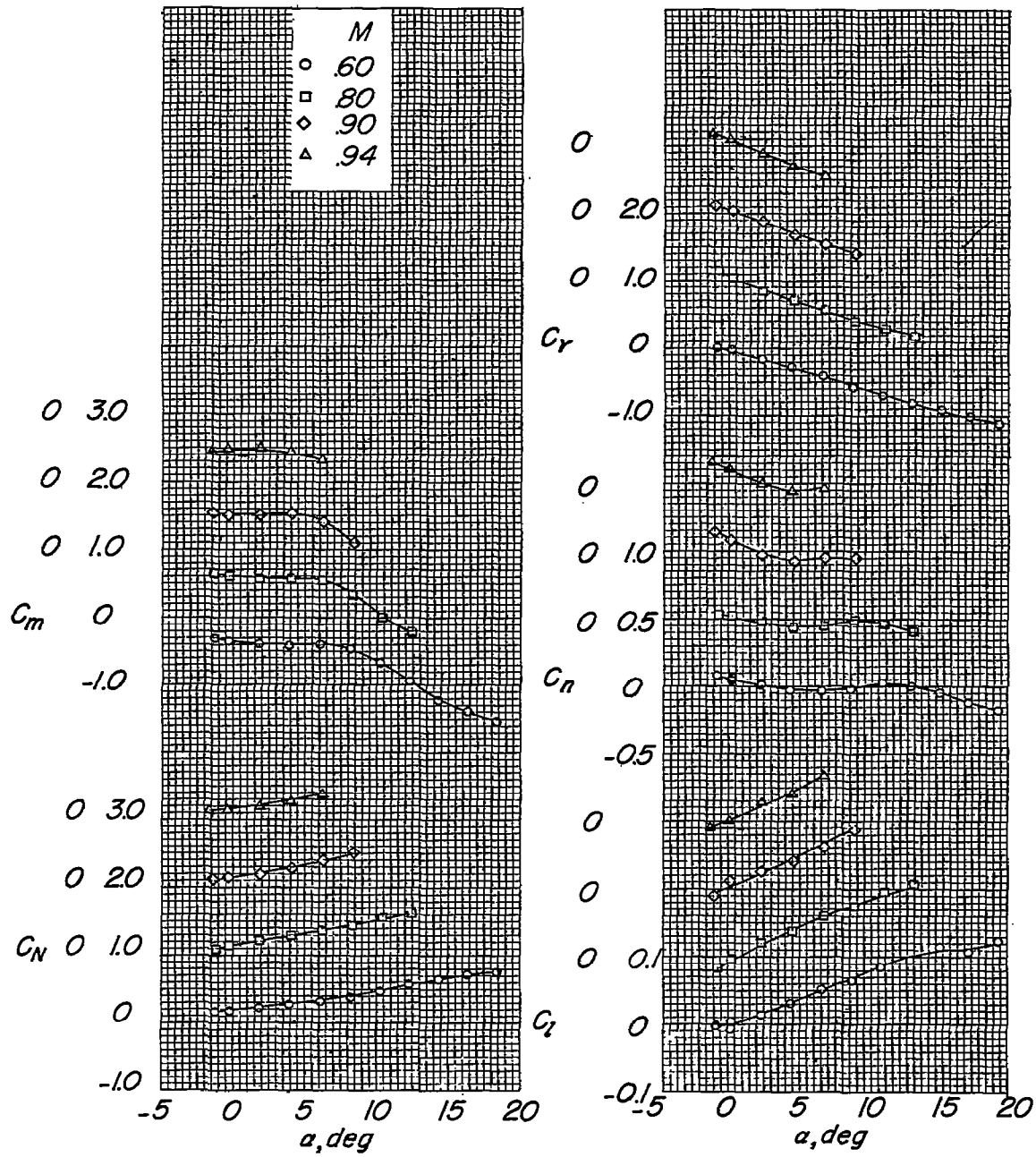

(a) x/c = 0.48

Figure 12.- Missile aerodynamic forces and moments in the presence of the modified-delta-wing—fuselage combination. $z/\bar{c}_A = -0.12$; $y/\frac{b}{2} = -0.50$.

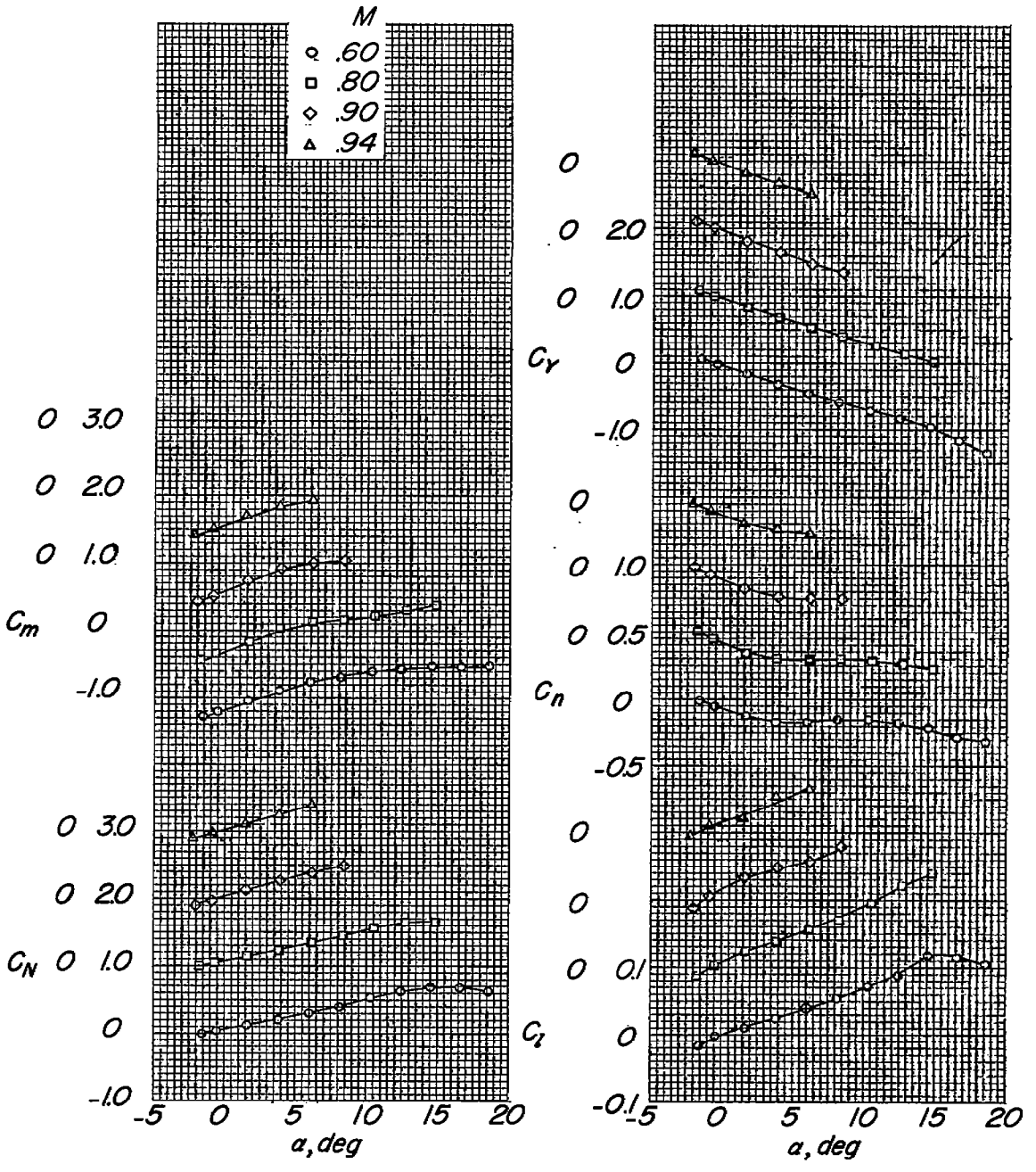

(b) x/c = 0.27.

Figure 12.- Continued.

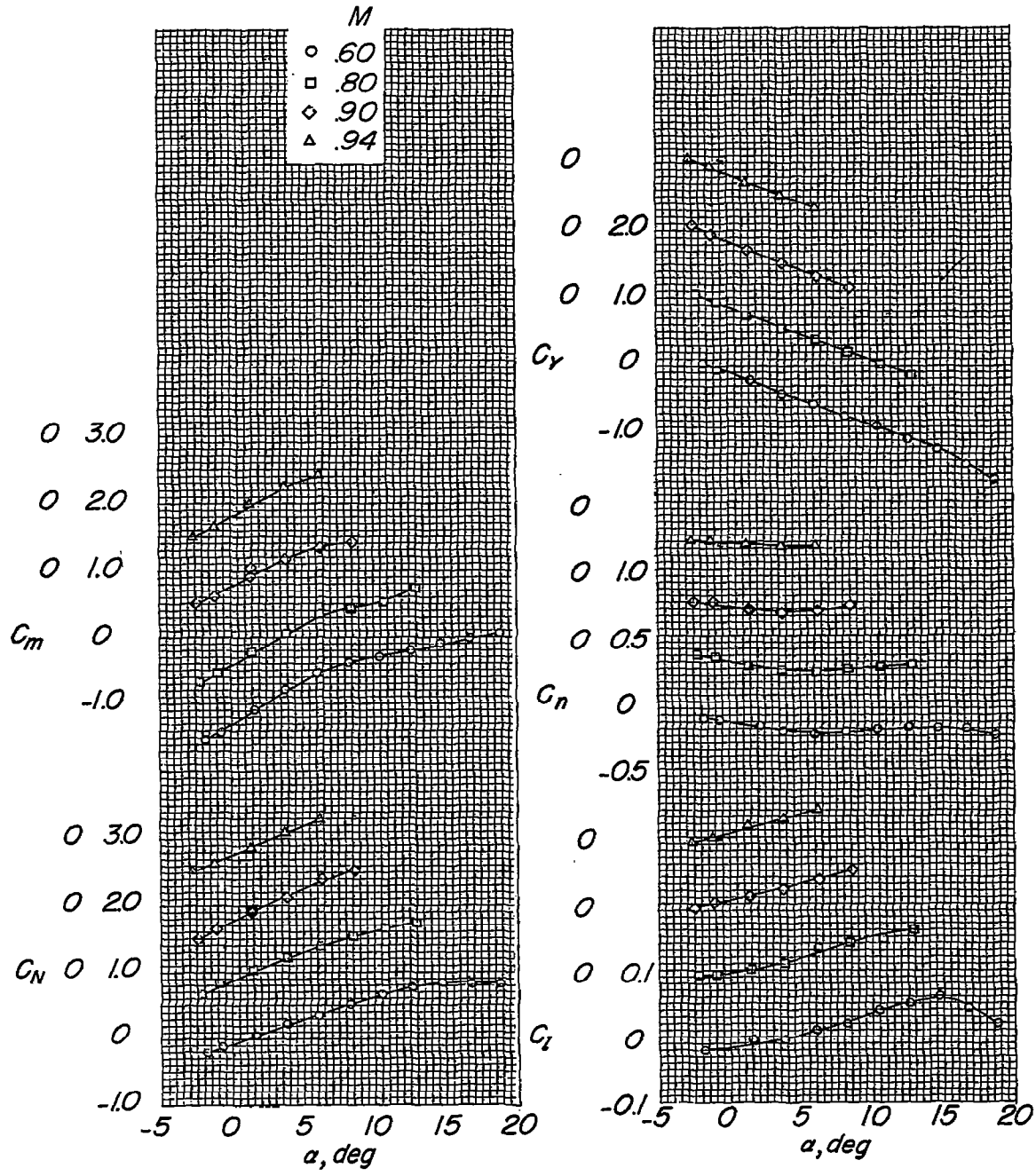

(c) x/c = 0.11.

Figure 12.- Continued.

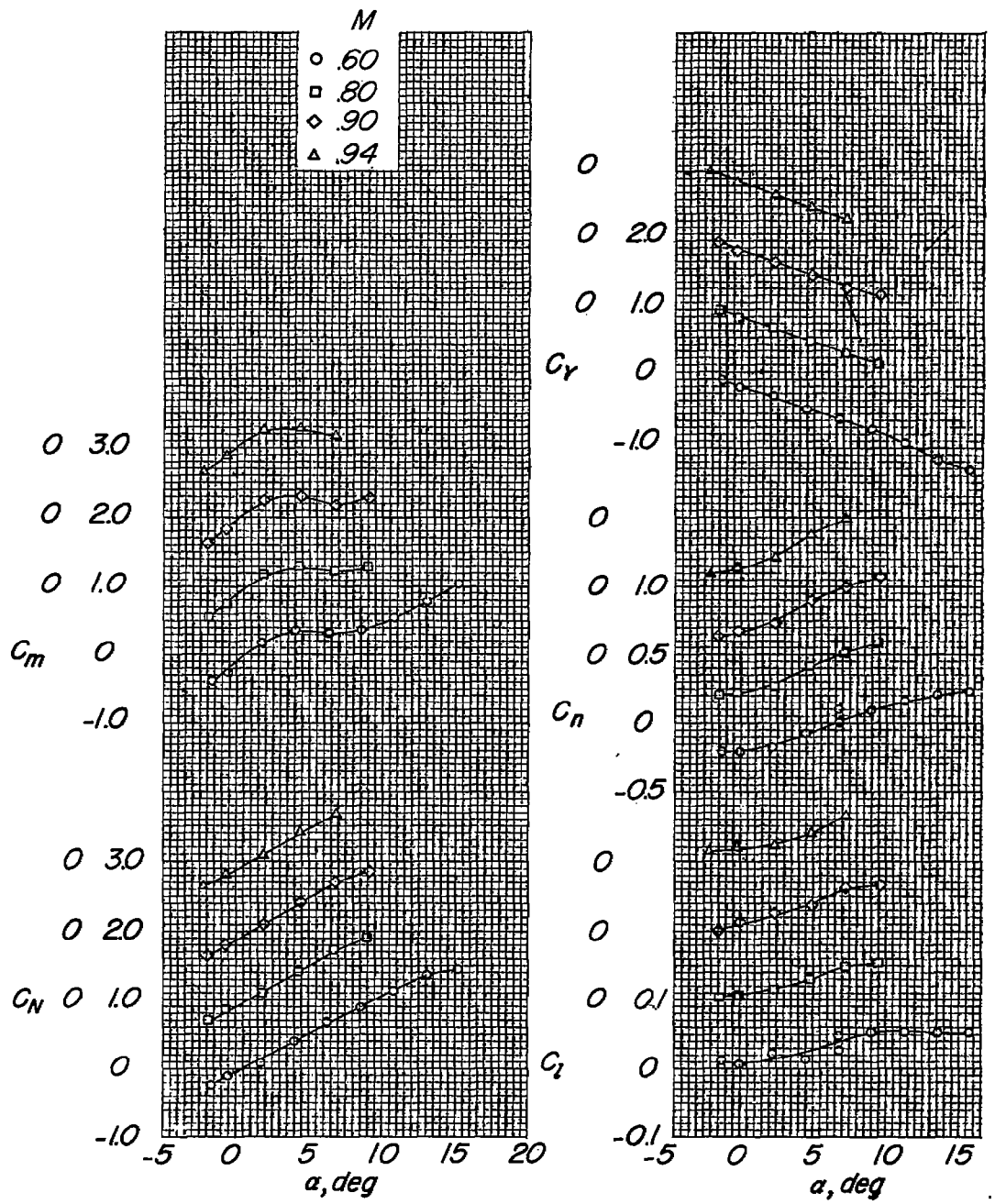

(d) x/c = -0.10.

Figure 12.- Continued.

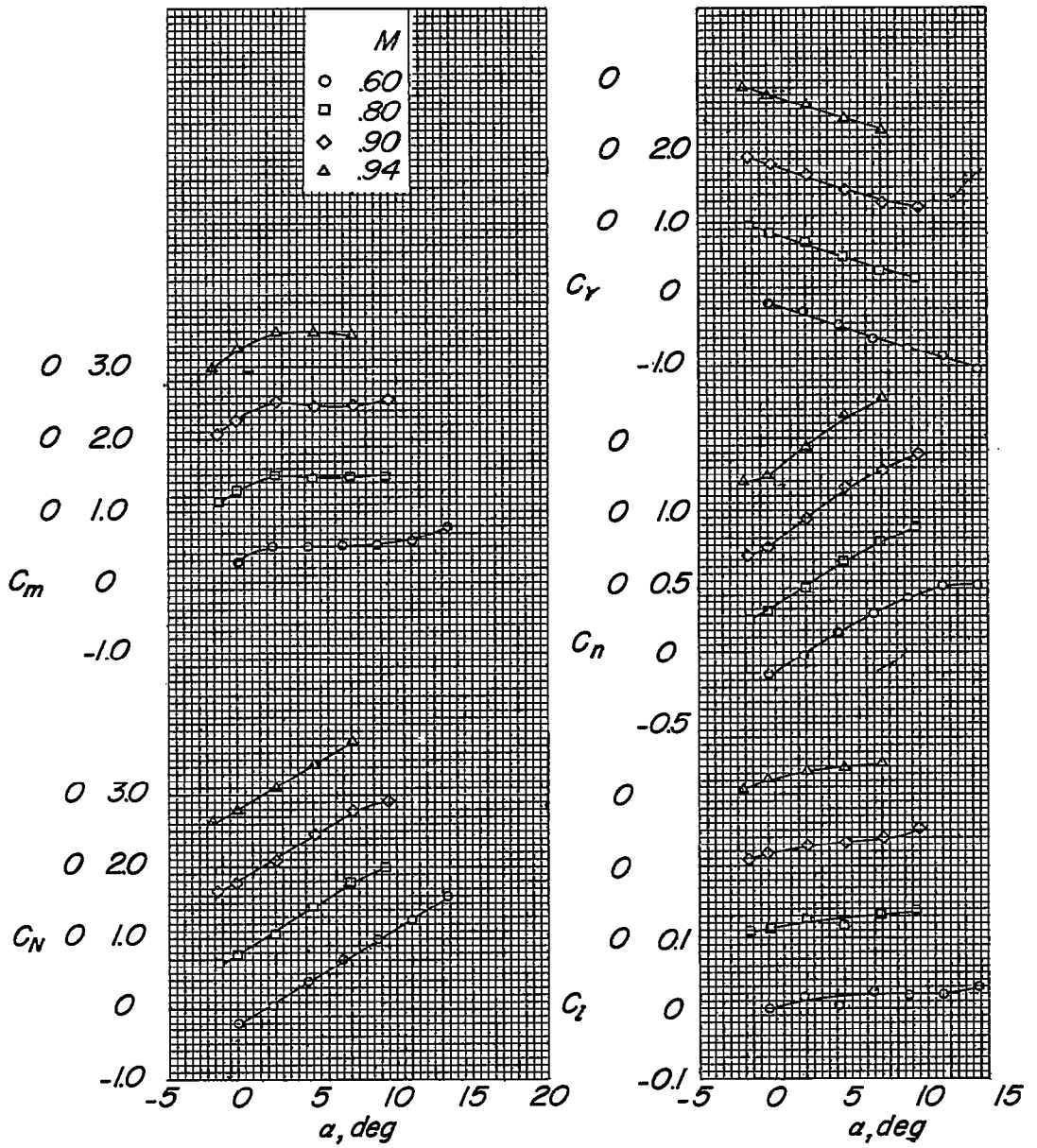

(e) x/c = -0.25.

Figure 12.- Continued.

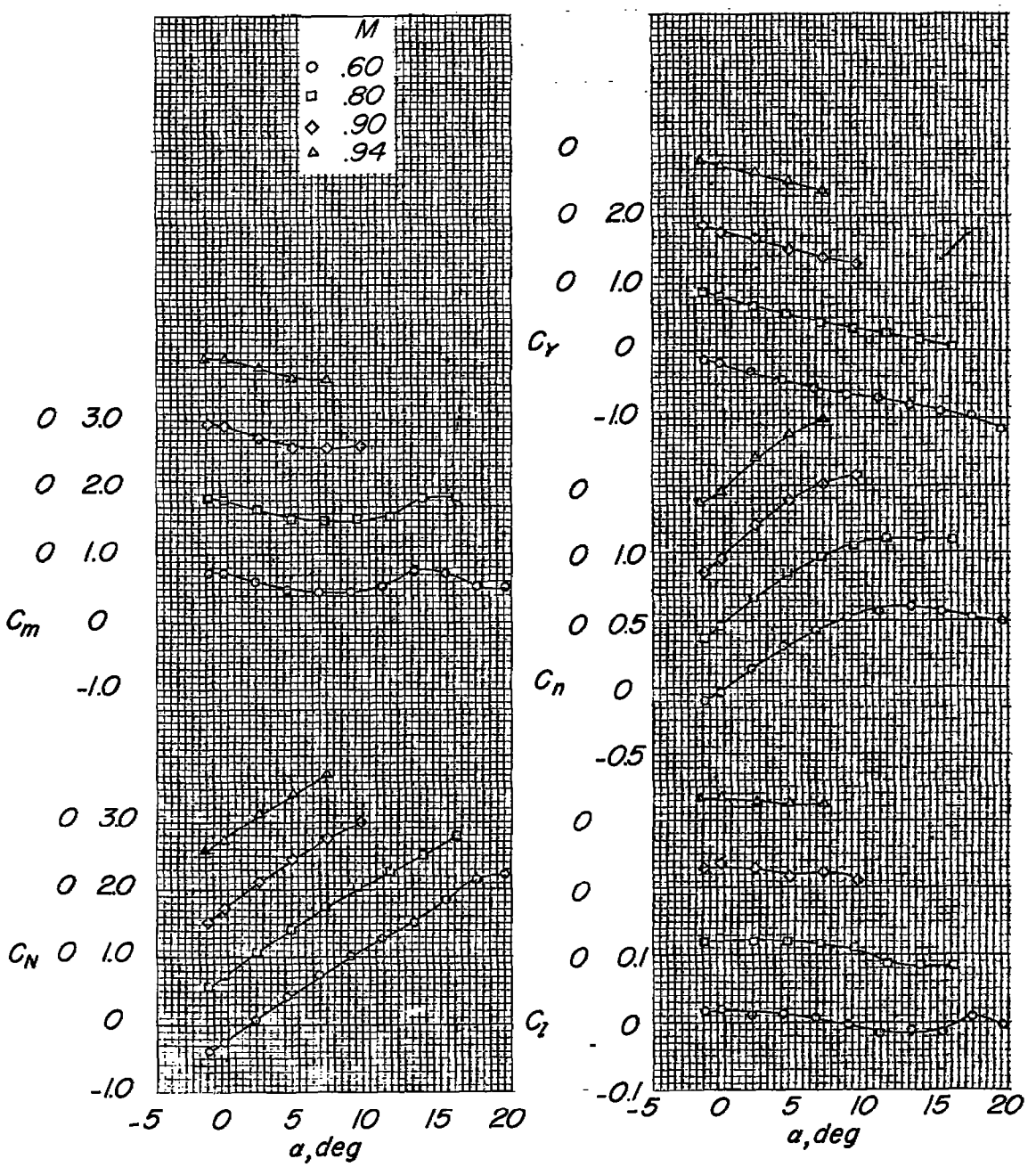

(f) x/c = -0.44.

Figure 12.- Continued.

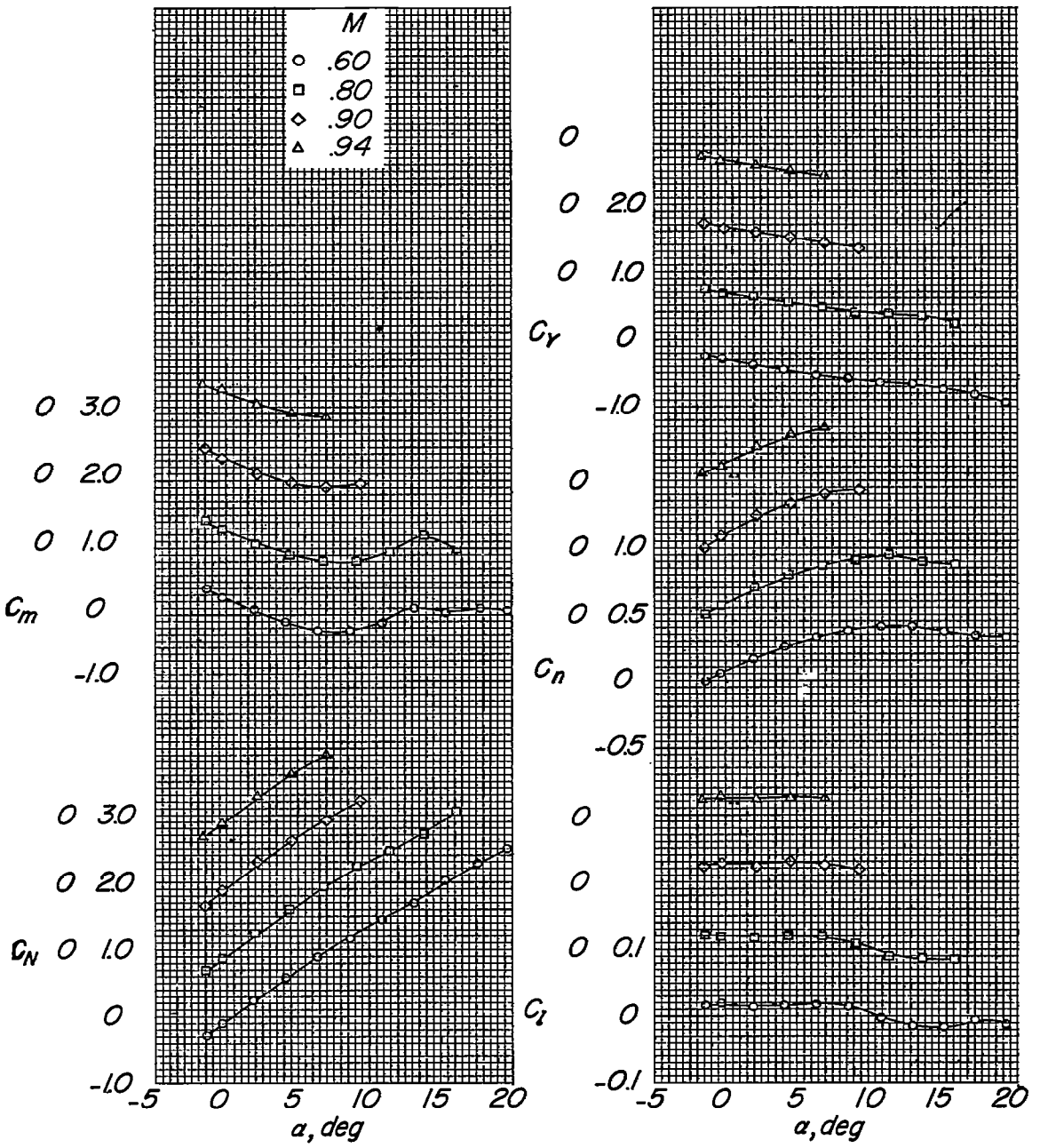

(g) x/c = -0.58.

Figure 12.- Continued.

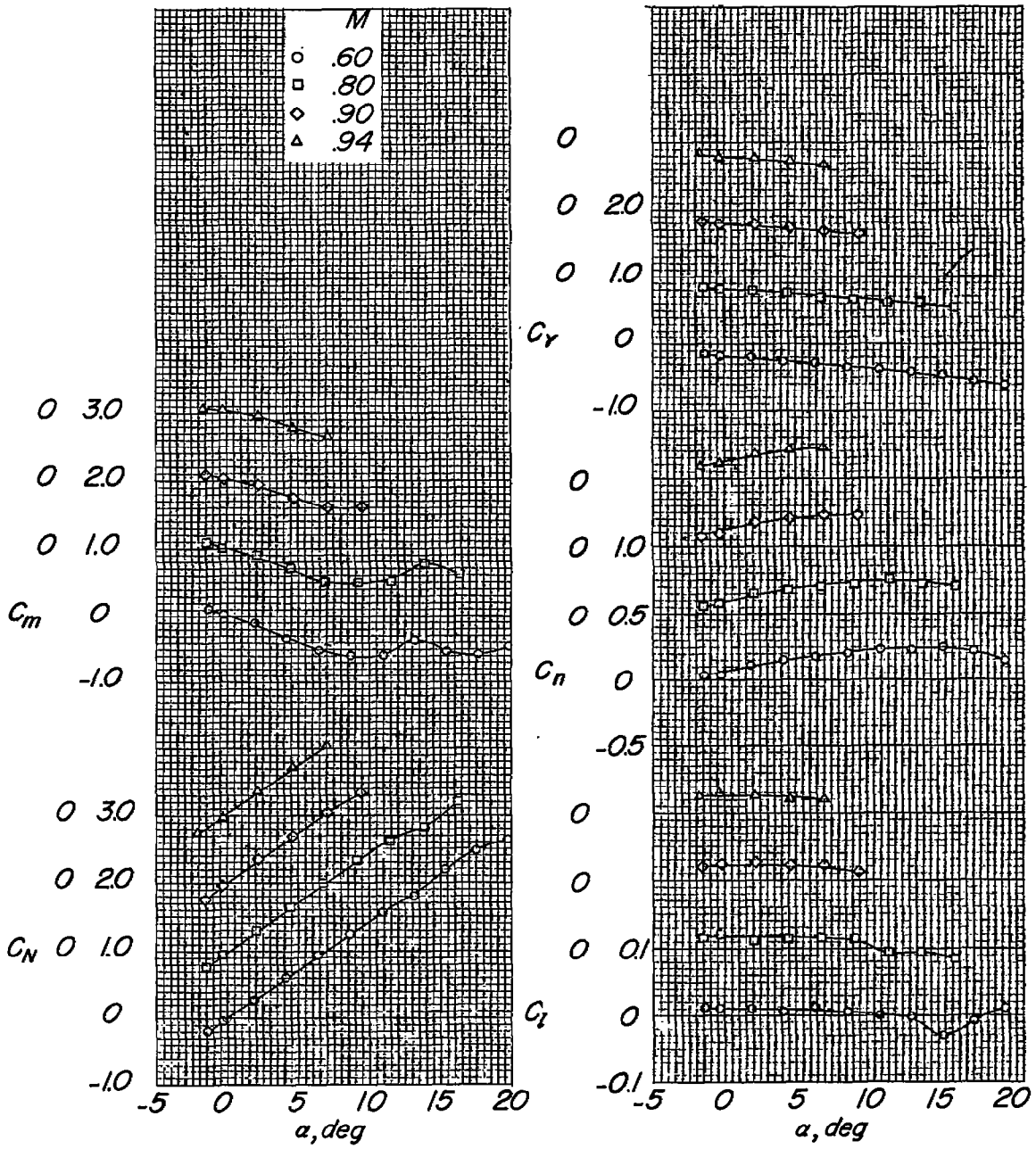

(h) x/c = -0.74.

Figure 12.- Continued.

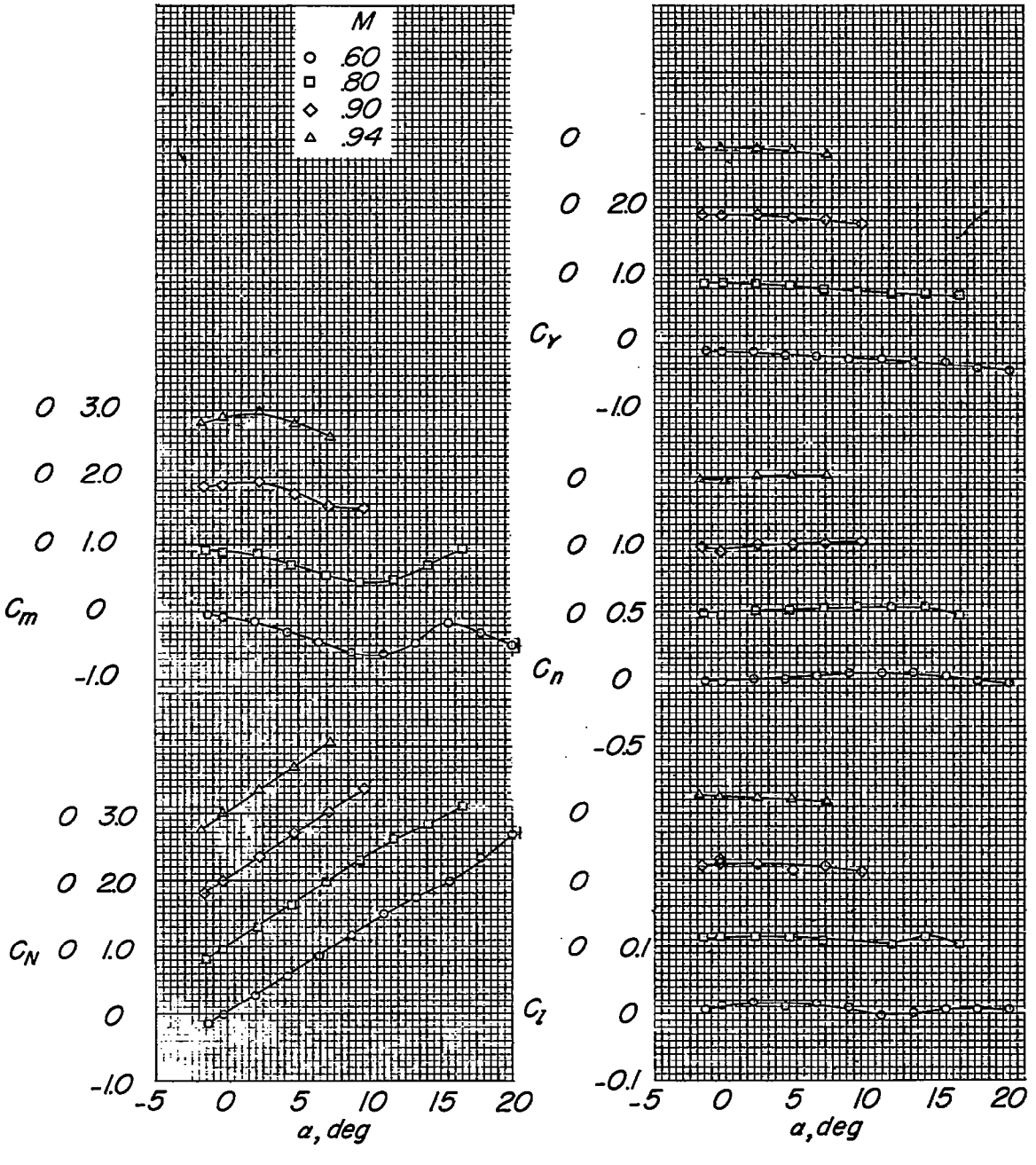

(i) x/c = -1.11.

Figure 12.- Concluded.

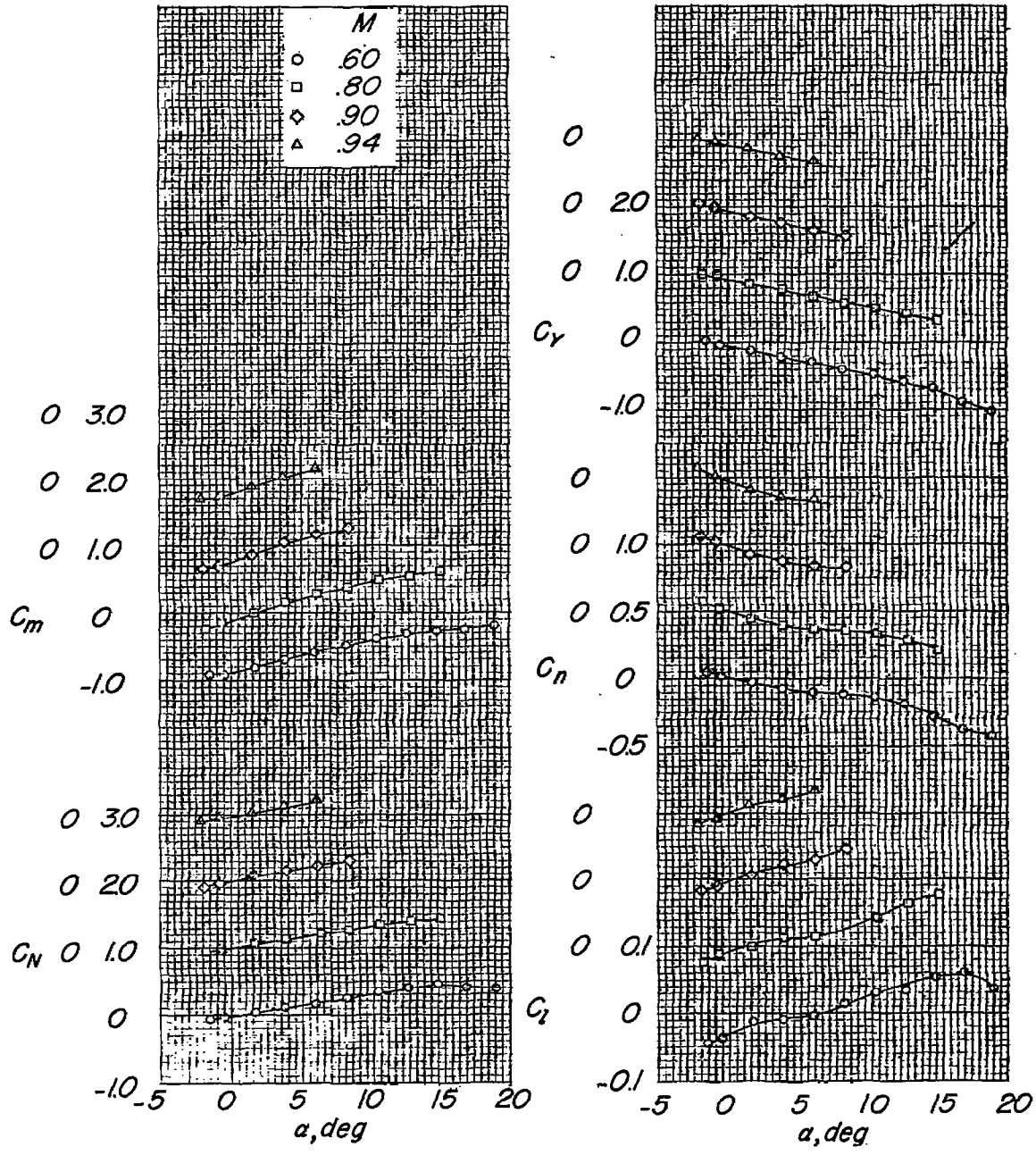

(a) x/c = 0.25

Figure 13.- Missile aerodynamic forces and moments in the presence of the modified-delta-wing—fuselage—pylon combination. $z/\bar{c}_A = -0.13$; $y/\frac{b}{2} = -0.25$.

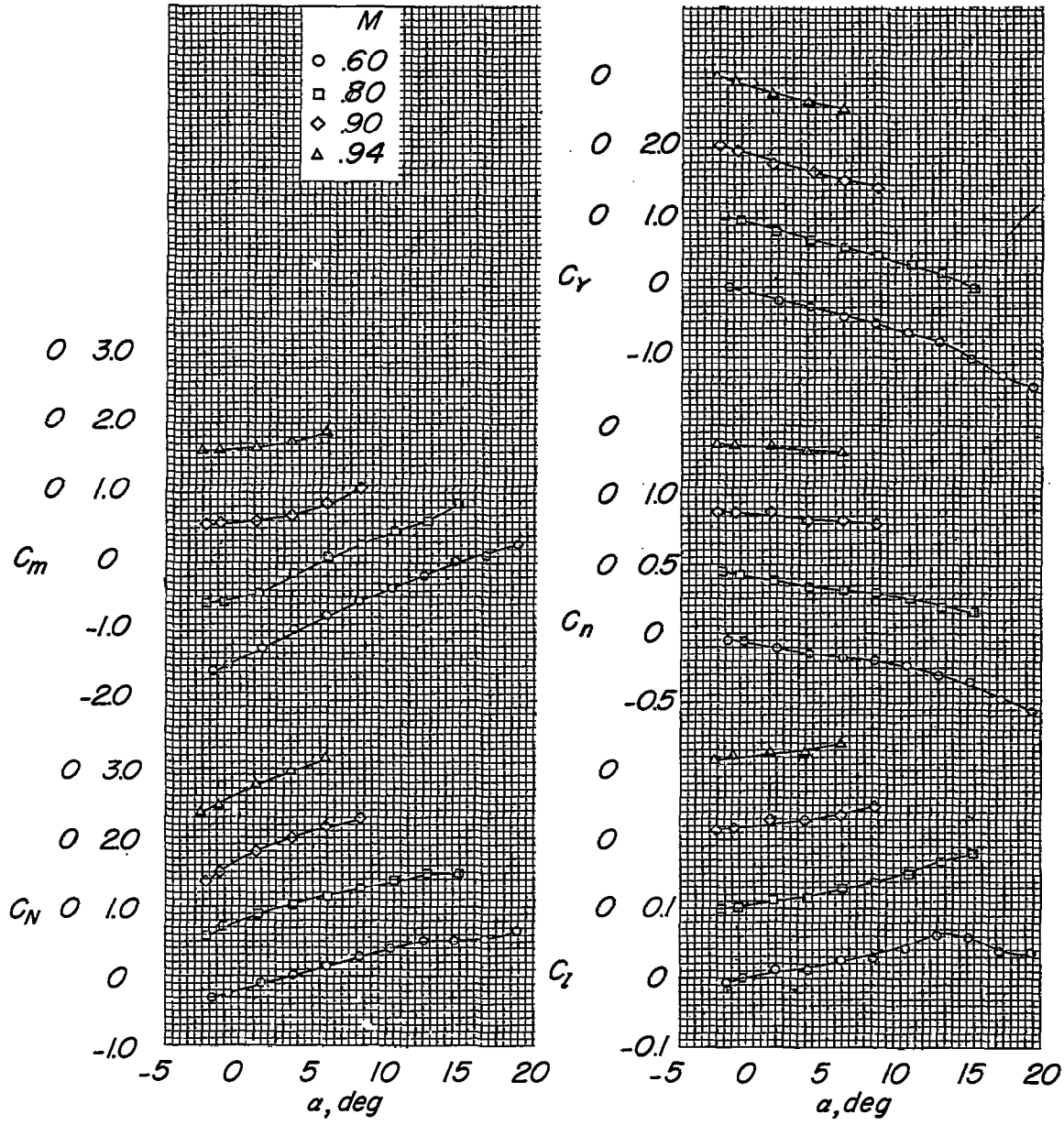

(b) x/c = 0.13.

Figure 13.- Continued.

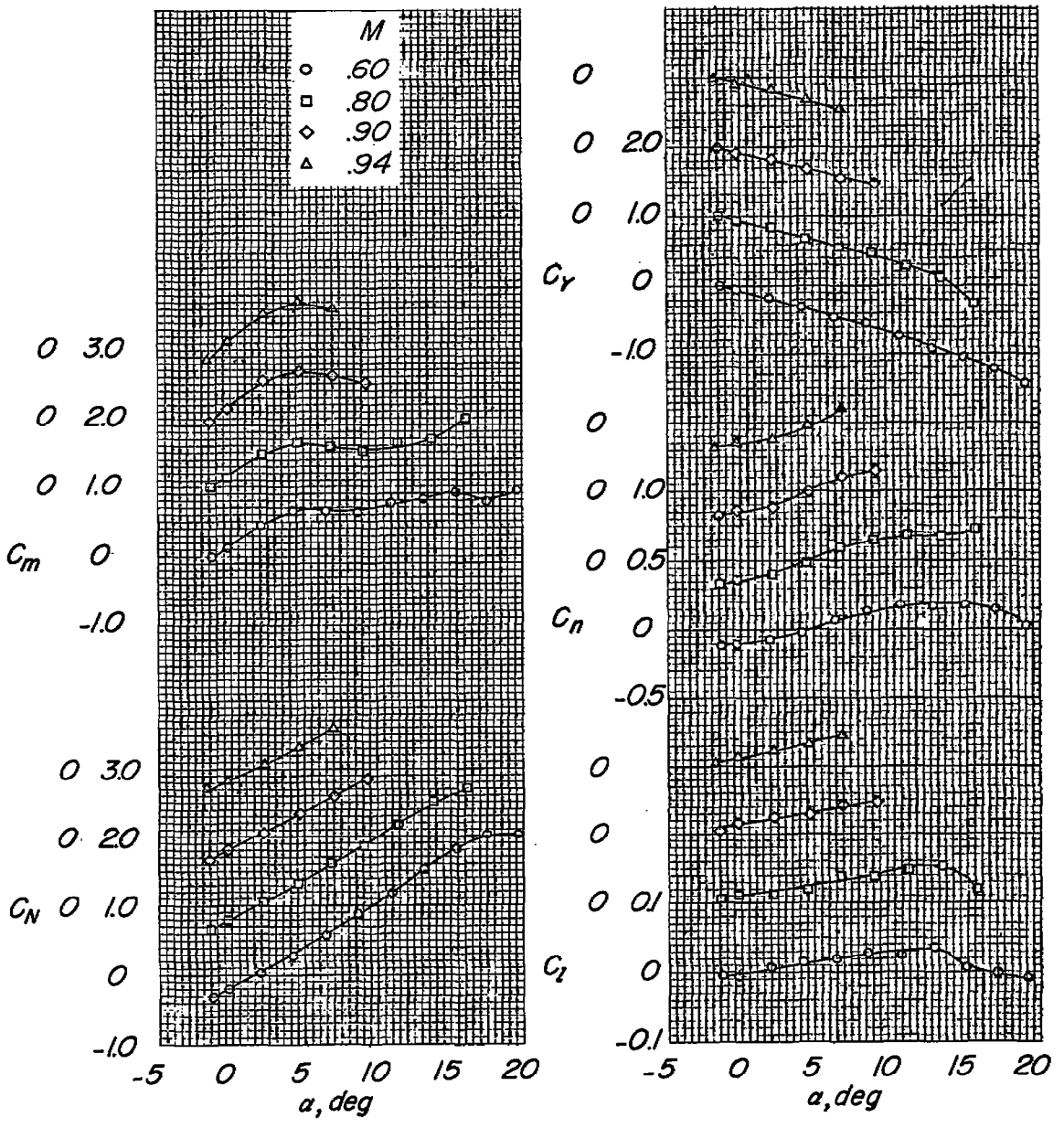

(c) x/c = -0.11.

Figure 13.- Continued.

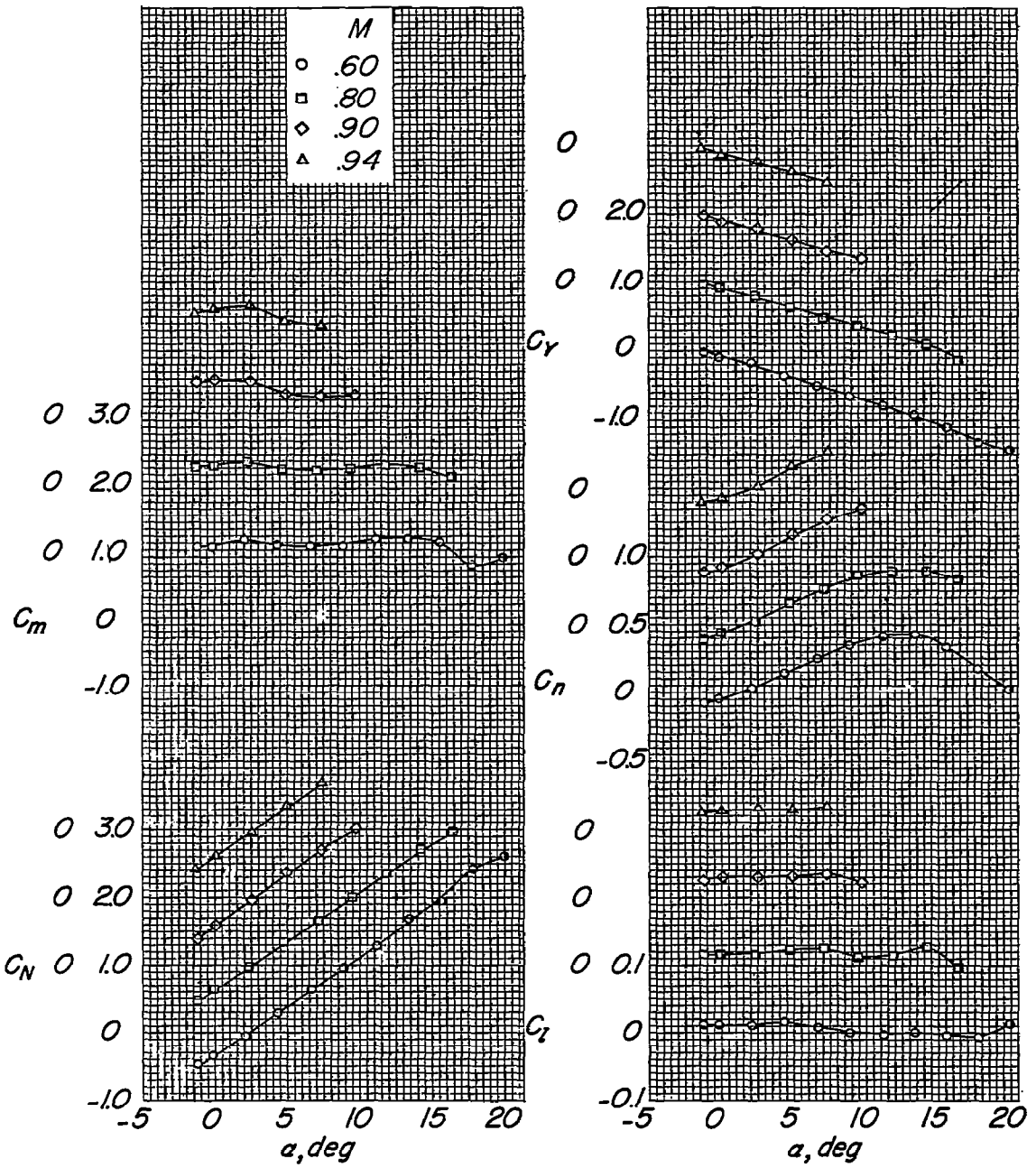

(d) x/c = -0.25.

Figure 13.- Continued.

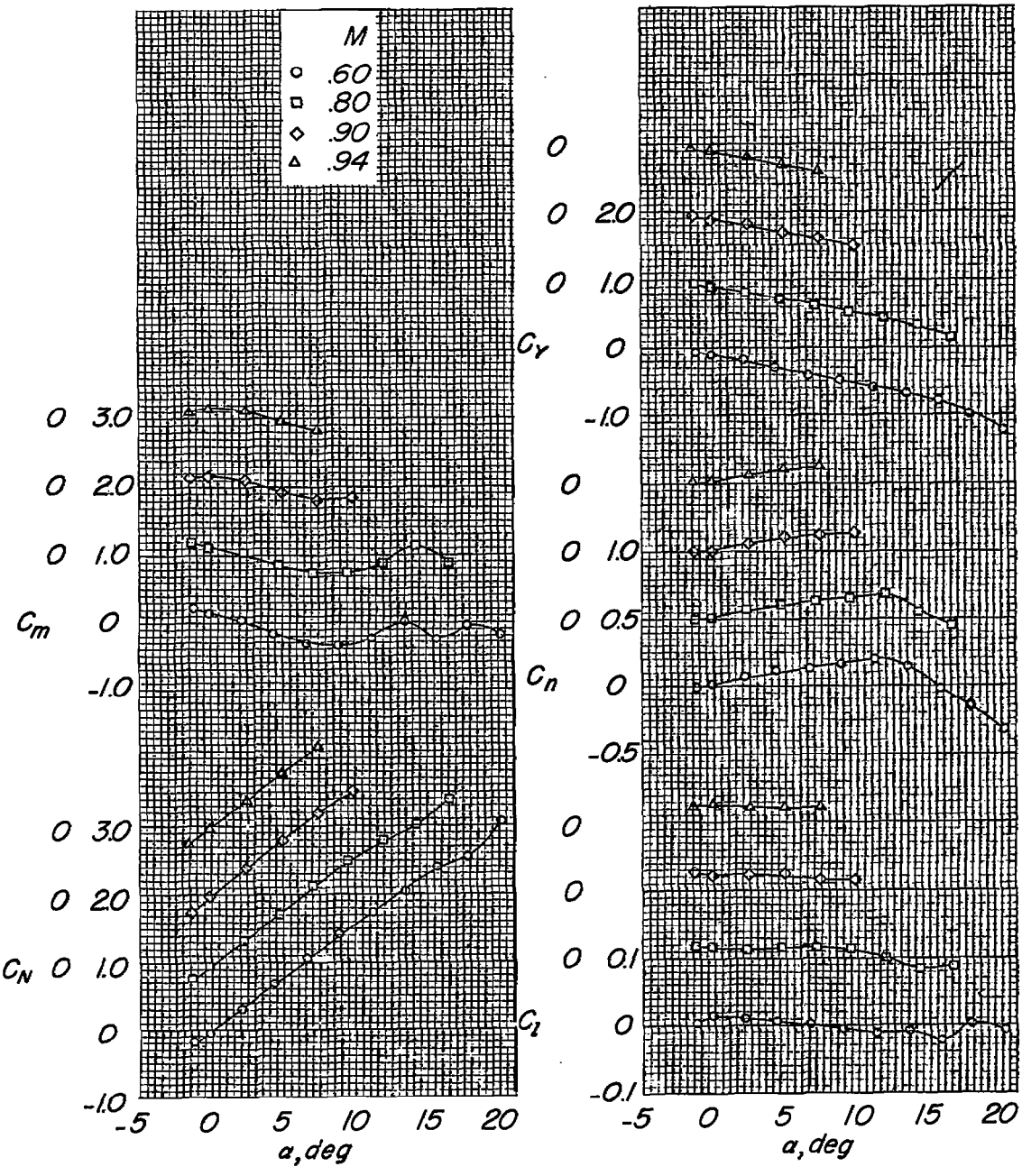

(e) x/c = -0.46.

Figure 13.- Continued.

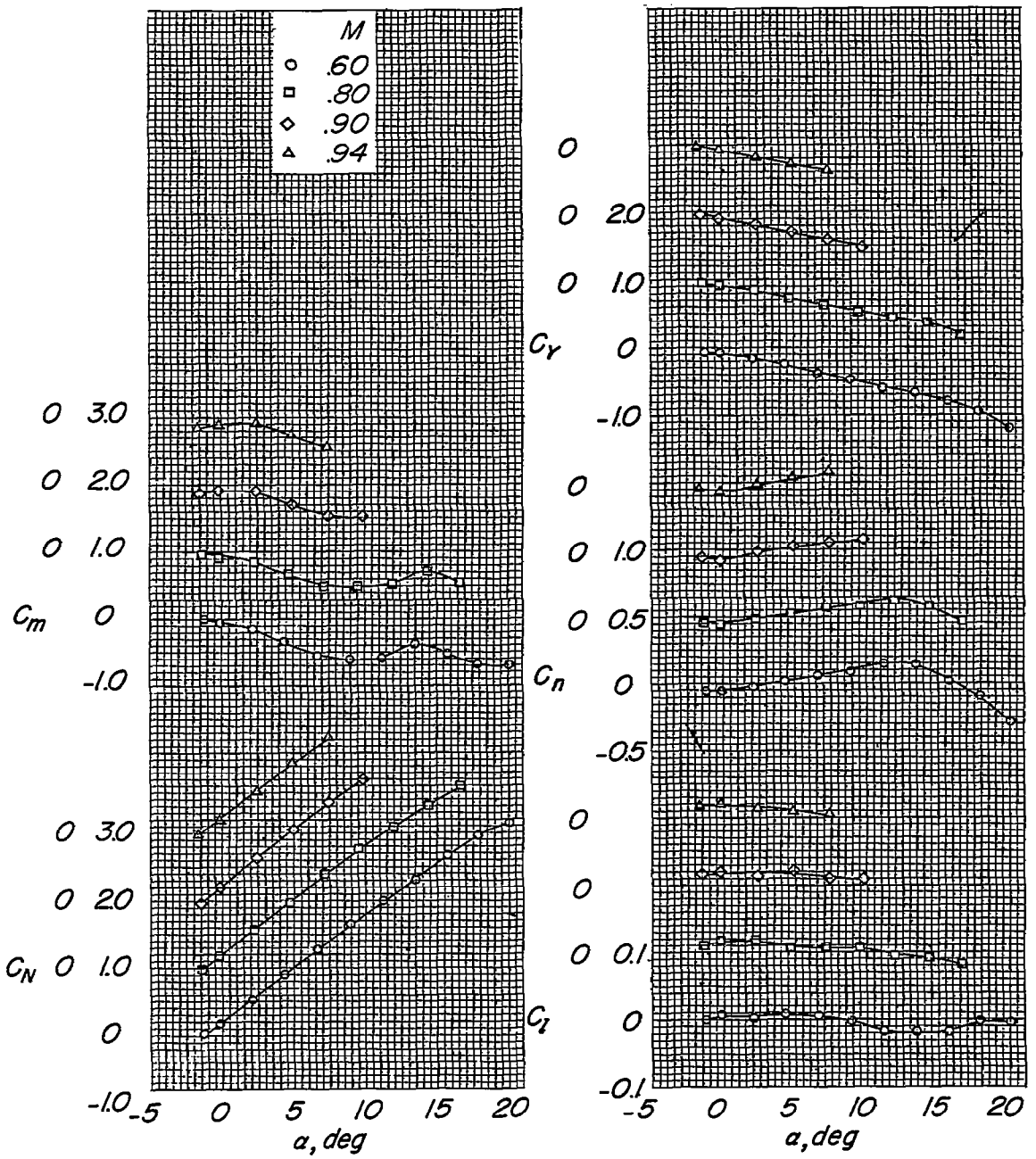

(f) x/c = -0.58.

Figure 13.- Continued.

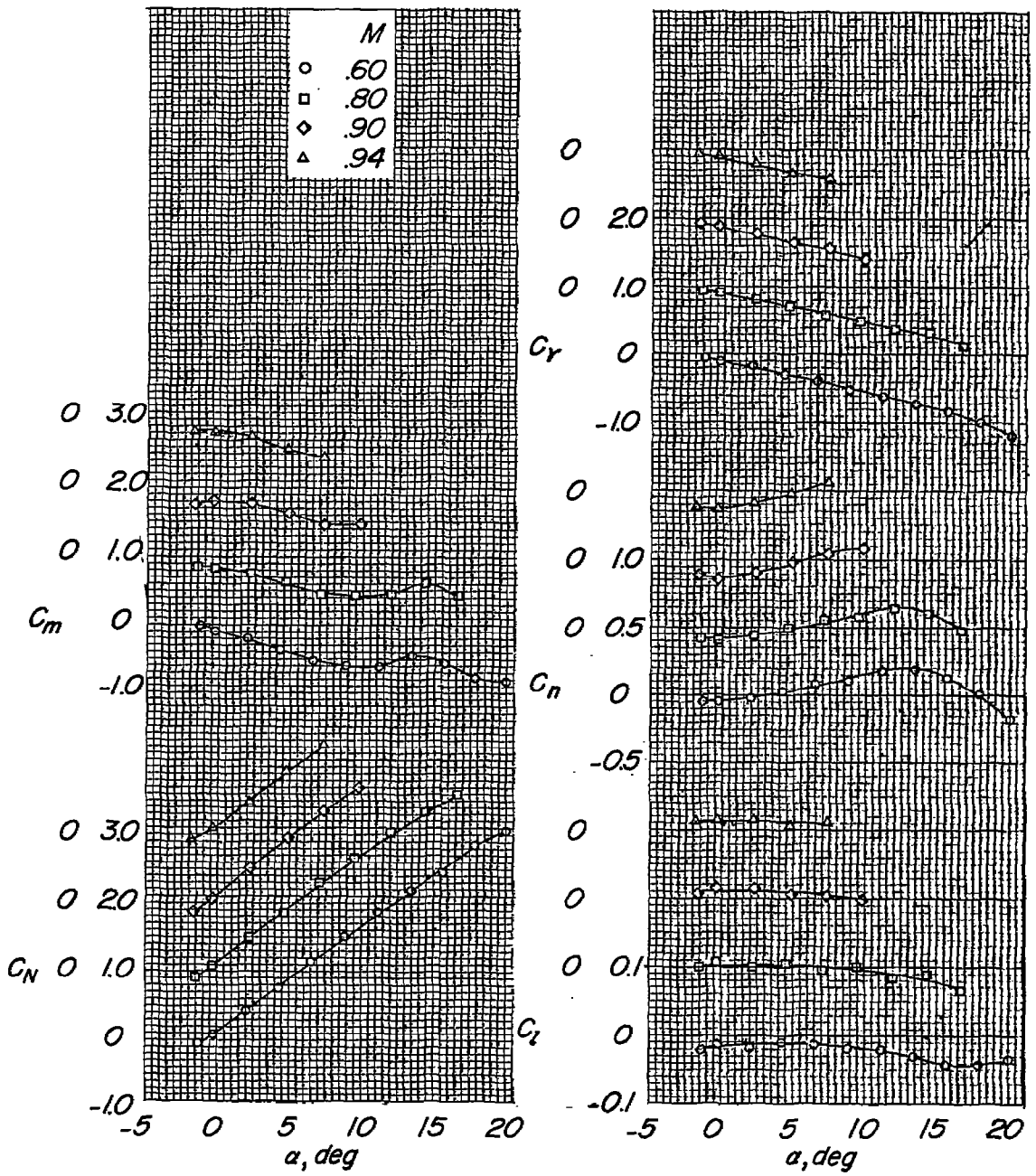

(g) x/c = -0.71.

Figure 13.- Concluded.

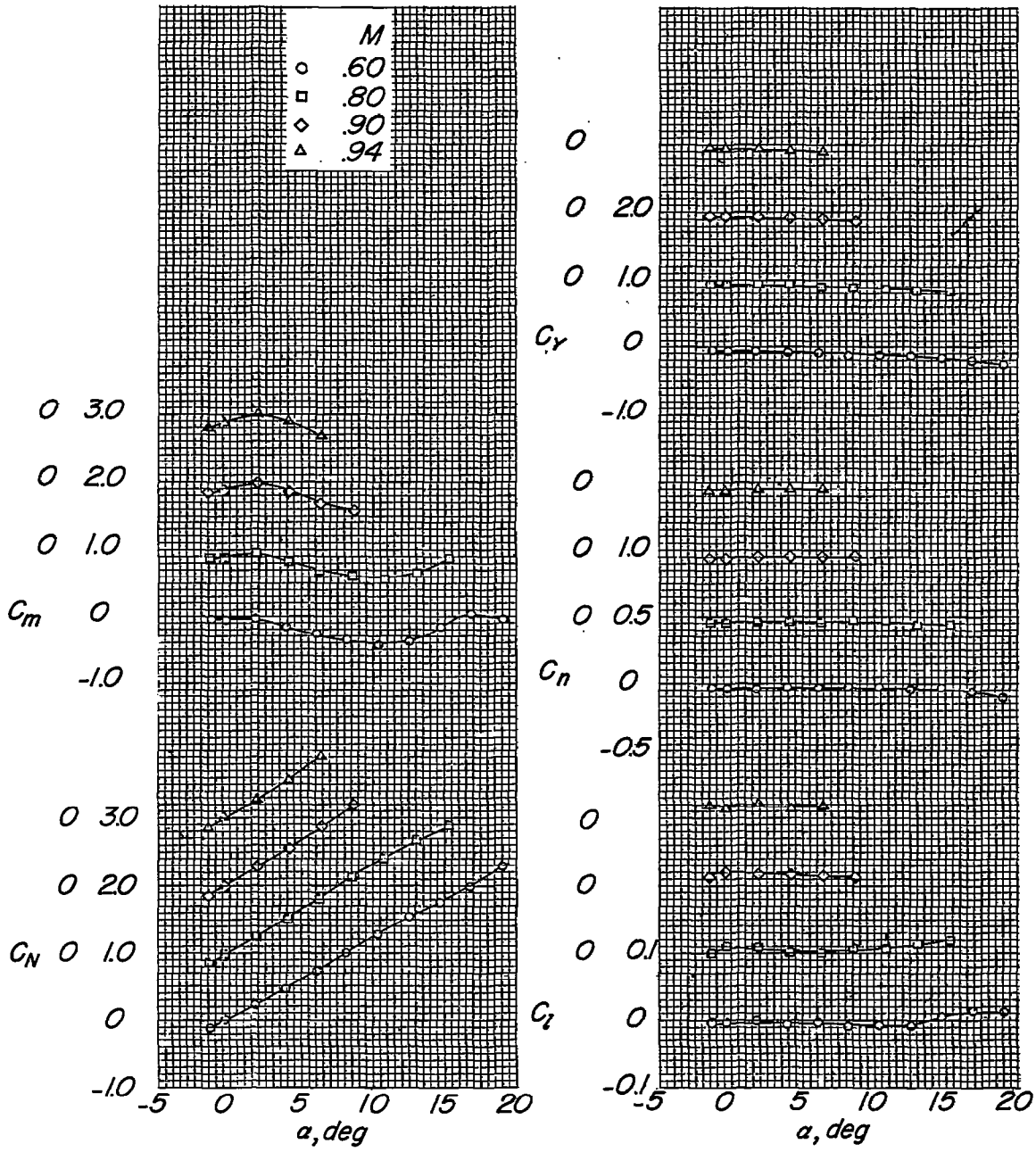

(a) x/c = 0.16.

Figure 14.- Missile aerodynamic forces and moments in the presence of the fuselage alone for various Mach numbers. $y/\frac{b}{2}$ = -0.50 (based on delta-wing semispan).

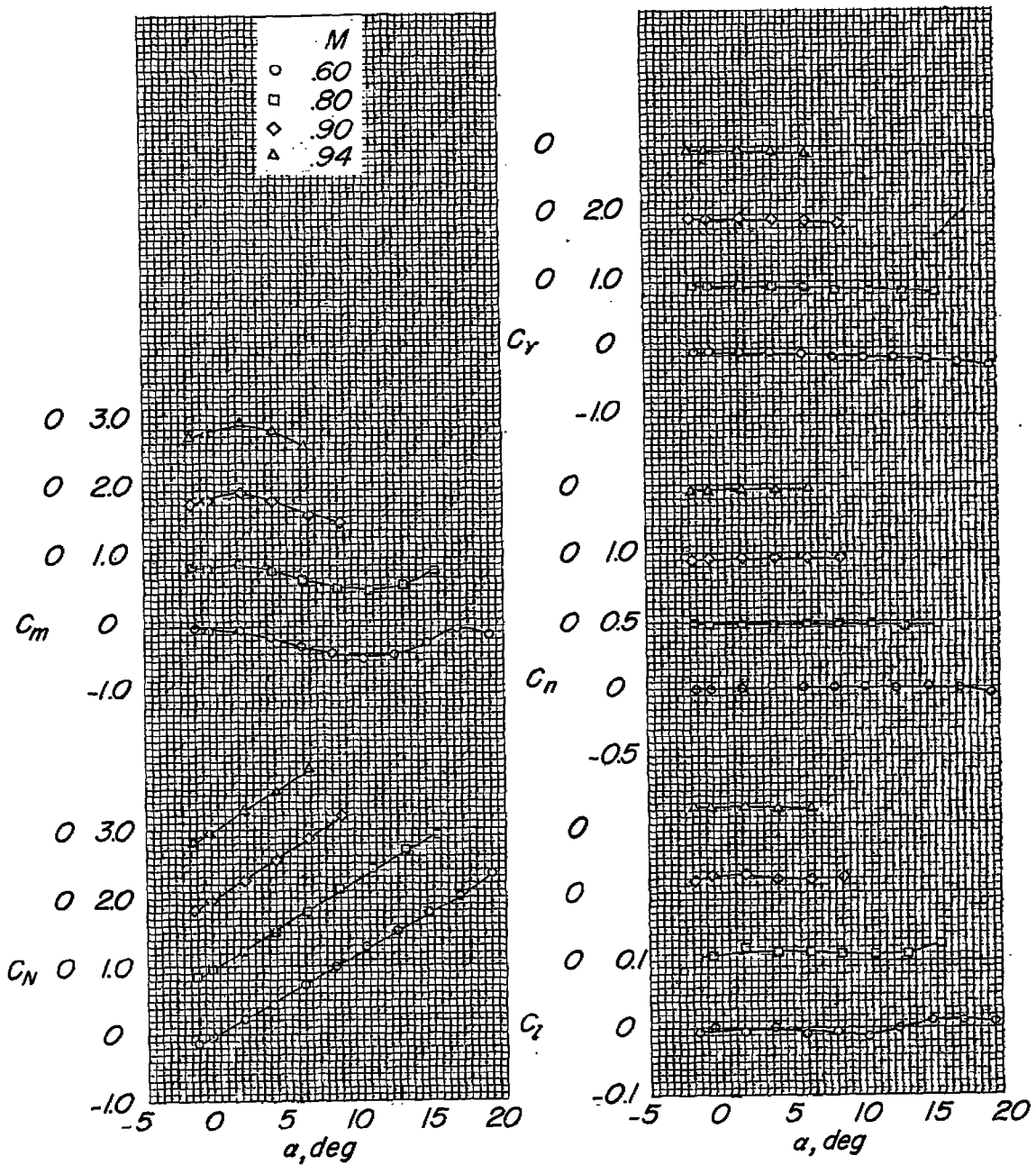

(b) x/c = -0.23.

Figure 14.- Continued.

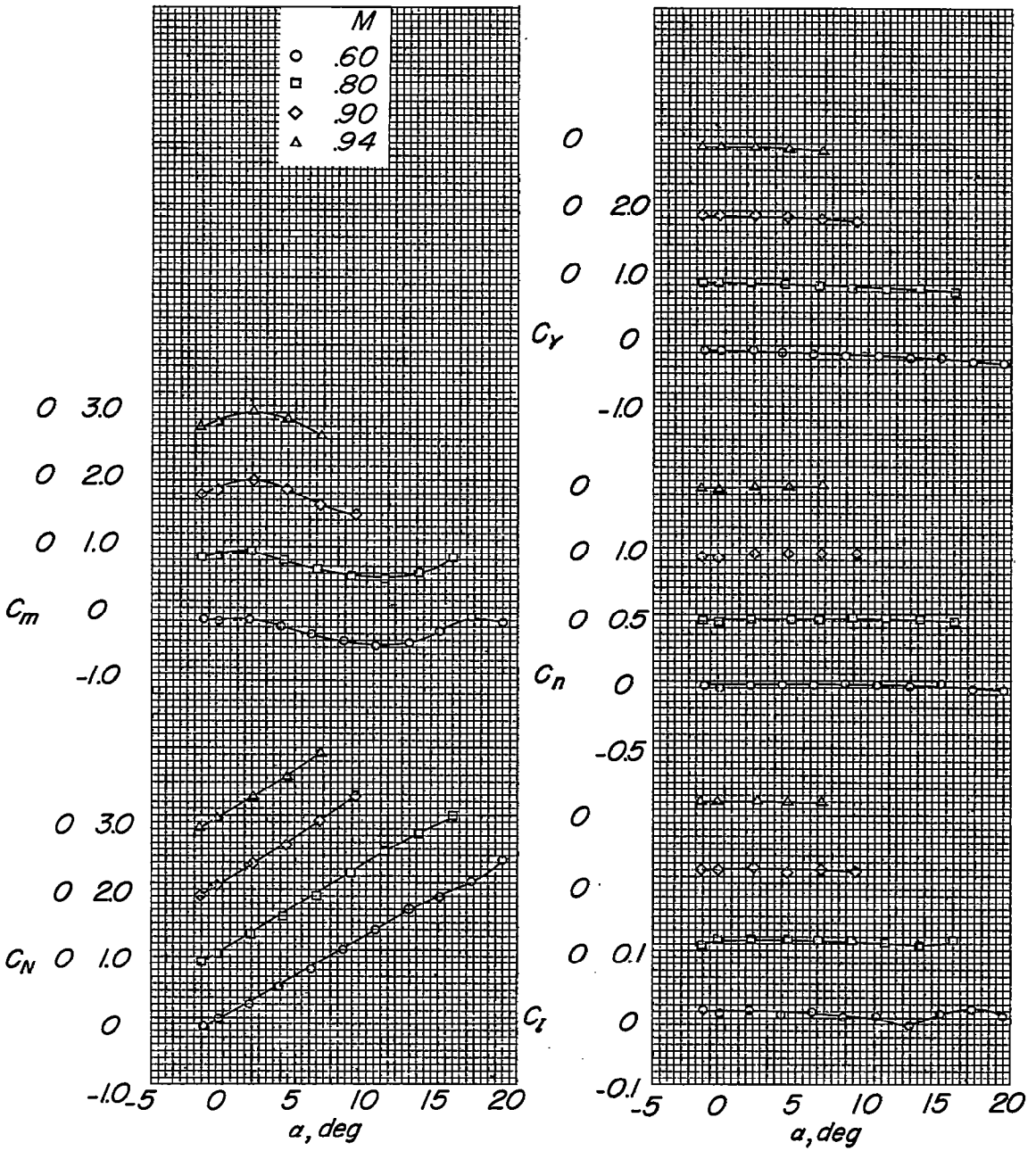

(c) x/c = -1.01.

Figure 14.- Concluded.

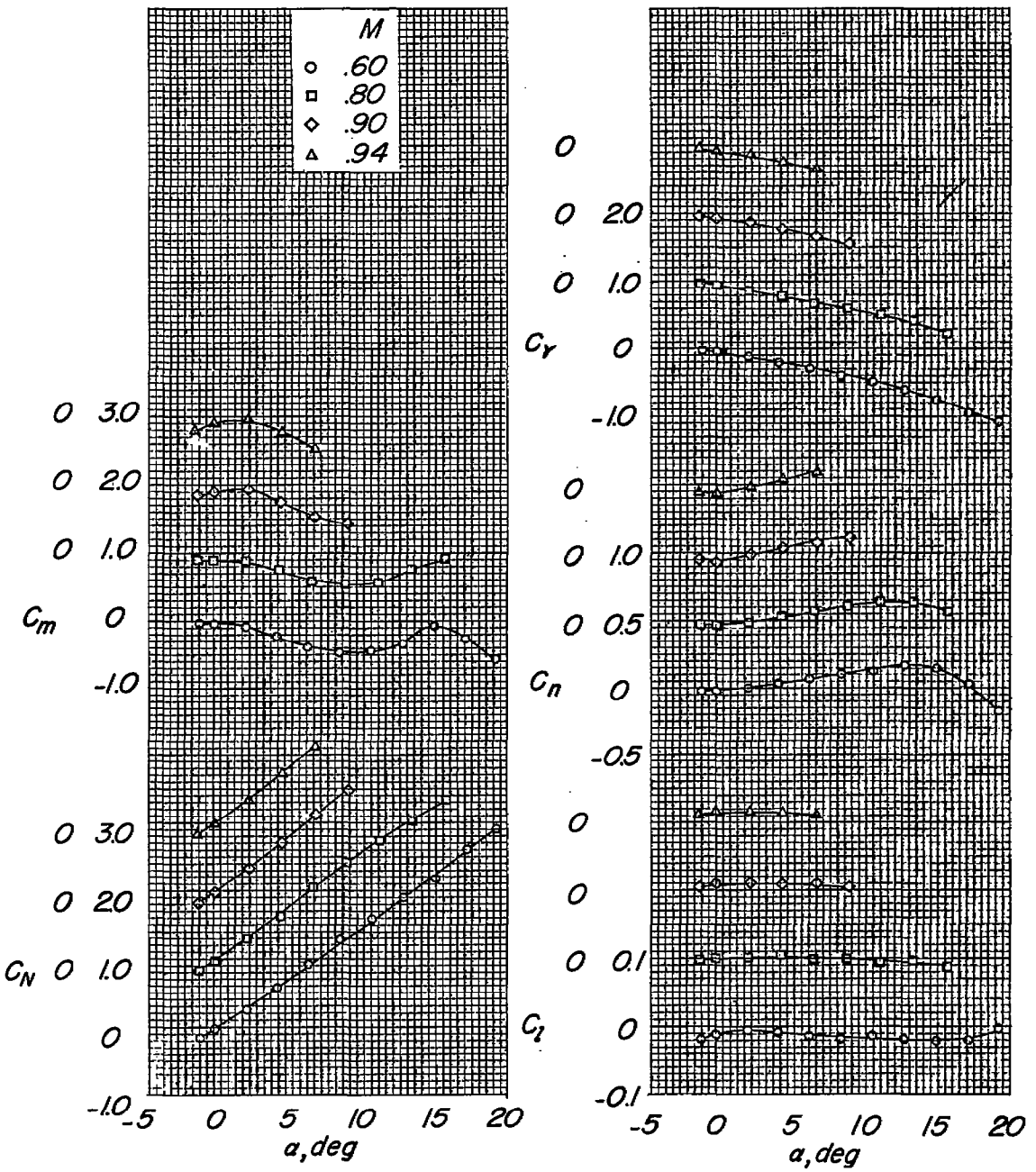

(a) x/c = 0.24.

Figure 15.- Missile aerodynamic forces and moments in the presence of the fuselage alone for various Mach numbers. $y/\frac{b}{2} = -0.25$ (based on delta-wing semispan).

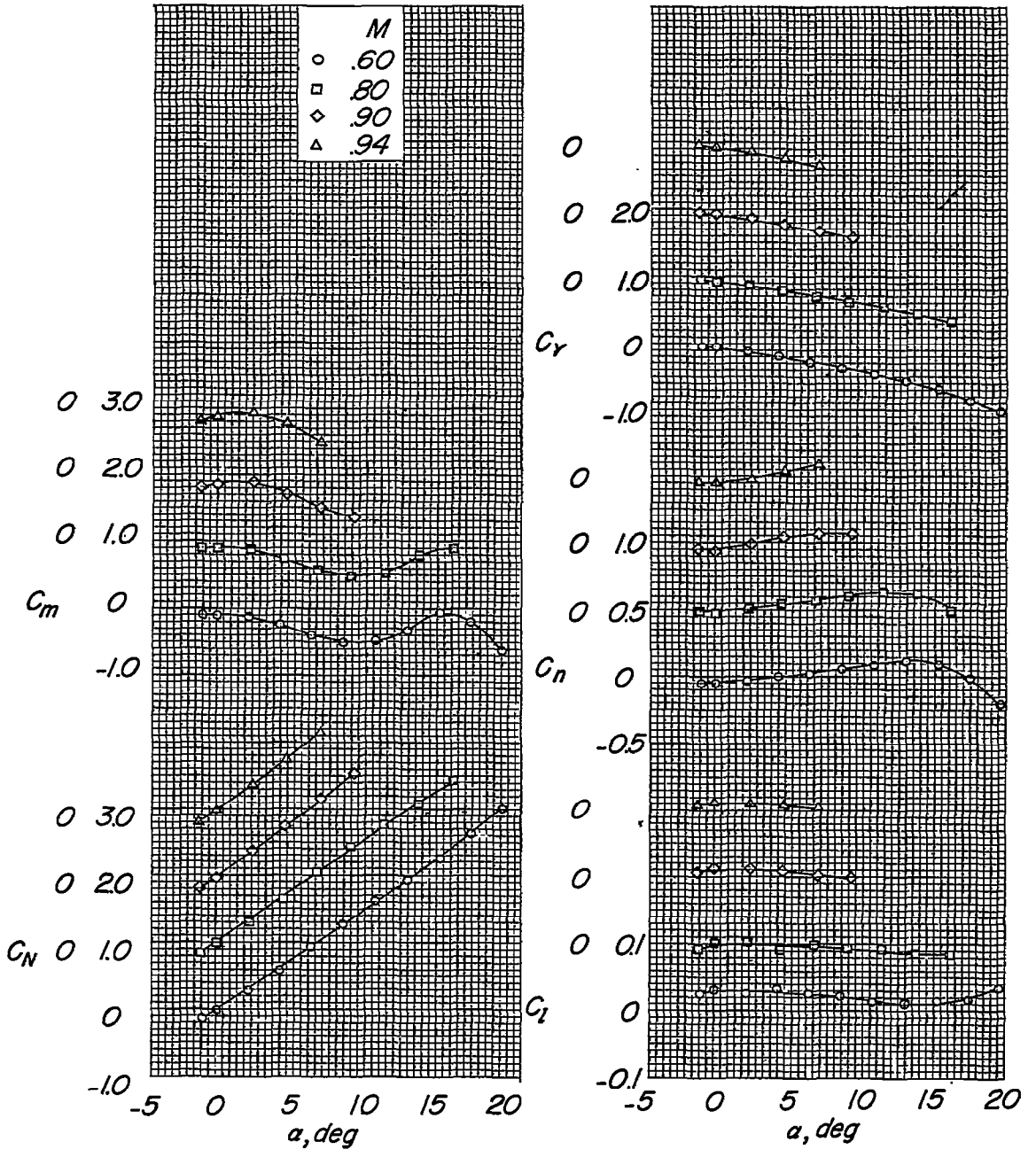

(b) x/c = -0.11.

Figure 15.- Continued.

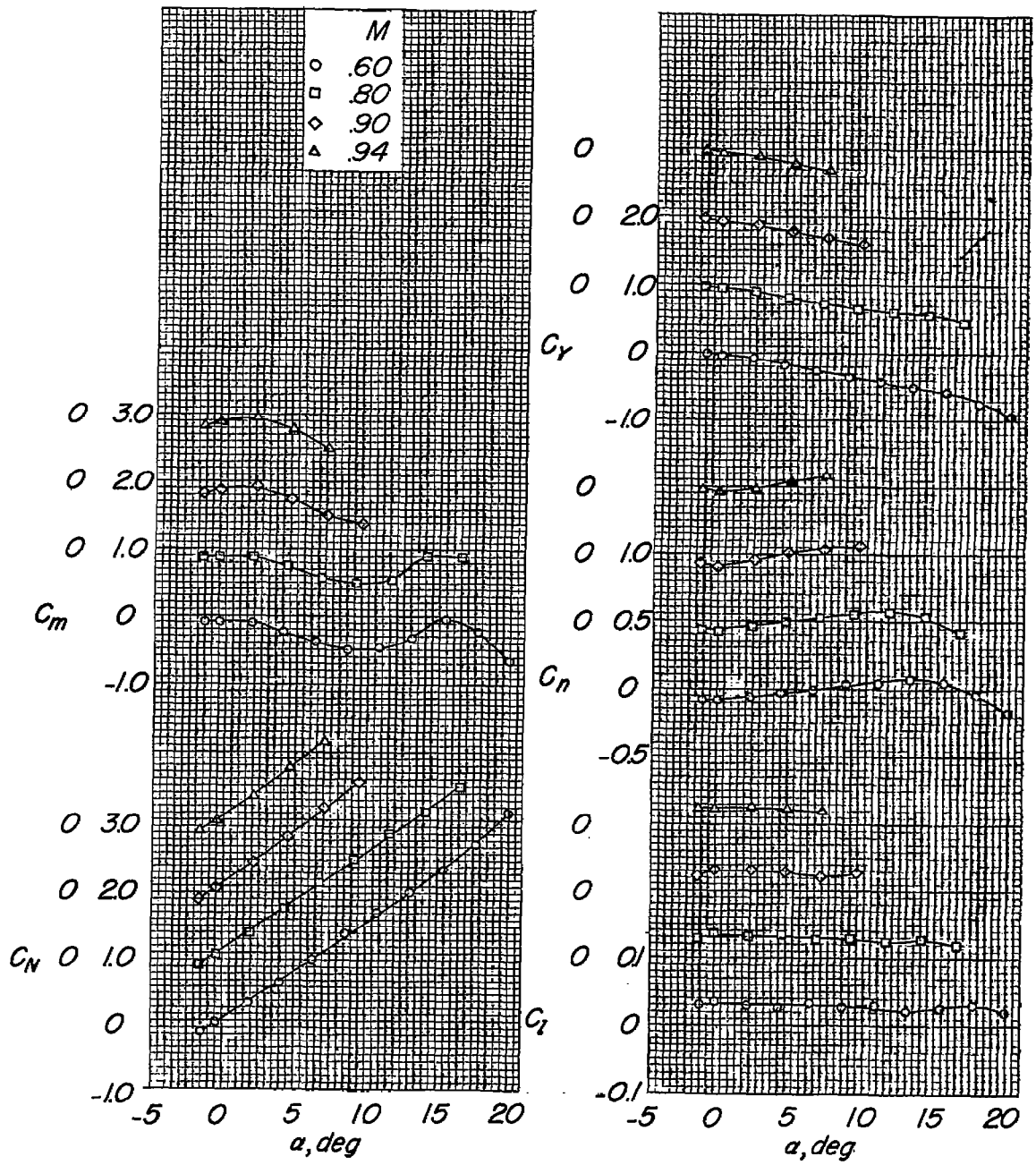

(c) x/c = -0.47.

Figure 15.- Concluded.

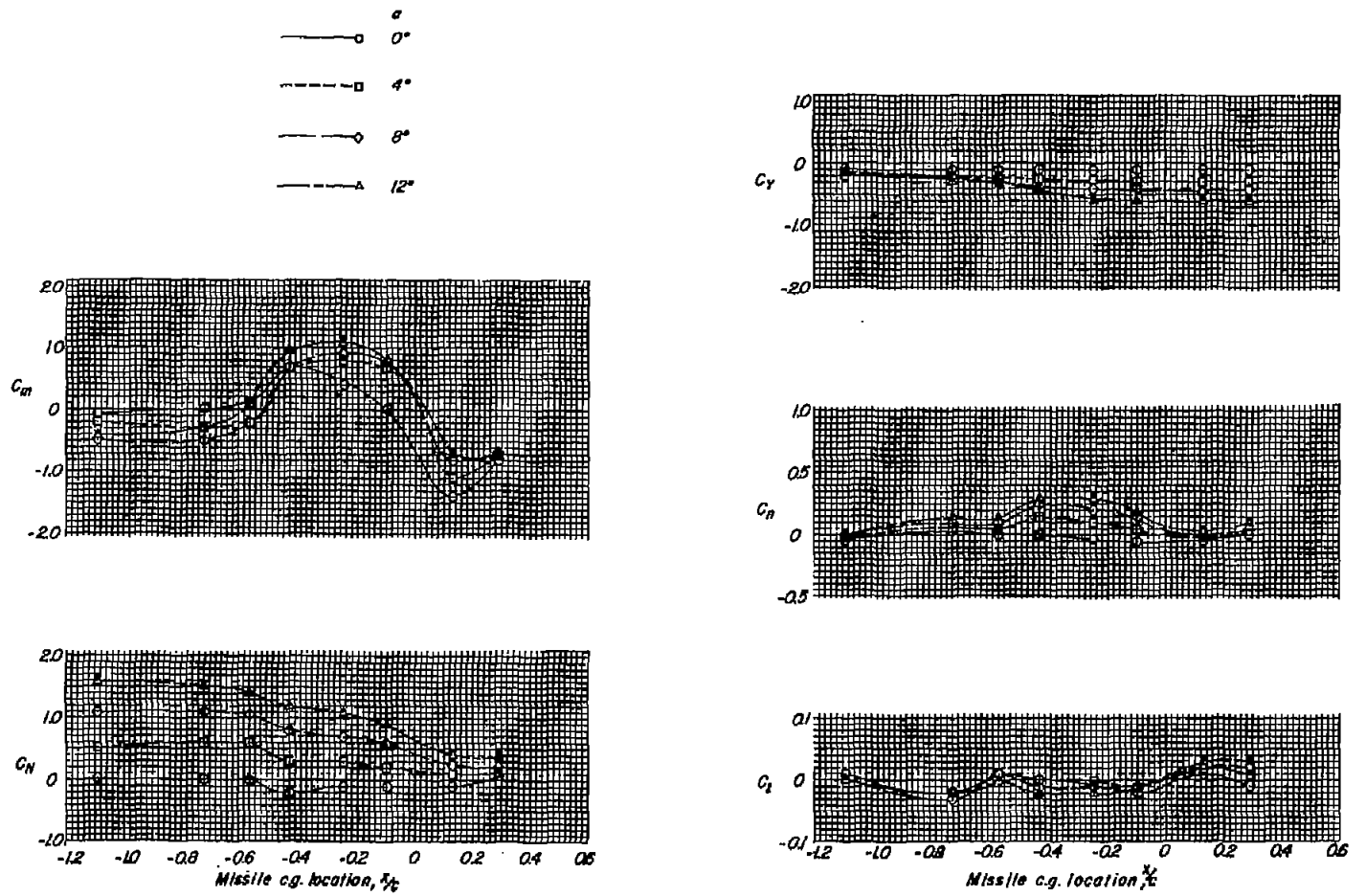

(a) M = 0.60.

Figure 16.- Effects of chordwise location on the missile forces and moments in the presence of the unswept wing—fuselage—pylon combination. $z/\bar{c}_A = -0.13$; $y/\frac{b}{2} = -0.50$.

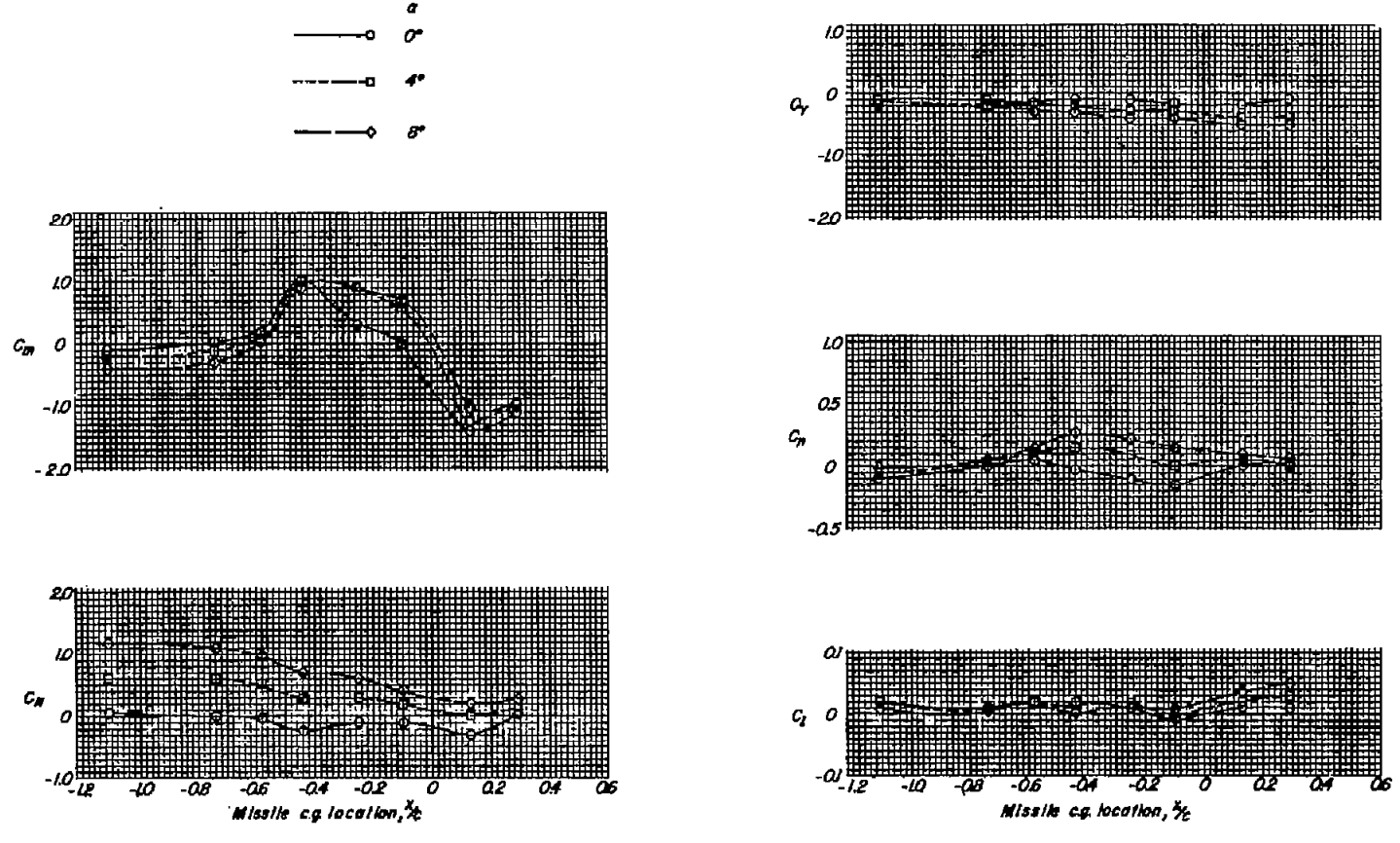

(b) M = 0.90.

Figure 16.- Concluded.

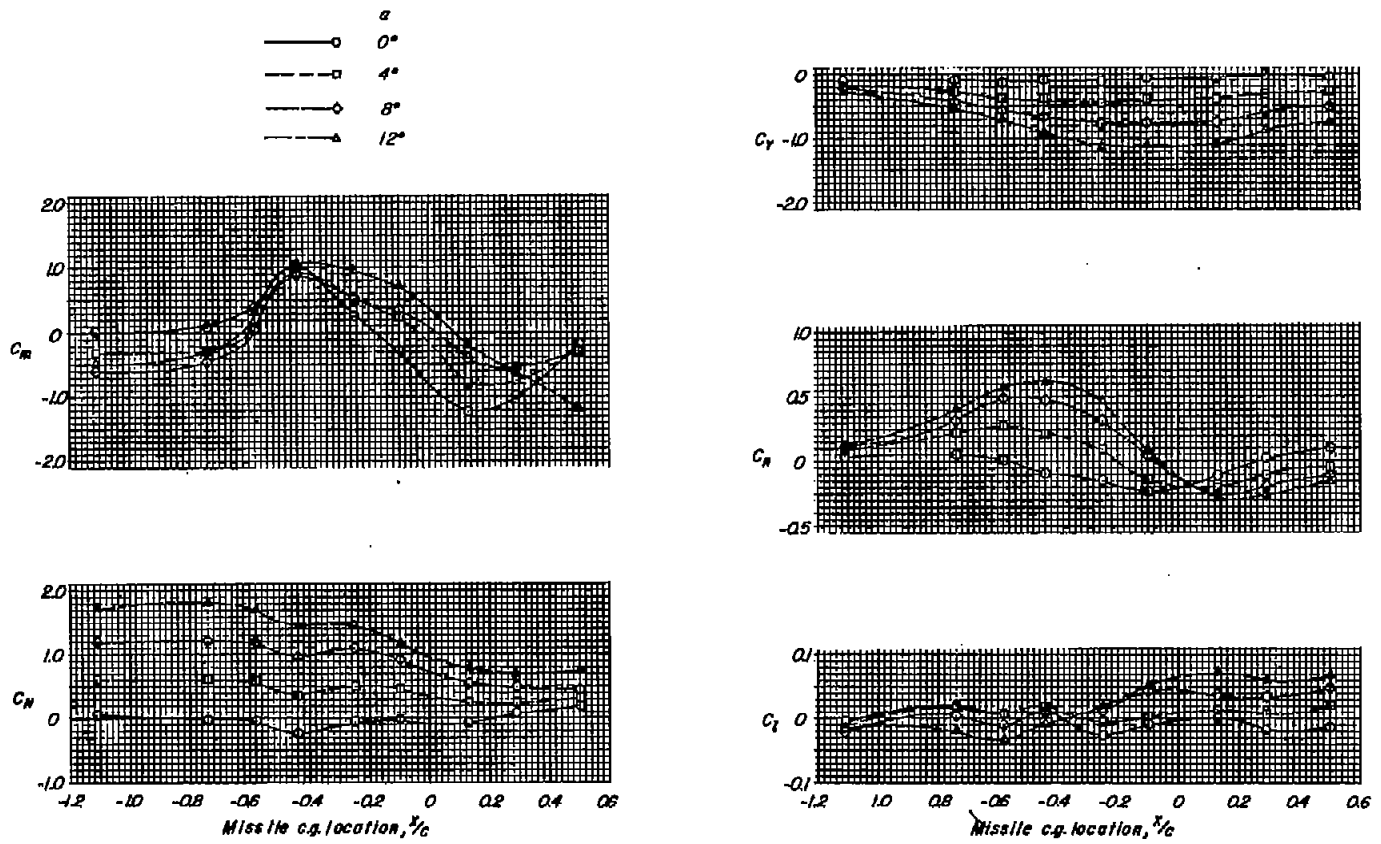

(a) M = 0.60.

Figure 17.- Effects of chordwise position on the missile forces and moments in the presence of the sweptback-wing—fuselage—pylon combination. $y/\frac{b}{2} = -0.50$; $z/\bar{c}_A = -0.15$.

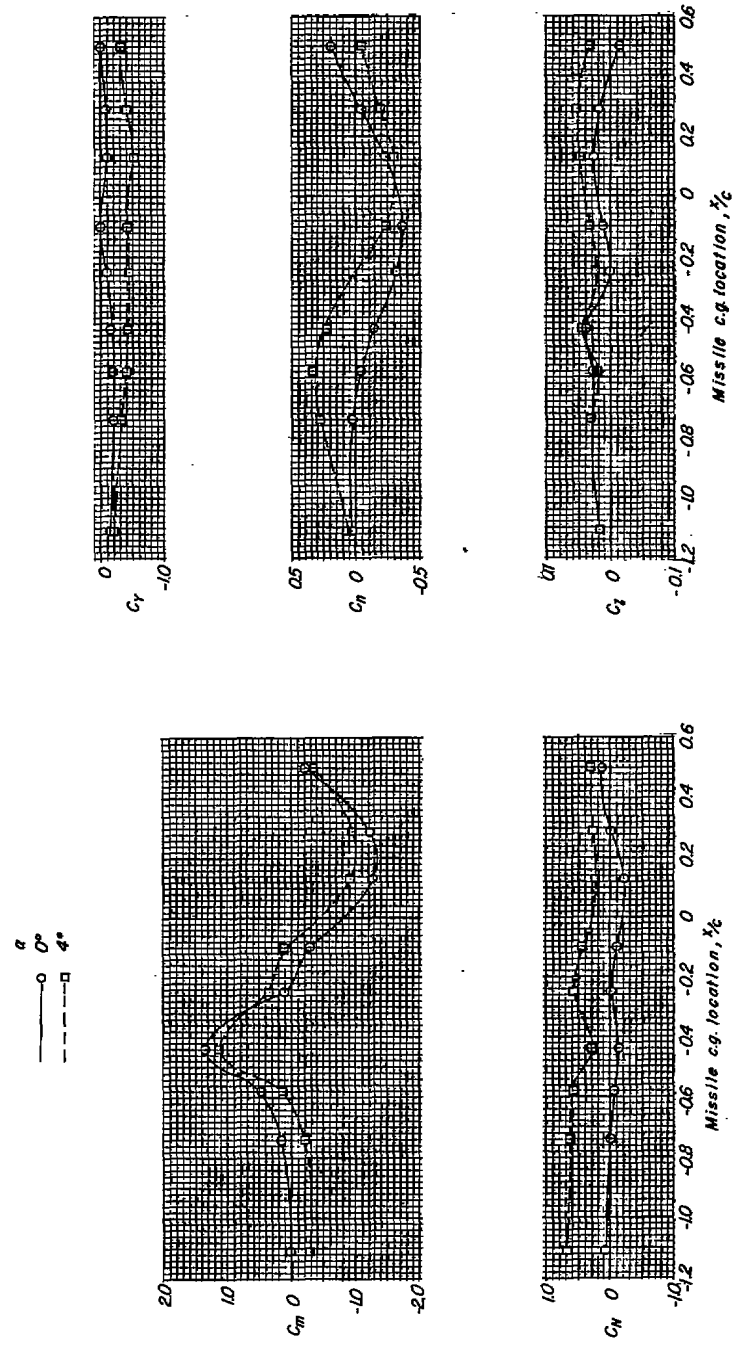

(b) M = 0.90.

Figure 17.- Concluded.

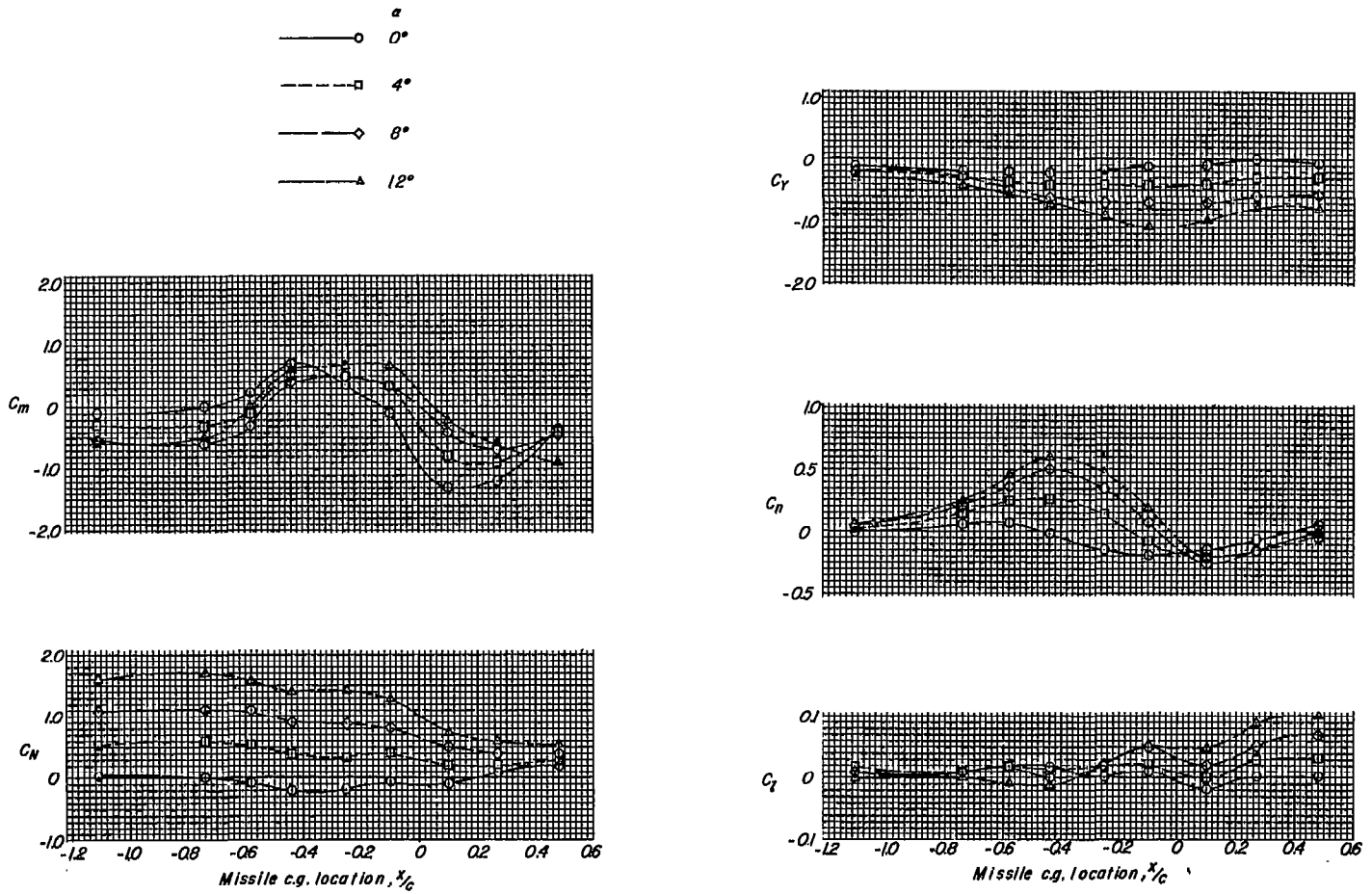

(a) M = 0.60.

Figure 18.- Effects of chordwise position on the missile forces and moments in the presence of the modified-delta-wing—fuselage—pylon combination. $y/\frac{b}{2} = -0.50$; $z/\bar{c}_A = -0.12$.

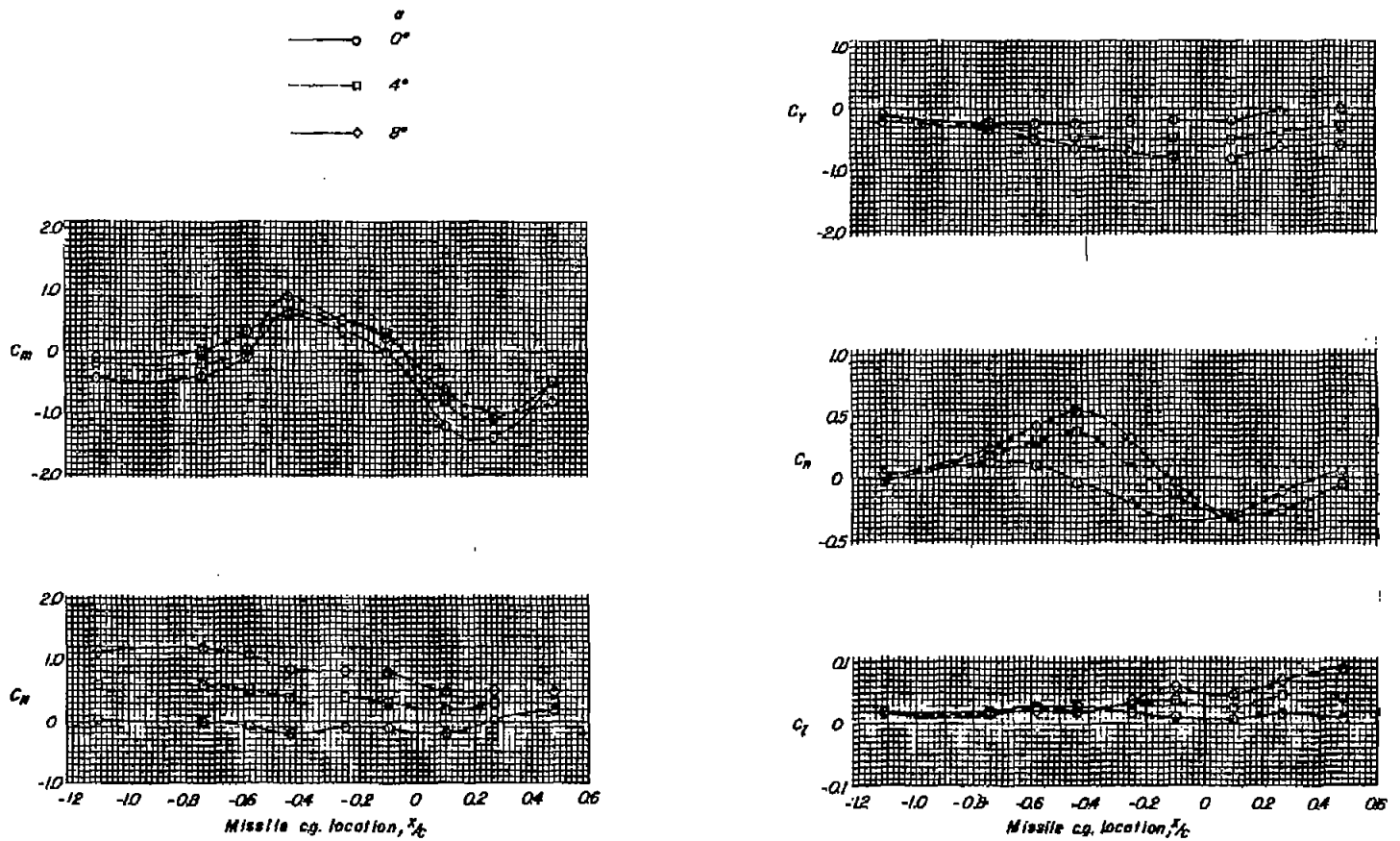

(b) M = 0.90.

Figure 18.- Concluded.

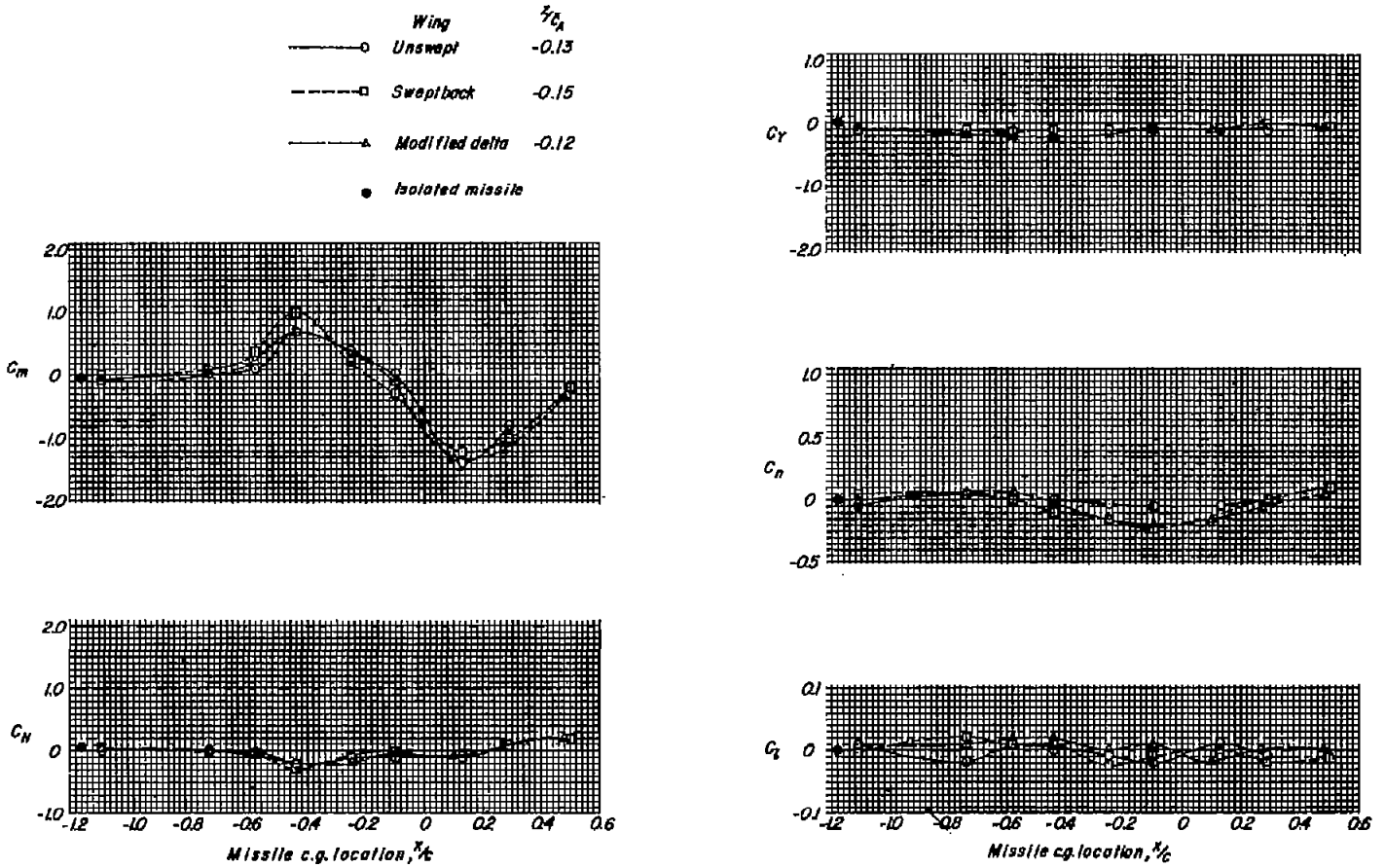

(a) M = 0.60; $\alpha = 0^\circ$.

Figure 19.- Effect of wing geometric characteristics on the missile forces and moments. $y/\frac{b}{2} = -0.50$.

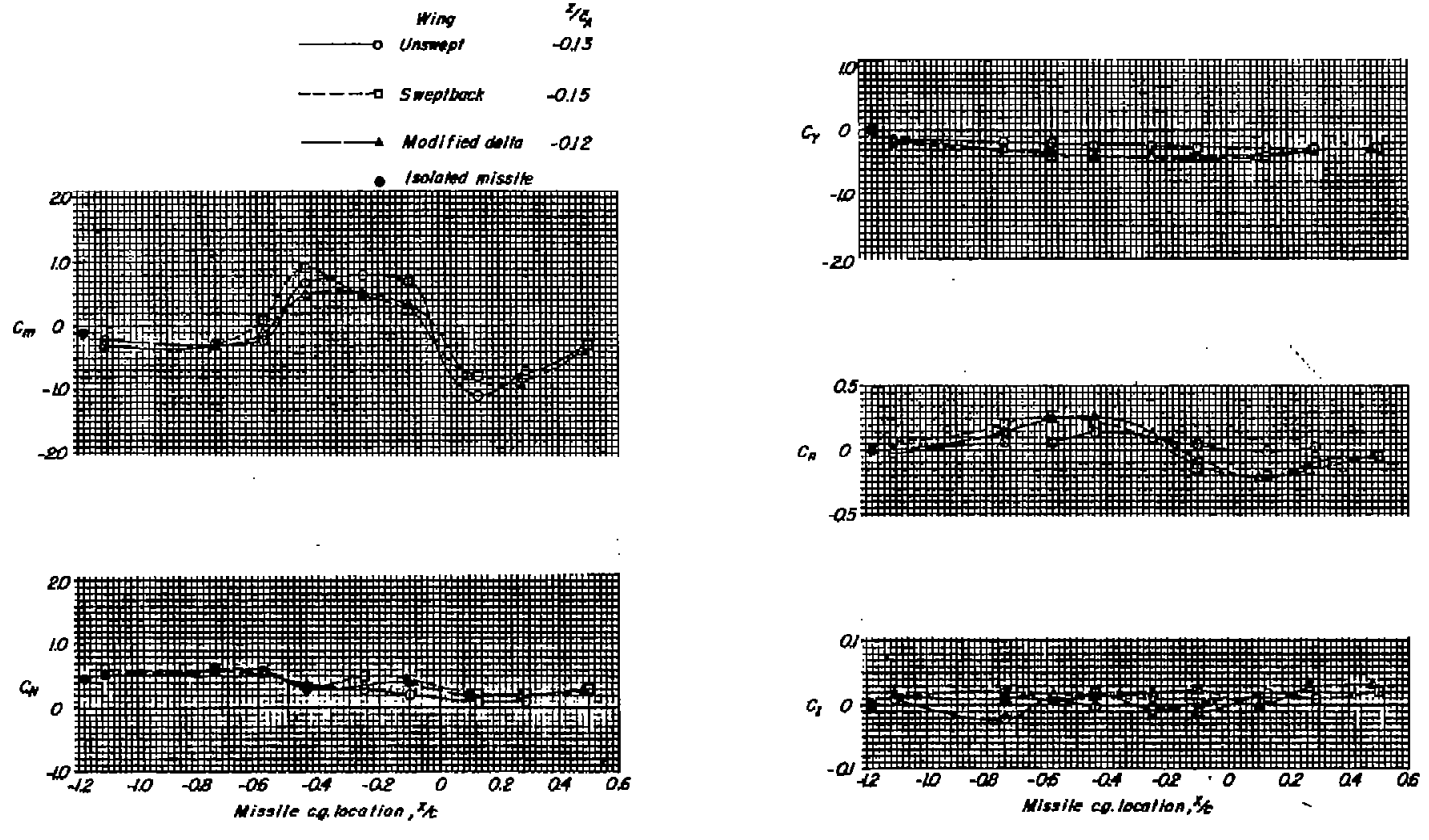

(b) M = 0.60; $\alpha = 4^{\circ}$.

Figure 19.- Continued.

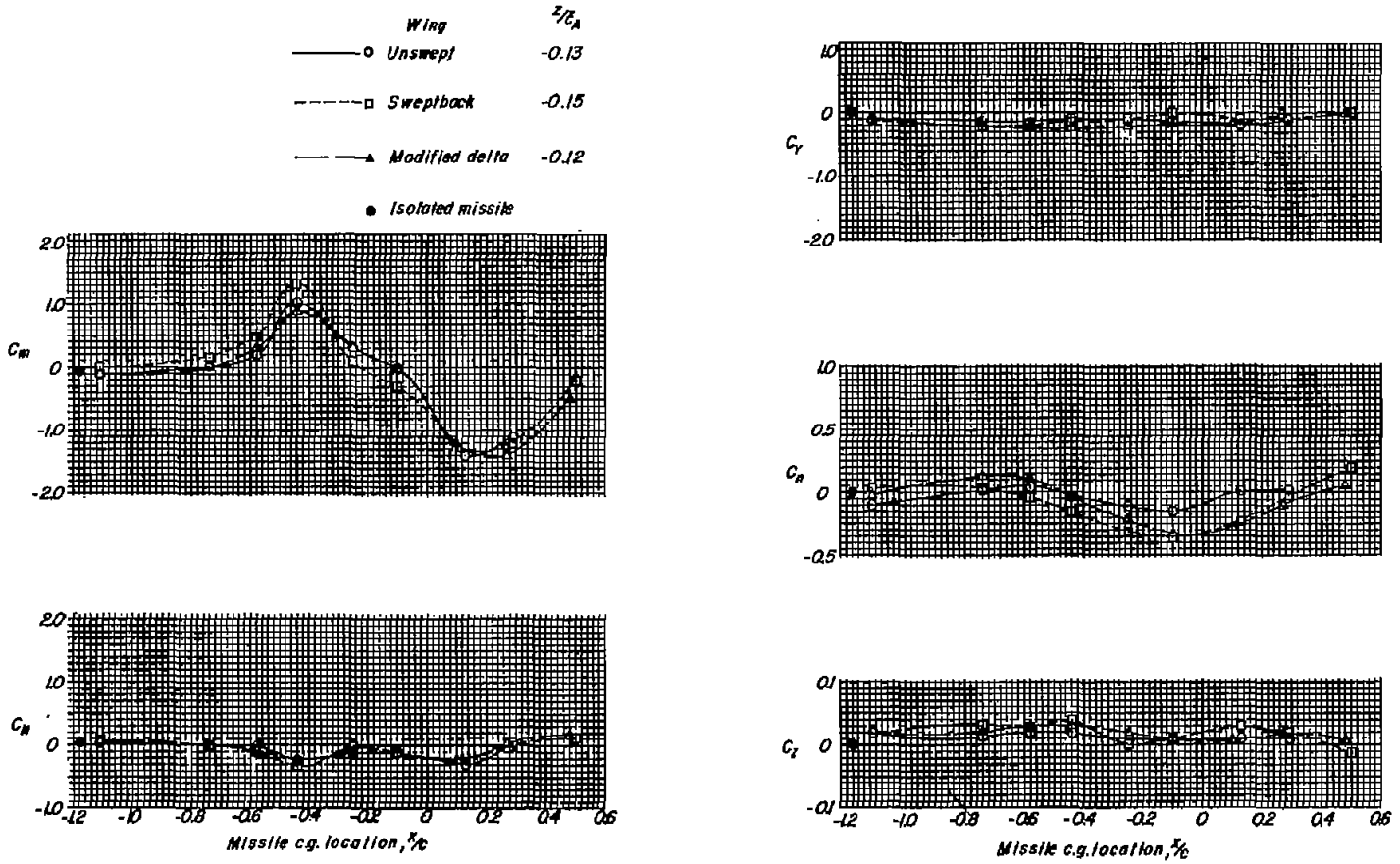

(c) M = 0.90; $\alpha = 0^{\circ}$.

Figure 19.- Continued.

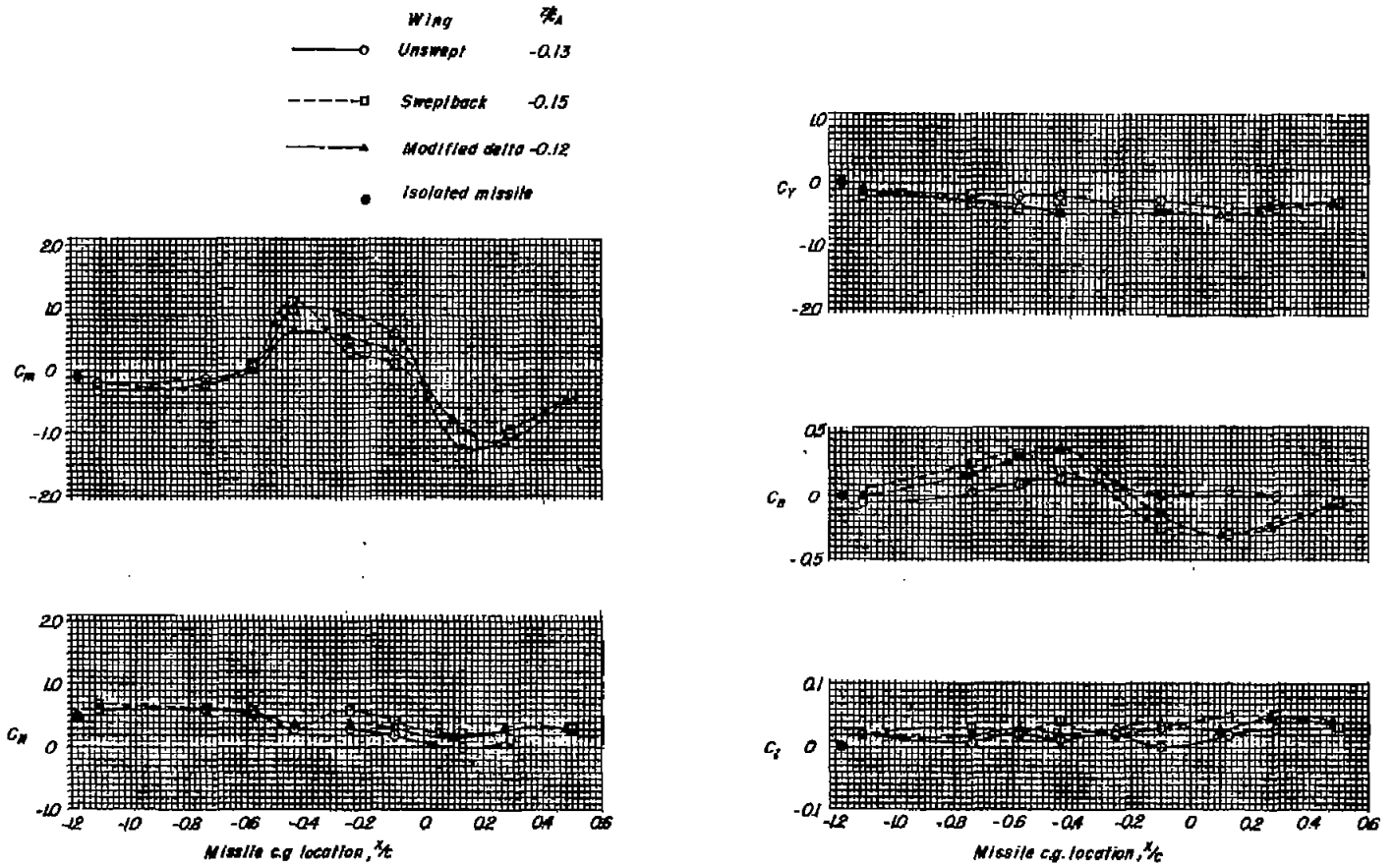

(d) $M = 0.90$; $\alpha = 4^\circ$.

Figure 19.- Concluded.

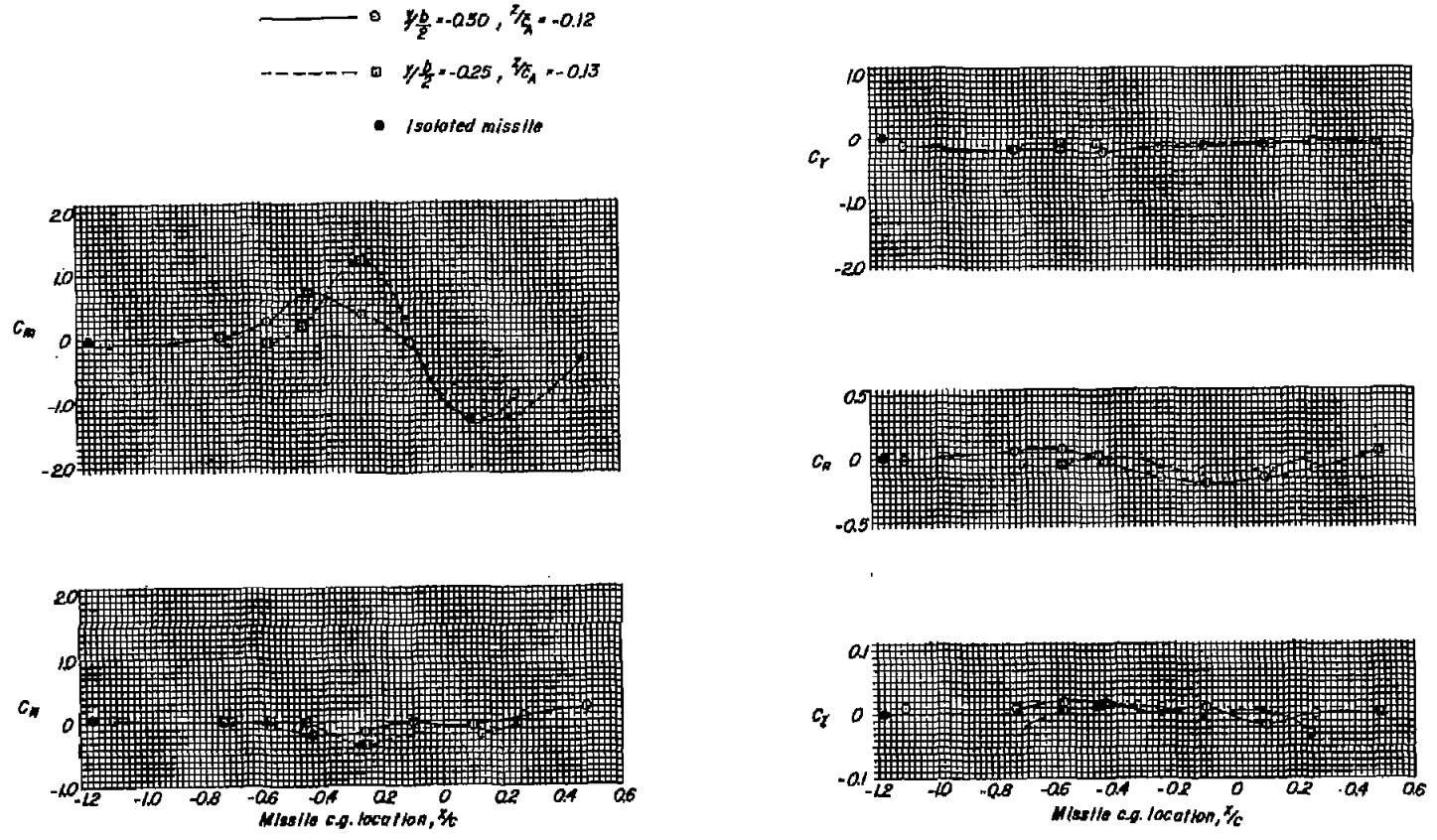

(a) M = 0.60; $\alpha = 0^{\circ}$.

Figure 20.- Effect of spanwise location on the missile forces and moments in the presence of the modified-delta-wing—fuselage—pylon combination.

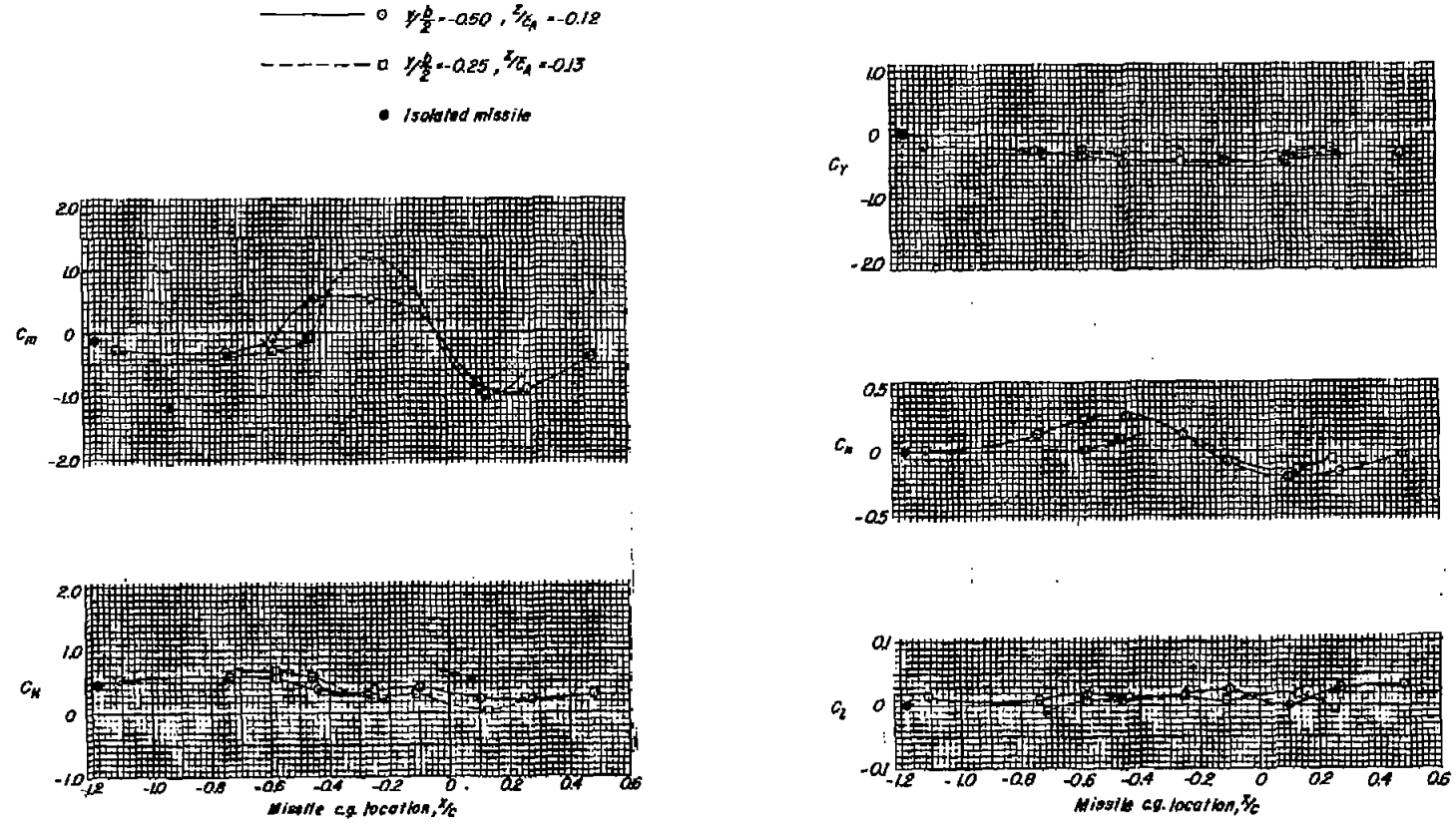

(b) M = 0.60; α = 4°.

Figure 20.- Continued.

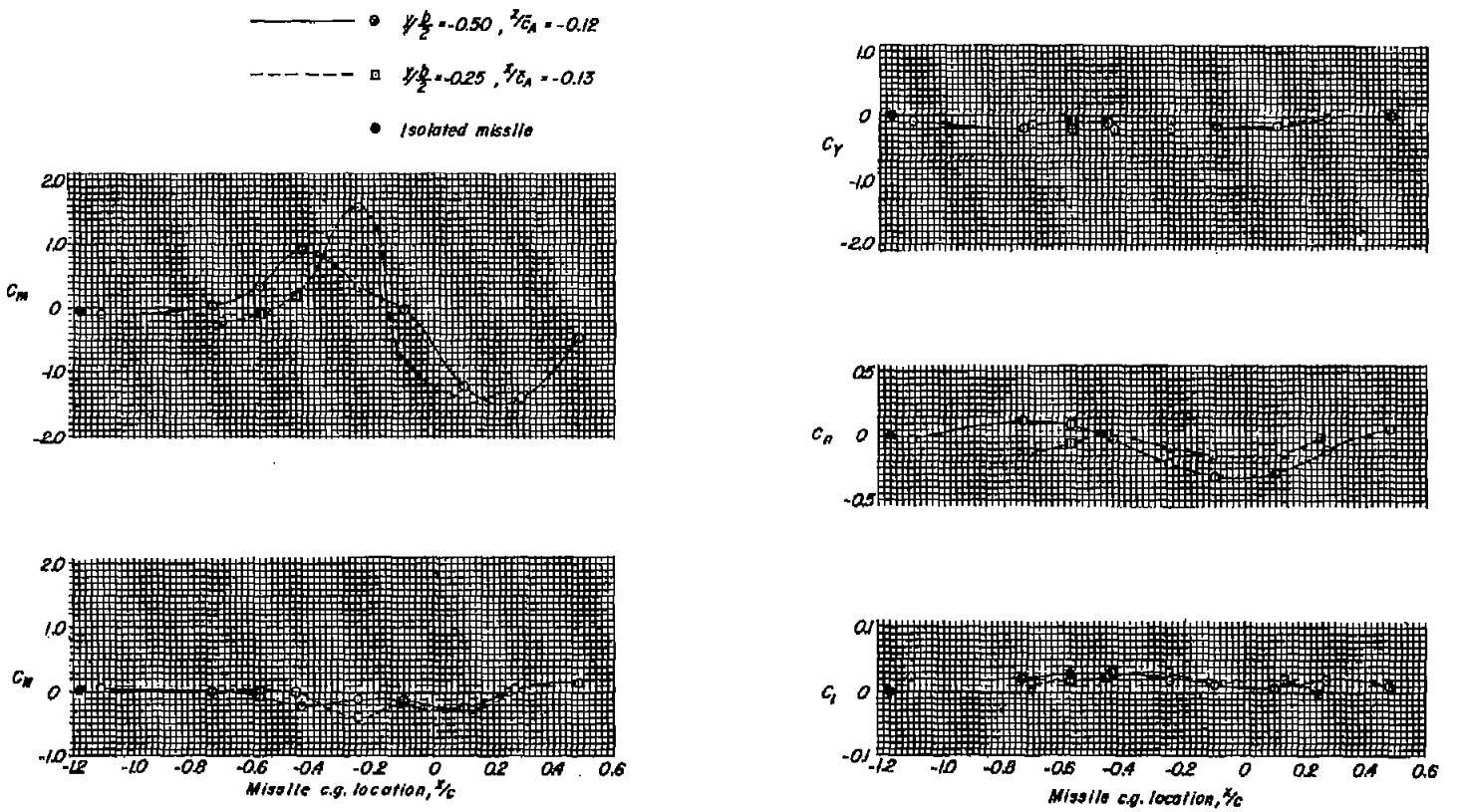

(c) M = 0.90; $\alpha = 0^\circ$.

Figure 20.- Continued.

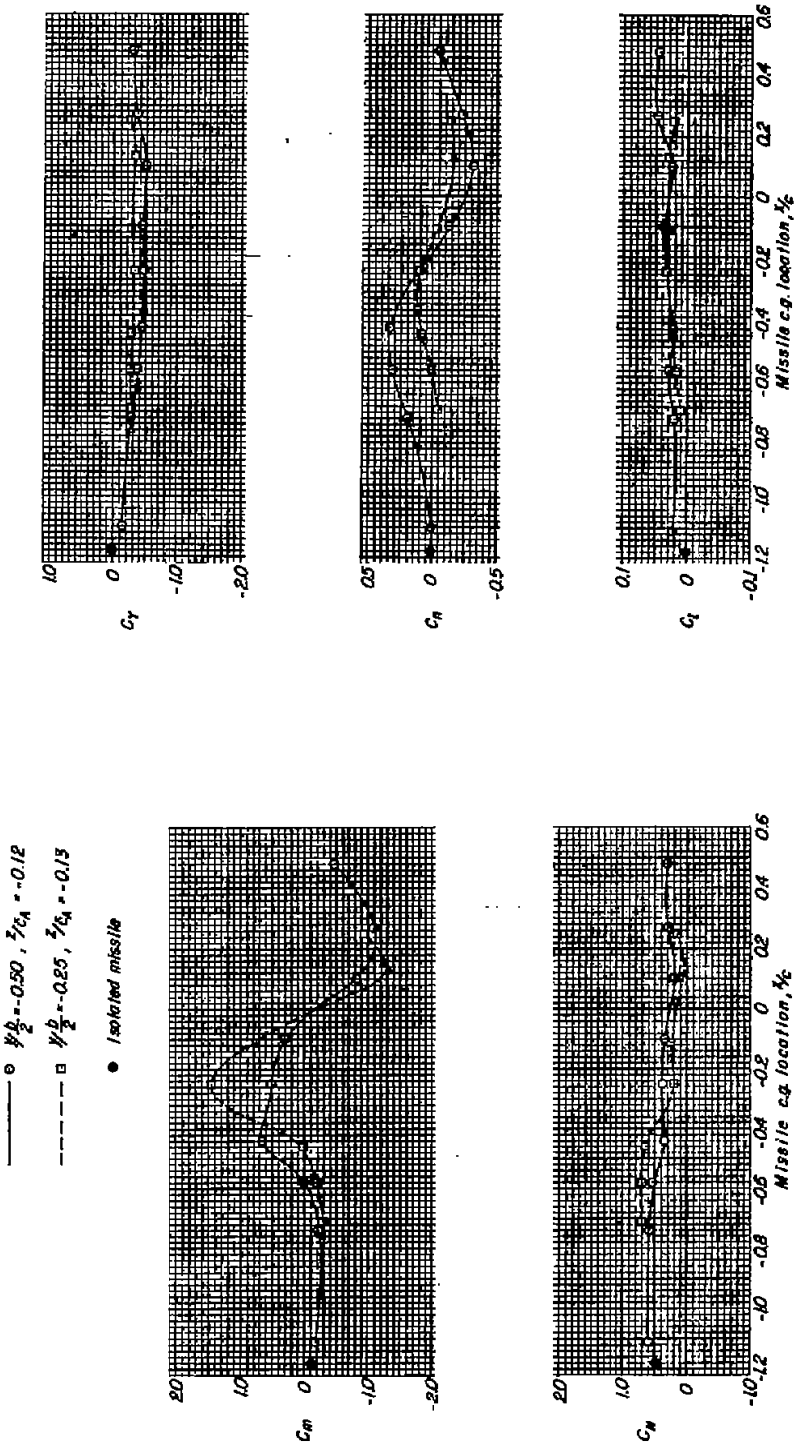

(d) M = 0.90; α = 4°.

Figure 20.- Concluded.

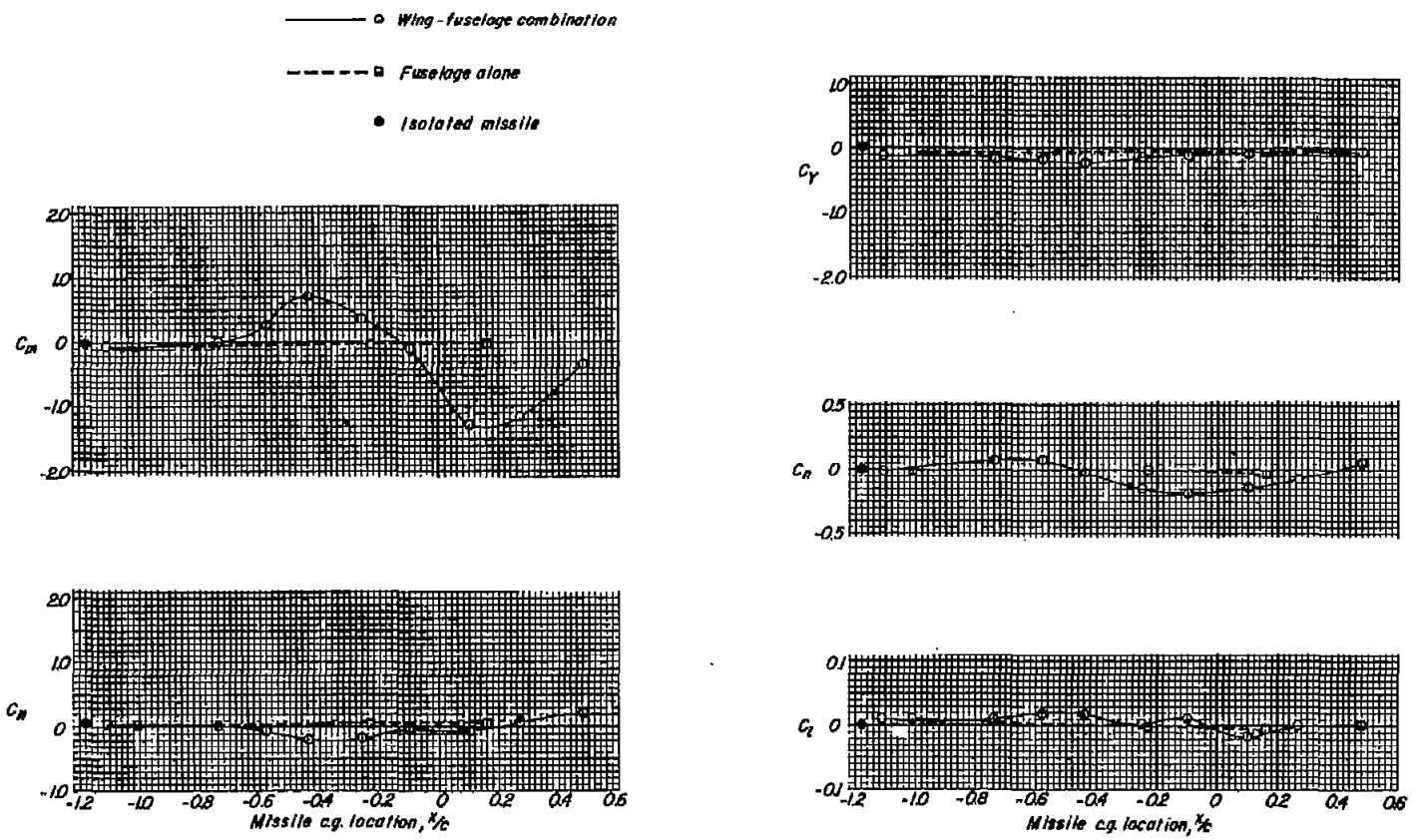

(a) M = 0.60; $\alpha = 0^\circ$.

Figure 21.- Comparison of missile forces and moments at the midsemispan location of the modified-delta-wing—fuselage—pylon combination with the missile forces and moments in the presence of the fuselage alone. $z/\bar{c}_A = -0.12$.

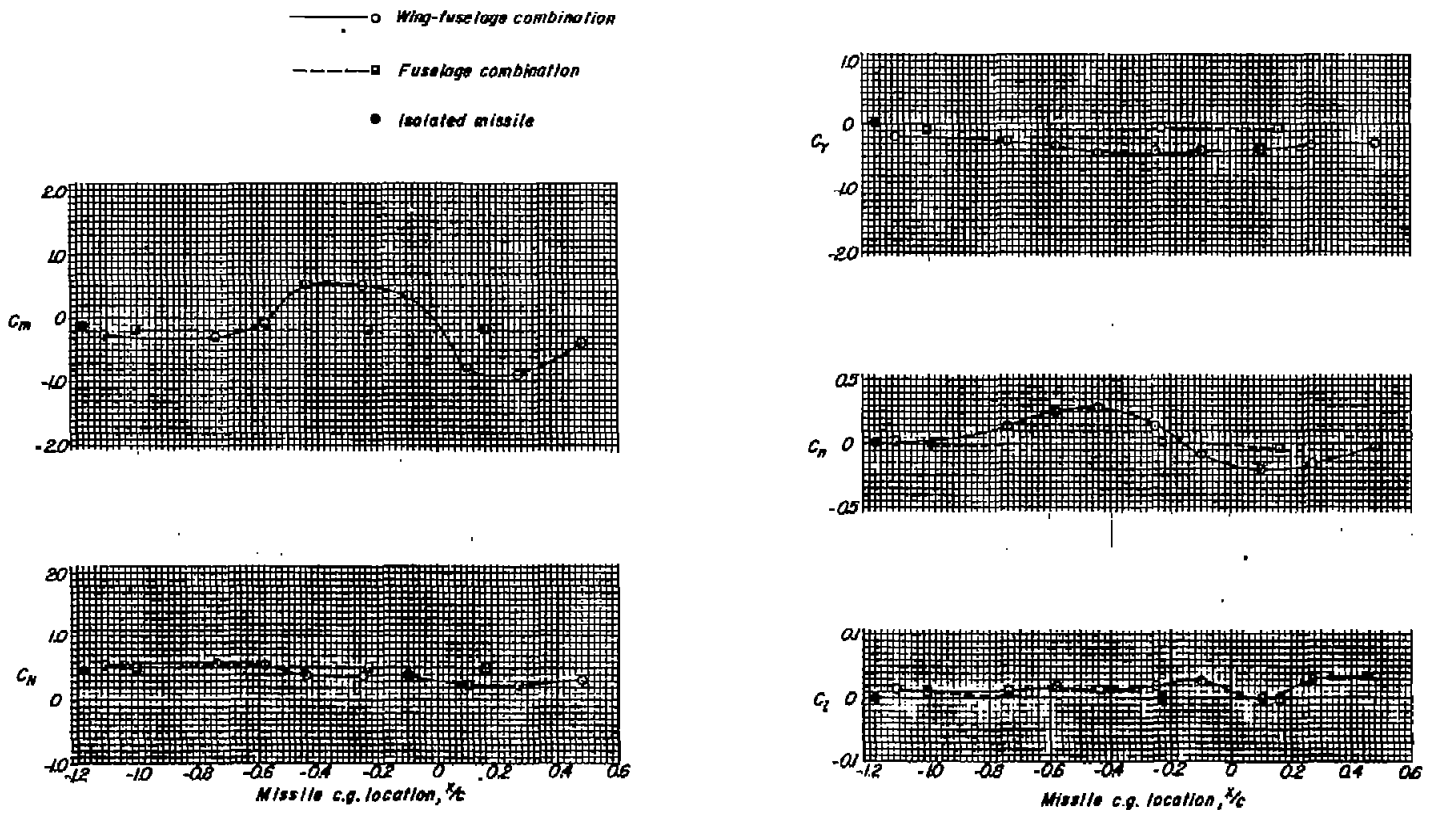

(b) $M = 0.60$; $\alpha = 4^\circ$.

Figure 21.- Continued.

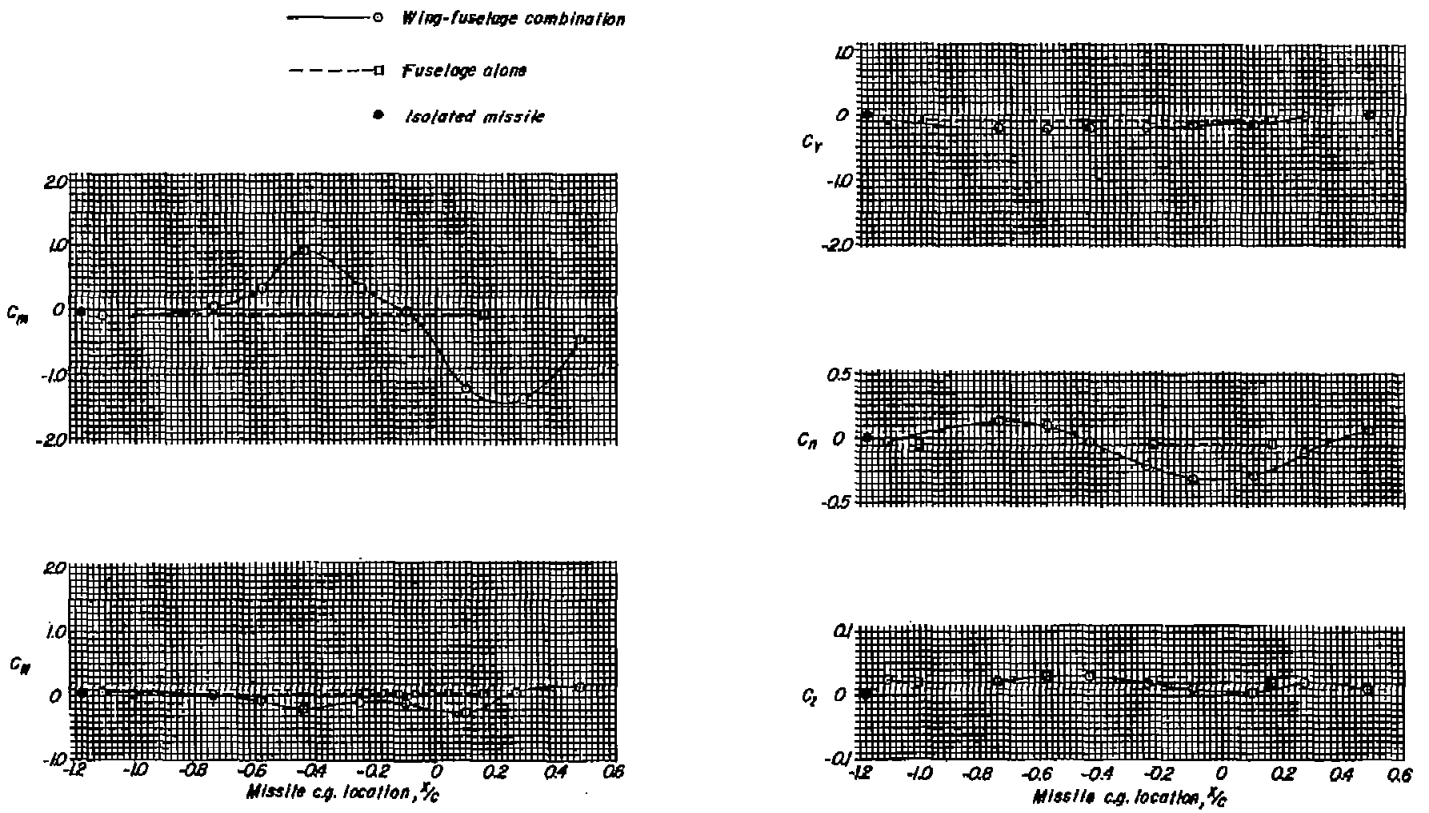

(c) M = 0.90; $\alpha = 0^{\circ}$.

Figure 21.- Continued.

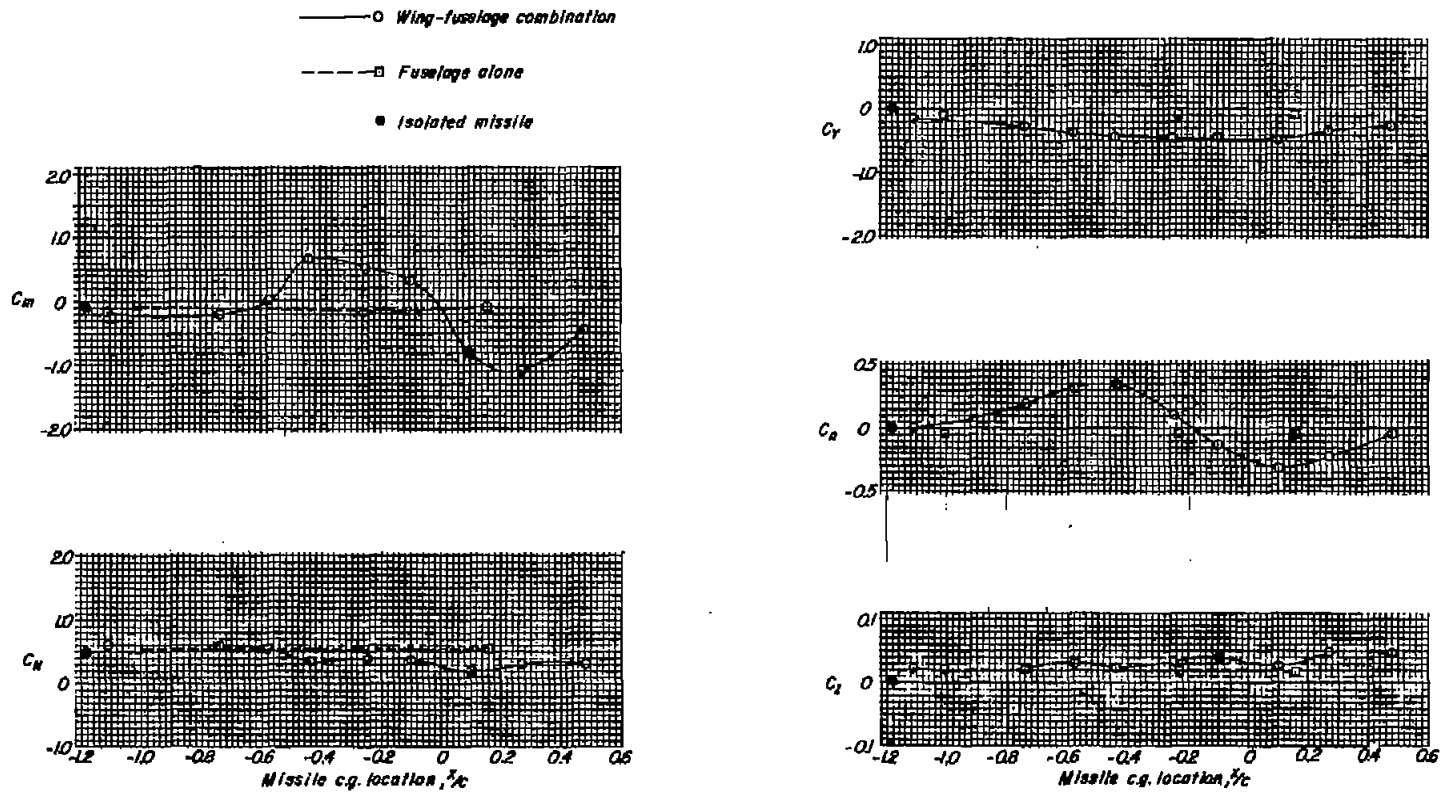

(d) M = 0.90; $\alpha = 4^\circ$.

Figure 21.- Concluded.

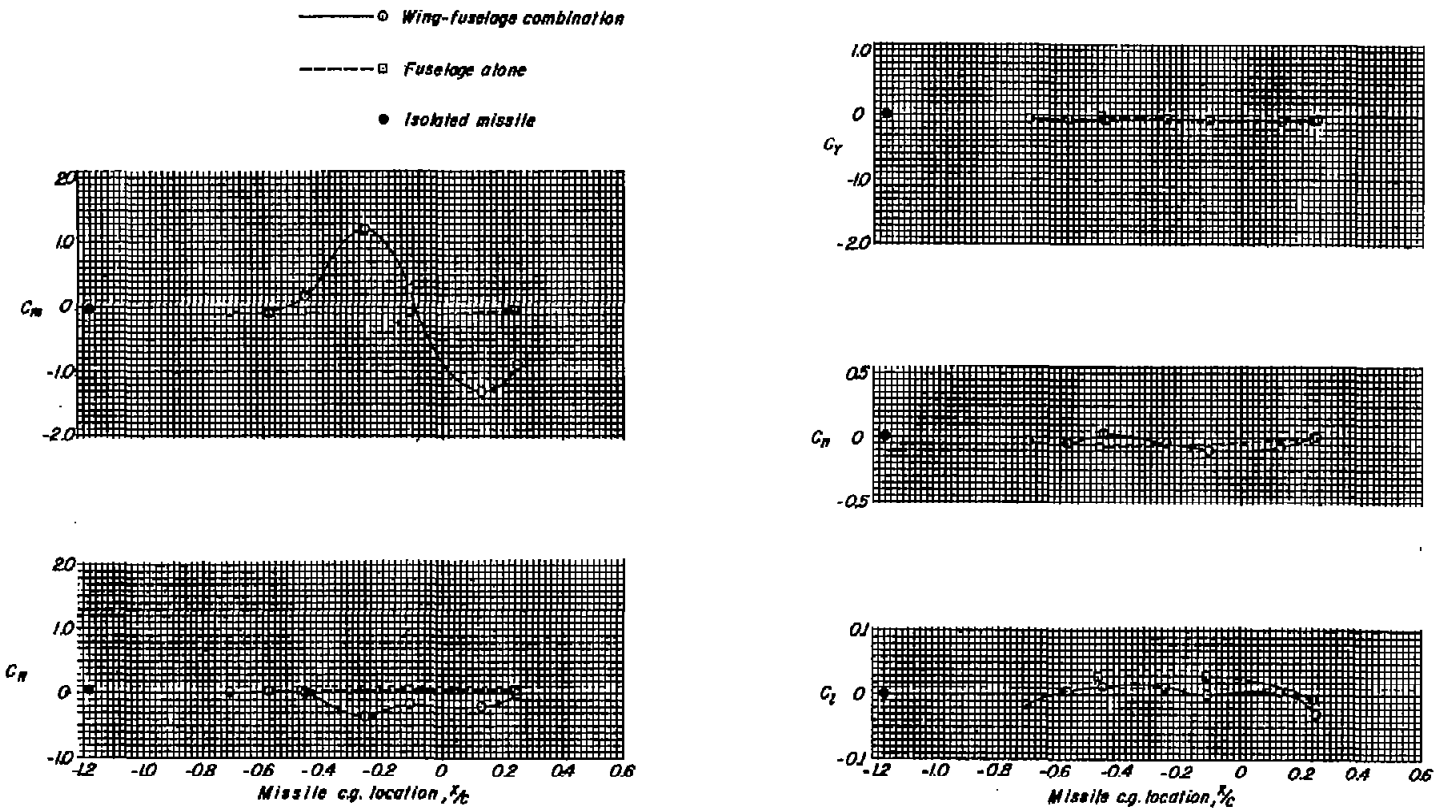

(a) $M = 0.60$; $\alpha = 0^\circ$.

Figure 22.- Comparison of missile forces and moments at the one-quarter semispan location of the modified-delta-wing—fuselage—pylon combination with the missile forces and moments in the presence of the fuselage alone. $z/\bar{c}_A = -0.13$.

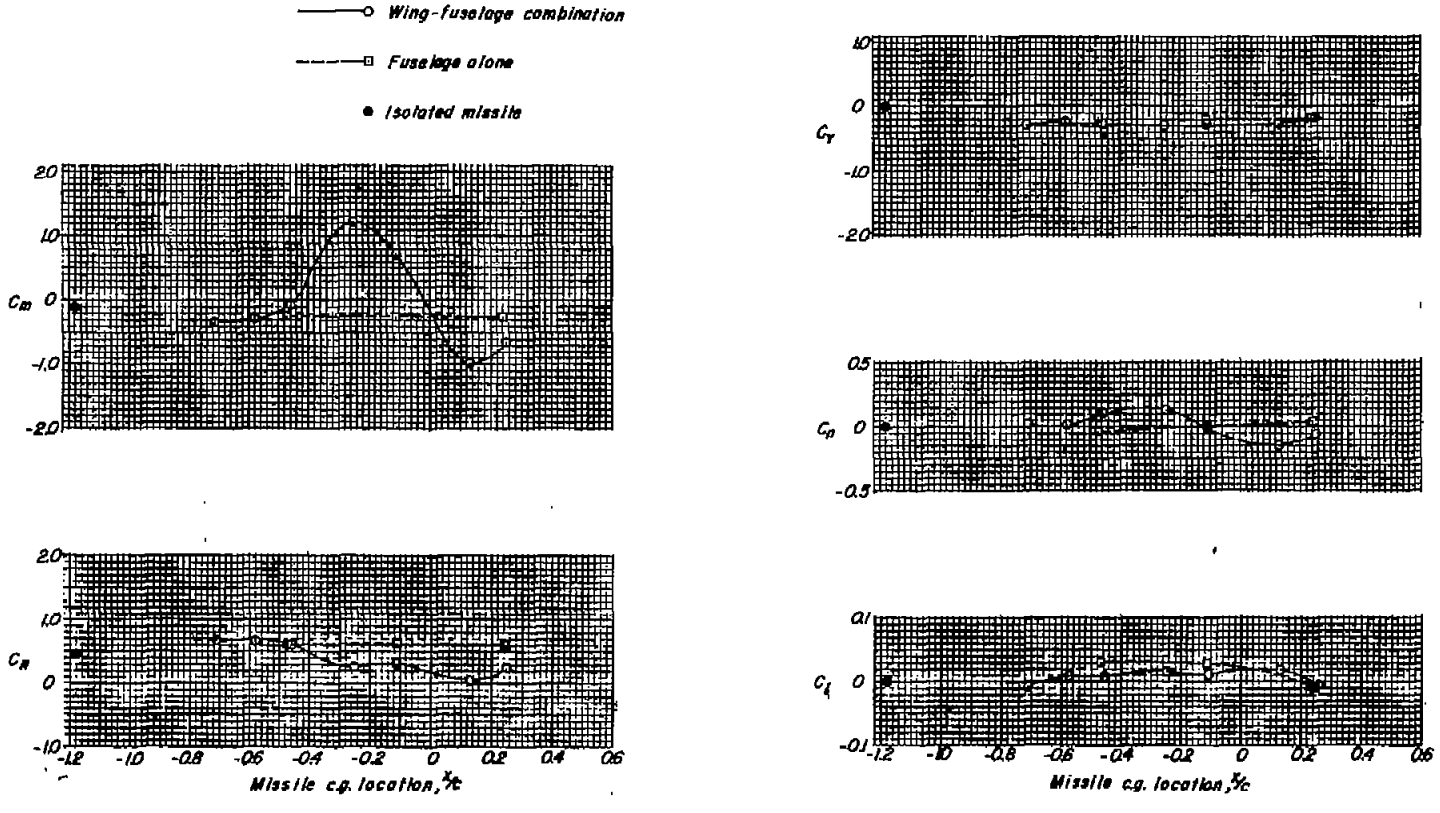

(b) M = 0.60; $\alpha = 4^\circ$.

Figure 22.- Continued.

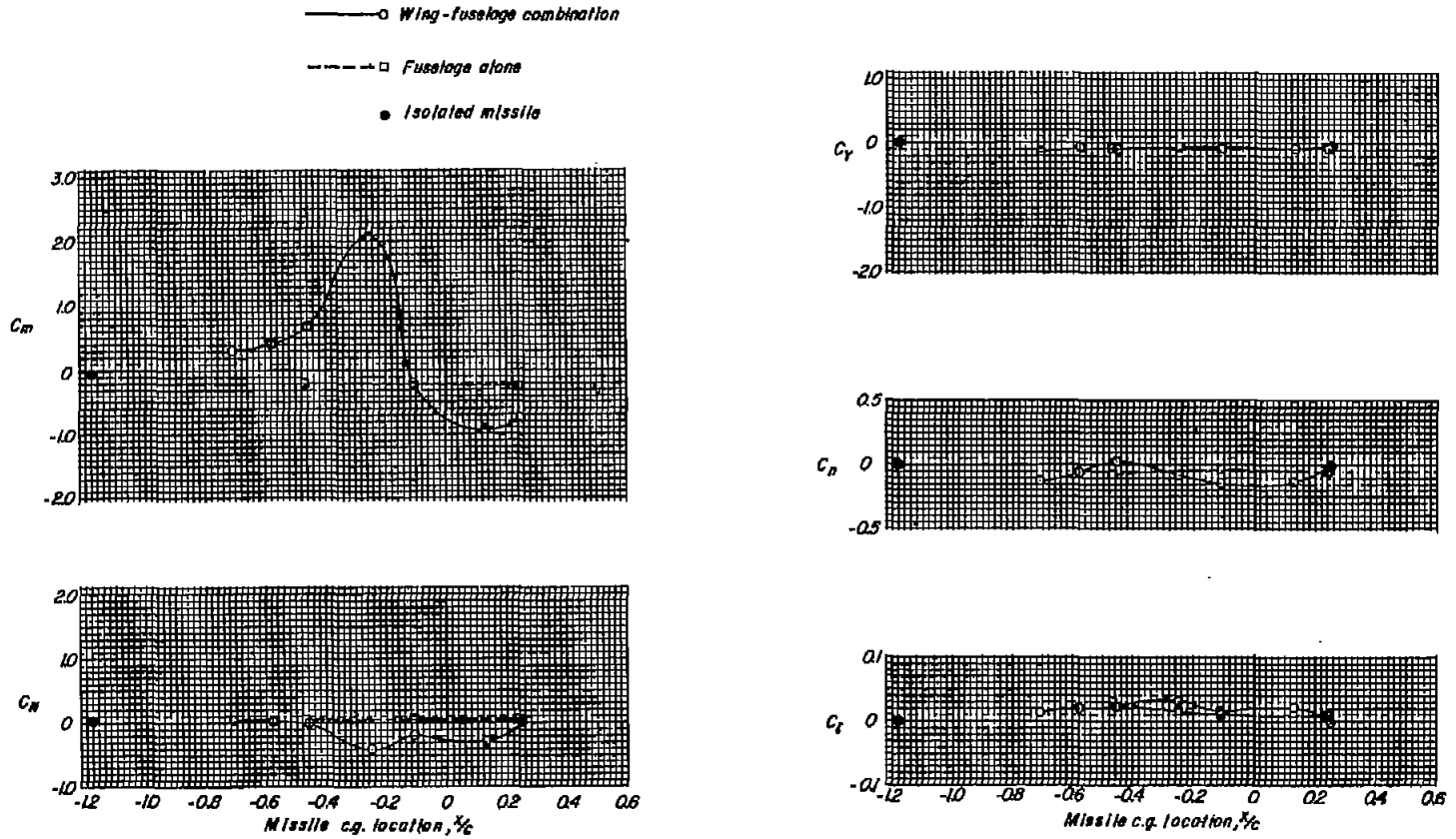

(c) M = 0.90; $\alpha = 0^{\circ}$.

Figure 22.- Continued.

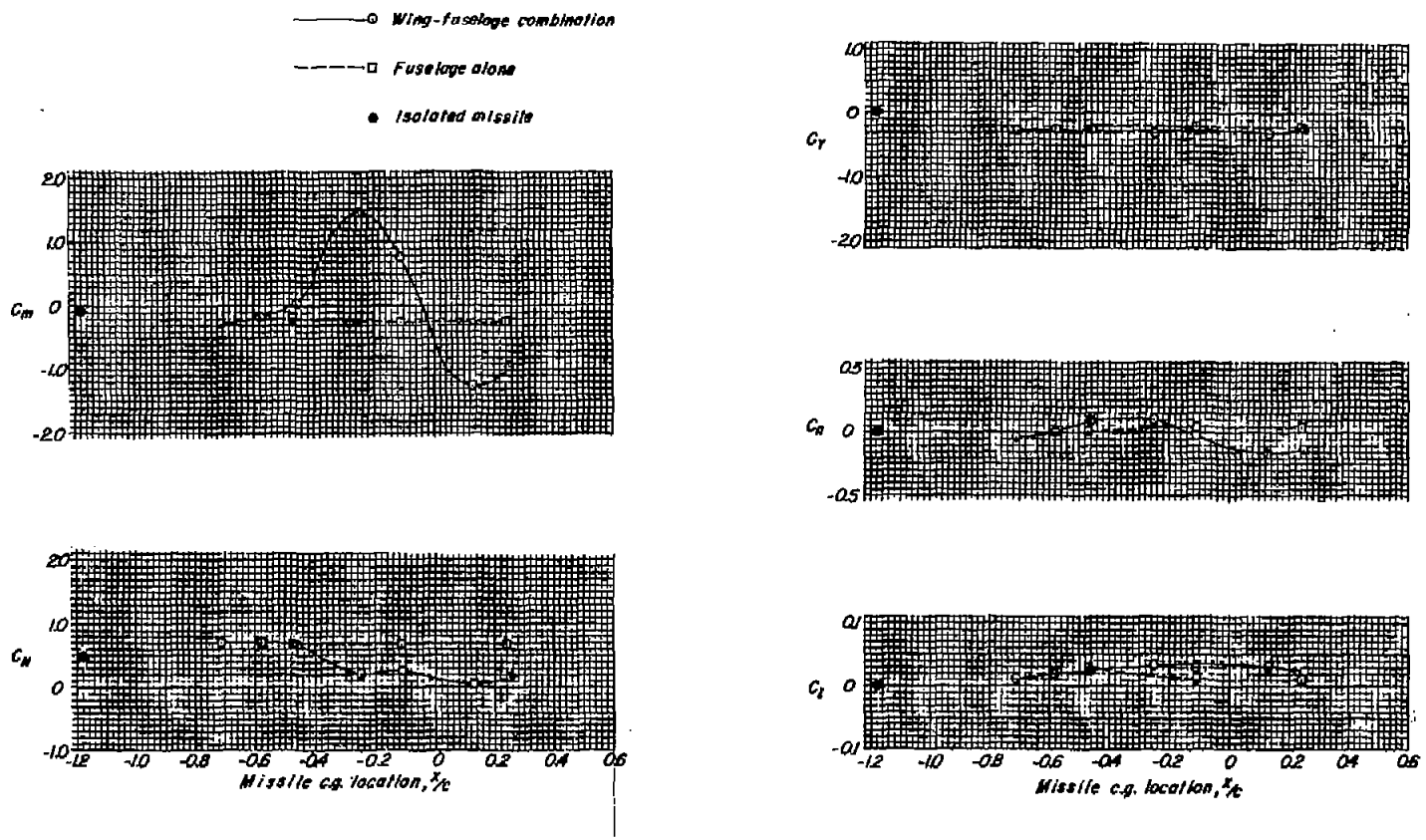

(d) M = 0.90; $\alpha = 4^{\circ}$.

Figure 22.- Concluded.

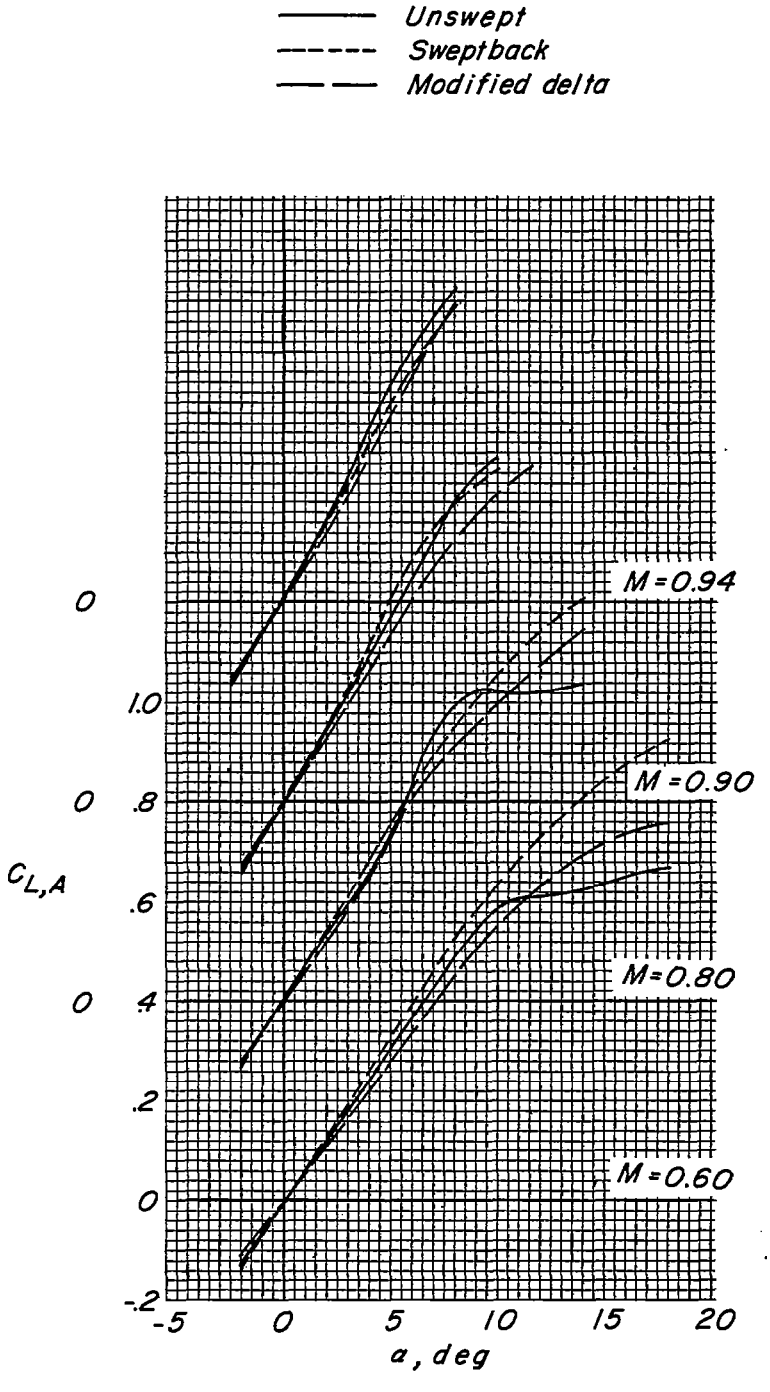

Figure 23.- Lift characteristics of the isolated wing-fuselage combinations.

NACA - Langley Field, Va.